Master's thesis

Master's Programme in Chemistry and Molecular Sciences

Chemical ionization mass spectrometry of ozonolysis-initiated autoxidation products of cyclooctene and 1,5-cyclooctadiene

Pyry S. Salomaa

February 4, 2025

Supervisor(s): Prof. Matti Rissanen

Examiner(s): Prof. Matti Rissanen
Dr. Siddhart Iyer

University of Helsinki
Faculty of Science
A.I. Virtasen aukio 1, PL 55 (Chemicum)
00560 University of Helsinki

HELSINGIN YLIOPISTO — HELSINGFORS UNIVERSITET — UNIVERSITY OF HELSINKI

Tiedekunta — Fakultet — Faculty	Koulutusohjelma — Utbildningsprogram — Degree programme
Faculty of Science	Master's Programme in Chemistry and Molecular Sciences

Tekijä — Författare — Author

Pyry S. Salomaa

Työn nimi — Arbetets titel — Title

Chemical ionization mass spectrometry of ozonolysis-initiated autoxidation products of cyclooctene and 1,5-cyclooctadiene

Työn laji — Arbetets art — Level	Aika — Datum — Month and year	Sivumäärä — Sidantal — Number of pages
Master's thesis	February 4, 2025	87

Tiivistelmä — Referat — Abstract

Aerosol affect air quality and the global climate. Air pollution causes serious health issues in the most polluted regions of the world. A significant part of air pollution consists of aerosol, which originate from both biogenic and anthropogenic emissions. In addition to the effects on global air quality, aerosol influence global temperatures through direct and indirect effects, which mainly cause a net cooling effect through cloud interactions. A large fraction of atmospheric aerosol are organic aerosol, which include primary and secondary organic aerosol. Secondary organic aerosol (SOA) are the major component of sub-1 μm particles. Secondary organic aerosol are formed in the atmosphere from gas-phase compounds that can be deemed aerosol precursor compounds, requiring low enough volatility to form SOA. Some aerosol precursor compounds are highly oxygenated organic molecules (HOMs) which have been found to form in the atmosphere from various volatile organic compounds (VOCs), such as alkanes, terpenes, and aromatics, via autoxidation on rapid time scales. The total contribution of HOM to SOA in the atmosphere is highly uncertain.

To understand the effects and mechanisms of formation of HOM in the atmosphere, it is essential to understand the autoxidation mechanisms of some of the VOCs with large emissions such as α-pinene and limonene, which are classified as monoterpenes. The study of compounds with similar chemical structures is beneficial in gaining insight into the autoxidation mechanisms of more complex VOCs, such as monoterpenes. For example, cyclohexene has been studied extensively because of its structural similarity to monoterpenes. The structure of limonene contains two double bonds, which likely results in similarities in the ozonolysis-initiated autoxidation mechanisms of limonene and 1,5-cyclooctadiene. Some compounds other than limonene such as terpinenes, especially those containing 2 cyclic double bonds, are chemically very similar to 1,5-cyclooctadiene.

In this thesis, the autoxidation of two cyclic precursors, cyclooctene and 1,5-cyclooctadiene, was experimentally studied over a wide range of precursor concentration and reaction time. No preexisting studies on gas-phase autoxidation of 1,5-cyclooctadiene were found, and a very scarce amount of studies on the autoxidation of cyclic dienes were found. One of the main goals was to find the time scale of formation of HOM, and also accretion product HOM formed by bimolecular radical reactions, that are expected to be very important for the first steps of atmospheric new particle formation. The results show that the accretion products form as rapidly as 0.35 seconds at a concentration of 3.49 ppm of 1,5-cyclooctadiene, and a concentration of 41 ppb of O_3. Accretion products were not detected at a reaction time of 0.33 s and a concentration of 3.94 ppm of cyclooctene, and an O_3 concentration of 37 ppb. The results show that the extra double bond of 1,5-cyclooctadiene significantly enhances the formation of accretion products, compared to cyclooctene.

Avainsanat — Nyckelord — Keywords

HOM, secondary organic aerosol, autoxidation, chemical ionization mass spectrometry, Orbitrap

Säilytyspaikka — Förvaringsställe — Where deposited

Helda

Muita tietoja — Övriga uppgifter — Additional information

Contents

1. Introduction

According to recent studies, air quality was a leading factor contributing to the reduction in life expectancy through cardiovascular diseases globally, even competing with smoking.[1–4] The effect of anthropogenic emissions on air quality is highly geographically variable. The most polluted areas worldwide, such as east Asia, are most drastically affected, with up to three years of decreased life expectancy due to anthropogenic emissions alone. Air pollution consists of harmful gases such as CO, NO_2, O_3 as well as suspended gases and particulates in the atmosphere, which are called aerosol. Atmospheric aerosol include larger particles such as dust, soil, vapor and liquids suspended in the atmosphere. A major part of submicrometer-sized atmospheric aerosol are organic aerosol (20-90%),[5] further classified as primary and secondary organic aerosol (POA, SOA, respectively). The largest share of organic aerosol are SOA. Secondary organic aerosol are formed from various precursors in the atmosphere, including highly oxygenated organic molecules (HOM).

Volatile organic compounds (VOCs) are transported to the atmosphere from both anthropogenic and biogenic sources. After being transported to the atmosphere, VOCs are oxidized, potentially forming HOM through a rapid oxidation process called autoxidation, which has only recently been found to occur in the atmosphere. Autoxidation is the process of sequential unimolecular peroxy radical hydrogen-shift (H-shift) reactions and pseudo-unimolecular oxygen additions, the H-shifts being the rate-limiting steps, but the complete autoxidation mechanisms of VOCs are often more complex. Autoxidation of VOCs lead to highly functionalized HOM that can be low-volatile enough to participate in the formation of SOA. Other reactions such as the cleavage of C=O groups or more complex reactions such as carbon structure rearrangements[6] can also be part of the autoxidation mechanisms of various compounds. Autoxidation has been known to occur in just about any kind of chemical conditions, such as combustion engines at high temperatures, cells in the human body or in the atmosphere for a wide variety of VOCs.[7–10] In the field of atmospheric chemistry, autoxidation has now gained interest in large scale, because it has been found to occur for a wide variety of precursors in the atmosphere. Even precursors, such as alkanes and aromatic compounds such as toluene, which were previously though not to undergo extensive autoxidation, have been found to quickly autoxidize.[6,11]

Atmospheric autoxidation is initiated by various oxidants, of which the most at-

mospherically relevant are O_3, NO_3 or OH radicals.[12] Most research has focused on ozonolysis-initiated autoxidation, but also hydroxyl radicals have been used as the initiator of autoxidation. The first studies on ozonolysis of α-pinene by Ehn et. al.[13] were motivated by the detection of HOM in the nocturnal ambient air over the boreal forest in Hyytiälä, Finland.[14] Because OH is not present in large quantities at night, it was proposed and later confirmed that O_3 is the source of these highly oxygenated molecules. Monoterpenes, the most abundant biogenic VOCs in addition to isoprene, were converted to HOM via ozonolysis. Other proposed sources of HOM production have been nitrate and chlorine radicals, although considered less important. For both the ozonolysis and the hydroxyl radical-initiated autoxidation process, autoxidation proceeds through formation of peroxy radicals (RO_2), which can then undergo autoxidation. The autoxidation mechanisms of atmospherically relevant VOCs are often very complex, which is why the use of surrogate compounds can give valuable information on the more complex autoxidation mechanisms of compounds such as limonene or β-caryophyllene.

In this thesis, the autoxidation of cyclooctene and 1,5-cyclooctadiene was experimentally investigated in the gas phase using a flow reactor connected to an Orbitrap mass spectrometer (Orbitrap Exploris 120). The autoxidation mechanism of cyclooctene, and especially that of 1,5-cyclooctadiene has a lot of resemblance to the autoxidation mechanisms of more atmospherically relevant VOCs with multiple double bonds in the initial structure of the molecule, which is why they were chosen. The measurements were performed in the molecular sciences research unit in the chemistry department of the University of Helsinki in the summer of 2024. The measurements were done by altering some conditions, such as the concentration of the precursor and the reaction time, and using both polarities of chemical ionization. The primary goal of these experiments was to investigate the time scale of autoxidation derived HOM formation and subsequently also the formation of accretion product HOMs originating from RO_2 + RO_2 reactions, signifying the involvement of considerable bimolecular chemistry. The time scale of the formation of the accretion product is an important aspect of autoxidation reactions because accretion products are generally the least volatile products of the formed HOM, which can be classified as radical monomer species, closed-shell monomer species, and accretion products. The low volatility of the accretion products allows these HOM to participate more efficiently in the formation of SOA.

There has only been one study in which autoxidation of cyclooctene was investigated, and no experimental studies into the gas phase autoxidation of 1,5-cyclooctadiene was found from the existing literature. Only one study on the autoxidation of cyclic dienes was found, in which Richters et al. studied the autoxidation of cyclohexadiene.[15] Surrogate compounds such as cyclohexene have provided a wealth of information on the autoxidation mechanisms of more atmospherically relevant VOCs such as monoterpenes.

A structurally resembling sesquiterpene to 1,5-cyclooctadiene, the β-caryophyllene has been studied before,[16,17] but a thorough autoxidation mechanism is lacking. The autoxidation mechanisms of more atmospherically relevant VOCs are often very complex, which is why the use of surrogate compounds can give valuable information on the more complex autoxidation mechanisms of compounds such as limonene or β-caryophyllene.

2. Theoretical

In this chapter, the relevant literature is reviewed and the theoretical basis is further established to solidify the understanding of the motivation, results, and significance of this research. This chapter begins with a discussion about SOA and proceeds to establish the connection between HOM and SOA. Next, the autoxidation mechanisms of cyclooctene and 1,5-cyclooctadiene are discussed. Finally, the detection of HOM is briefly discussed, as well as the vapor pressure and volatility of VOCs.

2.1 Secondary organic aerosol (SOA)

Aerosol are microscopic solid particles and/or liquid droplets dispersed in the atmosphere. Aerosol, in general, are a major component of the atmosphere and have substantial effects on climate, visibility, and human health. The main types of aerosol include inorganic aerosol (anthropogenic sulfates, nitrates), organic aerosol, black carbon, dust, and sea salt.[18] Organic aerosol (OA) are particles that contain suspended organic matter in the atmosphere. Organic aerosol are further divided into primary and secondary organic aerosol, (POA), (SOA) respectively. Primary organic aerosol is released directly into the atmosphere, largely from combustion process, while SOA is formed in the atmosphere from the oxidation of VOCs. According to estimations, SOA is the major constituent of OA.[19,20] The human health effects of aerosol include a decreased life expectancy, respiratory problems, cardiovascular issues and other health problems. Aerosol affect the climate by direct and indirect effects.[21] The direct effects are the scattering and the absorbing radiative effects of aerosol, while the indirect effects are the cloud albedo and lifetime effects.

Secondary organic aerosol are formed from low volatility vapors via gas-to-particle conversion by condensing on pre-existing condensed vapors such as clusters of sulfuric acid, ammonia, other bases, called new particle formation (NPF), a process which can be defined as an abrupt increase in concentrations of >3 nm particles and the growth of these particles. Vapors that participate in the formation of SOA via NPF are sometimes referred to as aerosol precursor gases. Secondary organic aerosol are formed from both biogenic and anthropogenic precursors in the atmosphere. Anthropogenic SOA precursors

are mainly alkanes (40%), aromatics (20%), alkenes (10%) and the rest are other oxygenated and unidentified compounds.[22,23] Biogenic emissions consist mainly of isoprene and terpenes. Biogenic emissions have been estimated to contribute most of the non-methane VOCs globally, with anthropogenic emissions being more important in urban areas. The oxidation of VOCs forms less volatile compounds such as HOMs, which can subsequently be partitioned into aerosol. New particle formation has been observed in many environments and conditions, such as coastal, polar, forested, and urban areas.[24–28]

Although organic compounds in the atmosphere have been known for a long time to influence the formation and growth of new particles, until recently it was not known how these low volatility organic compounds originate in the atmosphere. After the discovery of how HOM are formed in the atmosphere, it has been proven that HOM are a significant contributor to the mass and number of new particles. It is known that HOM can efficiently cluster with sulfuric acid and form new particles.[29,30] Sulfuric acid-HOM clusters have also been detected in boreal forest.[31] It is also known that HOM alone can form new particles under atmospheric conditions in the absence of sulfuric acid.[32] In the case of α-pinene, the monomer HOM are too volatile to participate in nucleation.[33] It is generally seen that only accretion products are involved in purely biogenic nucleation, as they have low enough volatility to do so.

2.1.1 Highly oxygenated organic molecules (HOM) in the context of secondary organic aerosol

The term HOM can easily be confused with just about any highly oxygenated organic compound, but in atmospheric chemistry, the term refers to oxygenated organic compounds formed by gas-phase autoxidation. Therefore, the term HOM is briefly defined in the following general guidelines for the usage of the term HOM, which have been suggested by Bianchi et. al.[12] to distinguish HOM from other organic molecules with high oxygen content and to clear any confusion with the usage of the term HOM. These guidelines are summarized as follows: 1. HOM are formed by the autoxidation of peroxy radicals. 2. HOM are formed in the gas phase under atmospherically relevant conditions. 3. HOM generally contain six or more oxygen atoms. There are some contradictions to these guidelines, as for example, sometimes molecules with less than 6 oxygen atoms have been referred to as HOM. Because HOM can act as precursors for secondary organic aerosol (SOA), HOM formation and the conversion of HOM to SOA have been an important topic of past and current research.

2.1.2 Oxidation of volatile organic compounds (VOCs) in the atmosphere

After being emitted into the atmosphere, the autoxidation process of VOCs is initiated by the formation of peroxy radicals (RO_2), which are formed under atmospheric conditions mainly by ozonolysis or reacting with OH/NO_3 followed by an addition of O_2. In the case of cyclooctene and 1,5-cyclooctadiene, ozonolysis is the main initiator for the autoxidation process under atmospheric conditions. The structures of cyclooctene and 1,5-cyclooctadiene are presented in Figure 2.1.

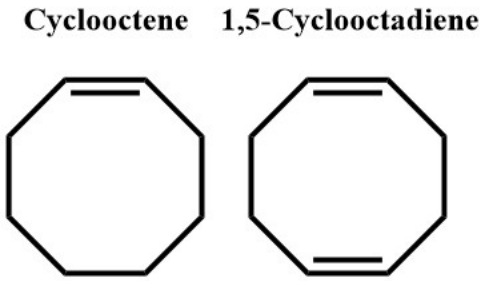

Figure 2.1: The chemical structures of the precursors used in this thesis.

Ozonolysis is initiated when O_3 reacts with an unsaturated carbon-carbon bond. The ozonolysis of cyclooctene is presented in Figure 2.2, adapted from the corresponding mechanism for cyclohexene by Rissanen et. al.,[34] because of the similarity of cyclooctene to cyclohexene.

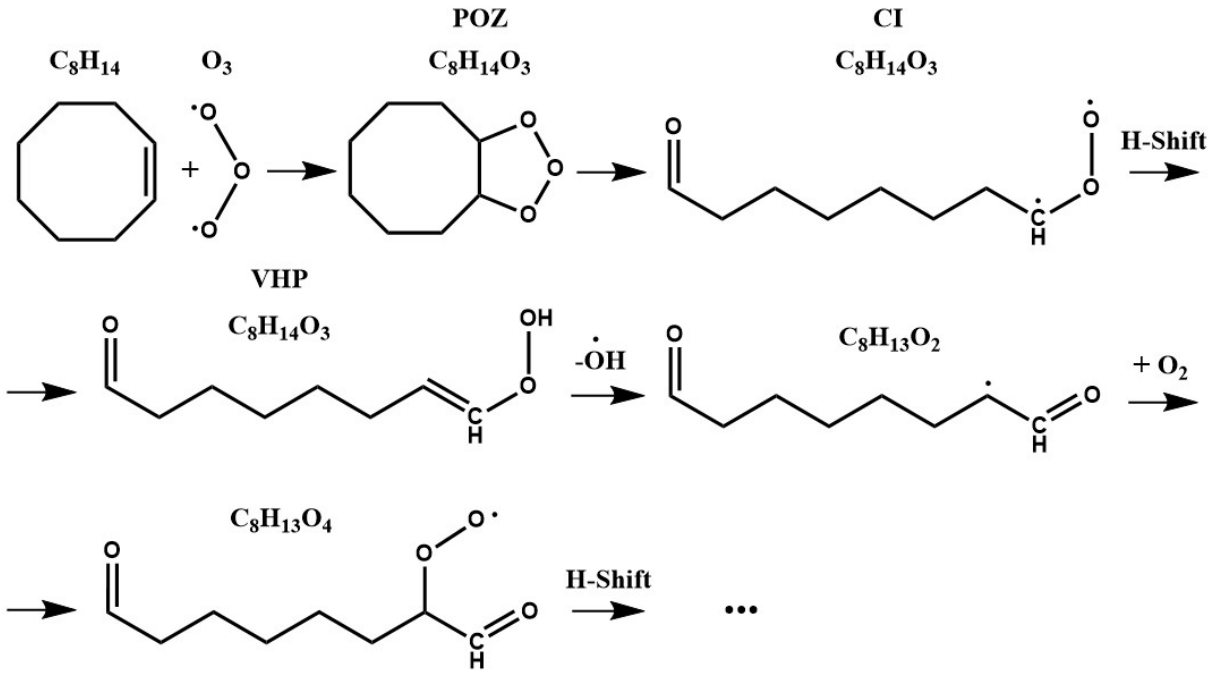

Figure 2.2: Ozonolysis of cyclooctene.

Ozone reacts with the double bond of cyclooctene, forming a primary ozonide (POZ), which subsequently decomposes into a Criegee intermediate (CI). The Criegee intermediate can undergo a 1,4 hydrogen shift to form a vinyl hydroperoxide (VHP), which rapidly loses an OH-radical. The resulting carbon-centered radical can add an oxygen molecule to form an oxygen-centered peroxy radical, which can be isomerized further. The expected ozonolysis mechanism of 1,5-cyclooctadiene is likely similar, except that the second double bond in the initial structure of 1,5-cyclooctadiene allows for additional reactions such as endoperoxidation and epoxidation, both of which will be explained in more detail later. In the case of 1,5-cyclooctadiene, which was also used in the experiments of this research, there is a double bond on the opposite side of the molecule after ozonolysis. Recently, Klippenstein et. al.[35] found that OH groups of VHPs formed from α-pinene can change location after elongation of the O-O bond of the OOH group of VHPs in a so-called roaming mechanism. Such reactions could provide an alternative branching point from the VHP in the ozonolysis mechanism presented above if those kinds of reactions were possible for cyclooctene in the first place. The rate coefficients of O_3 reaction with cyclooctene and 1,5-cyclooctadiene at 25 °C have been determined by Sharma et. al.[36] The determined rate coefficients were 4.10 ± 0.8 × 10^{-16} $cm^3molecule^{-1}s^{-1}$ for cyclooctene and 1.40 ± 0.2 × 10^{-16} $cm^3molecule^{-1}s^{-1}$ for 1,5-cyclooctadiene. In the troposphere, O_3 is formed primarily by reactions of NO_x. Peroxy radicals also have an effect on the amounts of O_3 indirectly due to the reactions with NO:

$$RO_2 + NO \rightarrow RO + NO_2 \tag{2.1}$$

$$NO_2 \xrightarrow{\text{Photolysis}} O + NO \tag{2.2}$$

$$O + O_2 \rightarrow O_3 \tag{2.3}$$

2.1.3 Unimolecular RO_2 reactions following ozonolysis

Unimolecular reactions involve only one reactant [A]. In an unimolecular reaction, the reactant [A] is converted to [B], as shown in equation 2.4.

$$[A] \xrightarrow{Rate} [B] \tag{2.4}$$

Common unimolecular reactions include H-shift or elimination reactions, in which some sort of functional group, such as a carbonyl group CO is cleaved off the molecule. The concentration of reactant [A] at time t in equation 2.6 can be solved from the differential form of the rate law 2.5 for reactant [A] by integrating:

$$\text{Rate} = -\frac{d[A]}{dt} = k[A] \tag{2.5}$$

$$[A] = [A]_0 e^{-kt} \tag{2.6}$$

In which k is the rate coefficient of the reaction, $[A]$ is the reactant concentration after time t and $[A]_0$ is the initial reactant concentration.

Unimolecular reaction rates of individual peroxy radical reactions are difficult to study experimentally, hence quantum chemical computations are used to determine the rates of these reactions. Bianchi et al.[12] summarized the most important unimolecular fragmentation reactions of peroxy radicals, and these are presented in Figure 2.3 (excluding the NO_2 loss reaction). The reactions in Fig. 2.3 are a) OH loss following H-abstraction from a carbon atom an -OOH group attached, b) hydrogen shift, followed by an O_2 reaction, during which a hydrogen is cleaved, c) CO loss after H-abstraction from an aldehydic carbon atom and d) an epoxide formation.

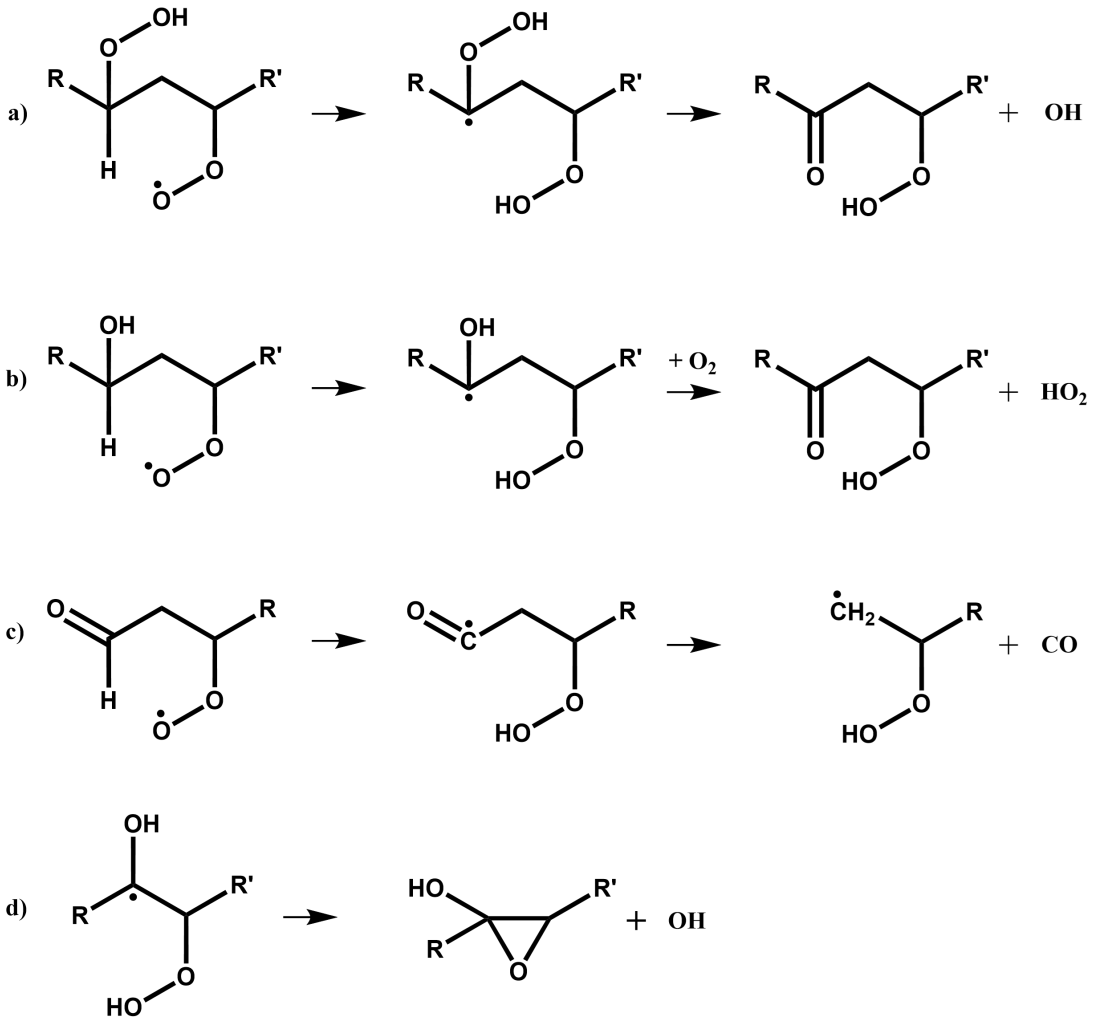

Figure 2.3: Common unimolecular fragmentation reactions of peroxy radicals.

The endoperoxidation reaction is also possible for some molecules with a suitable double bond functionality. This intramolecular reaction occurs when a radical center of RO_2 attacks the double bond, forming a cyclic structure called endoperoxide. The endoperoxidation reaction is explained later in the context of autoxidation of 1,5-

cyclooctadiene. Because of the similarity of cyclooctene to cyclohexene, the autoxidation mechanisms of cyclooctene and cyclohexene are likely similar. Figure 2.4, motivated by previous studies of Rissanen et. al.[34] and Berndt et. al.[37] as well as Hyttinen et. al.[38] presents likely follow-up reactions leading to the formation of HOM.

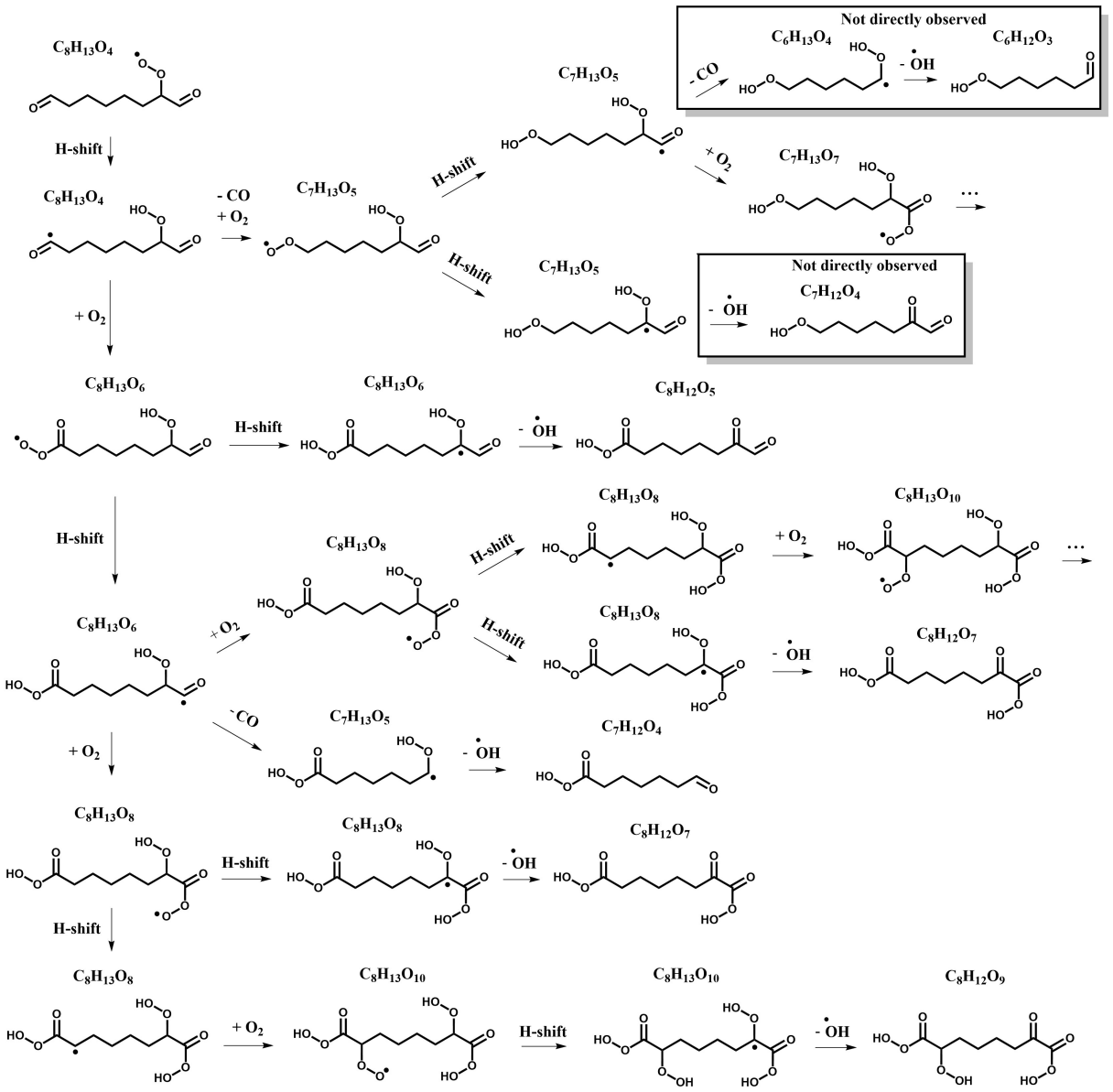

Figure 2.4: Reaction pathways leading to HOM formation starting from the $C_8H_{13}O_4$ radical formed in the ozonolysis of cyclooctene. This scheme is based on earlier studies by Rissanen et al.[34] and Berndt et. al.[37] as well as Hyttinen et. al.[38] Products $C_6H_{13}O_4$, $C_6H_{12}O_3$ and $C_7H_{12}O_4$ were not experimentally detected. Experimentally detected species are discussed in the results Section. The first H-shift could also be an 1,4 H-shift. Both 1,4 H-shift and 1,9 H-shift have unfavorable transition state geometries.

Rissanen et. al.[34] also presented computationally obtained rate coefficients for some of these reactions. The magnitudes of the rate coefficients they obtained for the O_2 addition (k_{O_2}) and the carbonyl elimination (k_{CO}) were in general: $k_{O_2} > k_{CO}$. Similar

magnitudes for the rate coefficients of these reactions are expected for cyclooctene (and also likely for 1,5-cyclooctadiene) as for cyclohexene.

The general trends for the H-shift rates of RO_2 in terms of substitute groups adjacent to the hydrogen being abstracted have been discussed previously.[12,39–41] The most favorable transition geometries are achieved for 1,5 - 1,7 H-shifts, leading to high H-shift rates. A crucial note from previous results of computational studies in the context of the reaction mechanism of 1,5-cyclooctadiene is that the rates of H-shifts of peroxy radicals are very dependent on the functional groups next to the hydrogen being abstracted. Autoxidation stands for autocatalytic oxidation, and the electron-withdrawing oxygen-containing substituents loosen the adjacent H-bonds. H-shifts for RO_2 with no adjacent oxygenated functional groups next to the abstracted hydrogen have the slowest rates. An allylic site can dramatically increase the H-shift rates of RO_2.[42] At least a partial explanation for this is the resonance stabilization of the alkyl radical by the double bond following the H-abstraction of the allylic H. For 1,5-cyclooctadiene, the extra double bond can potentially increase some H-shift rates very significantly for certain RO_2.

Although the autoxidation mechanisms of cyclooctene and 1,5-cyclooctadiene have similarities, there are some notable differences in the autoxidation mechanisms. The additional double bond of 1,5-cyclooctadiene allows for additional reaction pathways starting from the RO_2 radical formed in the ozonolysis. As discussed earlier, the double bond substituent next to the hydrogen being abstracted by H-shift reaction increases the rate of H-shift reaction. In addition to an alternative H-shift possibility for RO_2, there is a high probability of endoperoxide formation for 1,5-cyclooctadiene. In the endoperoxidation reaction, the radical center at the oxygen site attacks the other carbon of the double bond, forming a ring structure. An illustration of the branching point of RO_2 autoxidation formed of 1,5-cyclooctadiene is presented in Figure 2.5.

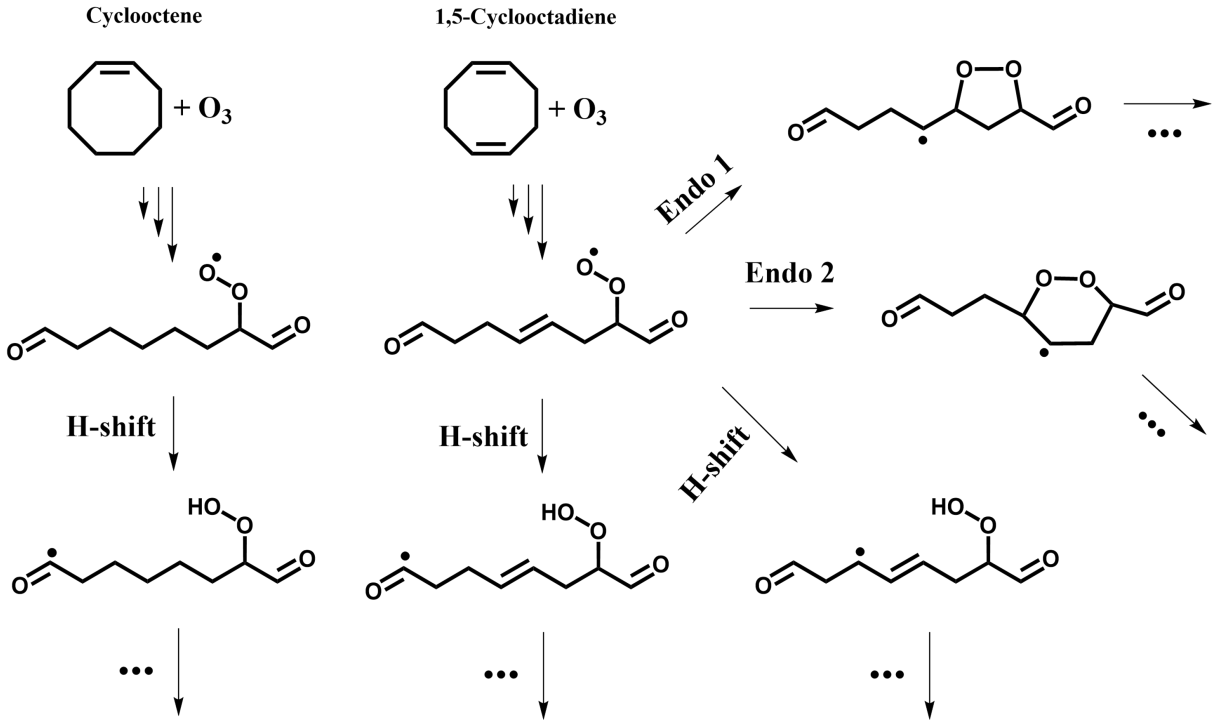

Figure 2.5: Competing reactions that the RO_2 can undergo after formation in ozonolysis of 1,5-cyclooctadiene. Of the two endo-cyclization reactions, Endo 1 is probably more likely because the double bond carbon is closer to the radical oxygen and the radical center is outside the formed ring structure after the reaction. The results obtained by Vereecken et. al. for the rates of endo cyclization reactions support this.[43]

The endoperoxidation frequently outruns common H-shift rates for some specific isomers of RO_2 formed from limonene and α/β-pinene,[42,44,45] which is why it is highly probable to occur in this case as well, and the formation of an endoperoxide is most likely another major reaction pathway of autoxidation of 1,5-cyclooctadiene.

2.1.4 Bimolecular RO_2 reactions

Bimolecular reactions involve two reactants, either two of the same reactants A, or two different reactants A and B. In a bimolecular reaction, these reactants collide, sometimes causing a reaction. The differential form rate law for a bimolecular reaction where A + B react, eq. 2.7:

$$\frac{d[A]}{dt} = \frac{d[B]}{dt} = -k[A][B] \tag{2.7}$$

If the initial reactant concentrations $[A]_0$ and $[B]_0$ are non-equal, the integrated form of the rate equation is:

$$\frac{1}{[B]_0 - [A]_0} ln \frac{[B][A]_0}{[A][B]_0} = kt \tag{2.8}$$

In the atmosphere, RO_2 radicals are relatively unreactive and react in significant amounts only with other RO_2, NO_x and HO_2 radicals.[12,46–48] These reactions can cause the autoxidation process to terminate or propagate. In propagation reactions, alkoxy radicals are formed. When NO_x and HO_2 are present, the reaction with these species is a significant sink of RO_2. The reactions between RO_2 with both NO and HO_2 have similar rate coefficients, in the order of 10^{-11}cm^{3}molecule^{-1}s^{-1}.[47,49] Typically [HO_2] is in the order of 10 pptv[12] in the atmosphere, and when [NO] is much higher than 10 pptv, it is expected to be the dominant bimolecular sink of RO_2. For acylperoxy radicals, the reaction with NO_2 can also be a very significant sink. The cross and self-reactions between RO_2 have widely varying rates, which are highly dependent on the structures of the reactants.

Cross- and self-reactions of RO_2 generally have slower rates than reactions with NO and HO_2. Because often HO_2 is more abundant than RO_2 under atmospheric conditions, self- and cross-reactions are not as relevant under atmospheric conditions as the reactions with HO_2 (and NO). However, for some RO_2, self- and cross-reactions are very fast, and even small yields of HOM can be atmospherically relevant. Furthermore, recent findings suggest that at low concentrations of NO (in the order of [NO] $<$ 82 pptv), NO can sometimes increase the HOM yields, contrary to previous assumptions, and does not completely inhibit the formation of HOM even at higher concentrations.[50] These low NO conditions are especially relevant to the present day in pristine areas and in the upper boundary layer. Low NO conditions are more probable in the future as NO concentrations are expected to decrease with better emission control. The most relevant bimolecular reactions in the context of this thesis are the cross- and self-reactions of RO_2. This is because the concentrations of NO_x and HO_2 are lower in the experiments of this thesis than under atmospheric conditions. Although there are more possibilities for reactions between RO_2 and HO_2, as explained by Bianchi et. al.,[12] only the most common termination reaction is considered here as presented in eq. 2.9.

$$RO_2 + HO_2 \rightarrow ROOH \tag{2.9}$$

A common tetroxide intermediate (ROOOOR') is formed in self and cross-reactions of RO_2 which decomposes into a complex of two alkoxy radicals (RO) and O_2, after which the alkoxy complex will react through one of three channels 2.10, 2.11 or 2.12.[51,52]

$$RO_2 + R'O_2 \xrightarrow{\text{ISC + recombination}} ROOR' + O_2 \tag{2.10}$$

$$RO_2 + R'O_2 \xrightarrow{\text{H-shift}} ROH + R'C{=}O + O_2 \tag{2.11}$$

$$RO_2 + R'O_2 \xrightarrow{\text{Dissociation}} RO + R'O + O_2 \tag{2.12}$$

Reaction channels 2.11 and 2.12 are terminations channels while 2.10 is a propagation channel. If one of the reactants is an acylperoxy radical (RC(O)OO•), the reactions are very fast.[53–55] The reaction channel 2.12 is the main source of the accretion products. The reaction channel 2.10 forms alkoxyl radicals, which can react in a H-shift reaction, and add more oxygen to form HOM with an odd number of oxygen. Closed-shell monomer HOM are formed mainly by the reaction channel 2.11. The yield of accretion products depends on the relative branching ratios of 2.10, 2.11 and 2.12. In the absence of other mechanisms, a higher branching ratio of 2.12 results in higher yields of the accretion products. In addition, a new channel producing ester products through β-scission of CH_2O has recently been found significant for α-pinene.[56]

2.2 Detection of HOM in the gas phase

Mass spectrometry, and more specifically Atmospheric Pressure interface Chemical Ionization Mass spectrometry (APi-CIMS) is the only method of detection of HOM. A very commonly used instrumental setup for HOM experiments has been the chemical ionization APi-TOF (CI-APi-TOF) setup with different chemical ionization reagents. In CIMS experiments, the most commonly used chemical ionization reagent for HOM studies is the nitrate ion (NO_3-). The nitrate was initially found to be selective for HOM with multiple hydrogen-bonding functional groups.[10] Other chemical ionization reagents that have been used are acetate ion, lactate, pyruvate, iodine and bromine on the negative polarity ionization mode, as well as protonated amines, such as ethylamine and n-propyl amine on the positive-polarity ionization mode.[11,57–59] There are some limitations to mass spectrometric methods, especially with the identification of the molecular structures and functional groups, as mass spectrometric methods provide only the molecular formulae of ions. Some complementary techniques have been developed to better allow the identification of molecules when using mass spectrometry, such as using D_2O mediated deuterium exchange.[34] Using deuterium exchange, one can identify some functional groups of molecules based on the easy switching of hydrogen atoms with deuterium. Labile acidic hydrogen can easily be exchanged and therefore if starting from a system containing purely C and H, then the number of exchangeable H equals the number of H-shifts (both RO and RO_2 mediated). Other ways to aid in the structural identification of molecules using MS-based methods are MS-MS fragmentation experiments, ion mobility spectrometry[60] (IMS) and the use of different chemical ionization reagents, which selectively bind to functional groups of HOM.

In addition to MS-based methods, spectroscopic and chromatographic methods have been proposed. Using spectroscopy or chromatography, one could very efficiently identify the structures and functional groups of HOM. The reason why these methods are not

used for the detection of HOM is that there are some fundamental problems with the use of these methods.[61] With spectroscopy-based methods, the main problem is that there is a very high amount of spectral overlap between functional groups of HOM. The largest problem with chromatographic methods is that the transfer limitations of the elution columns generally prevent the highly functionalized and polar HOM from passing through. In addition, many species of HOM are very reactive, which prevents them from going through the column unchanged. Finally, the very small concentration of HOM in experiments is a challenge for most detection methods.

2.2.1 Measuring the concentrations of HOM using nitrate CI-APi-TOF

In many measurement techniques, including mass spectrometry, the concentration of a compound can be determined by measuring the intensities of the signals of the compound at known concentrations and constructing a calibration curve. The problem with measuring the concentrations of HOM by using a calibration curve is that there are no commercially available standards for HOM. Sometimes, a reference compound can be used to determine the concentration of a compound if the actual compound cannot be used.

No accurate methods have been developed for the universal concentration determination of HOM. Sulfuric acid has been used as a calibration compound for the determination of HOM concentrations in past studies. To obtain the concentration of the HOM compound, sulfuric acid is photochemically produced at known concentrations and afterward the known concentration of sulfuric acid is compared to the signal of HOM.[62] The method relies on the assumption that the ionization efficiencies of HOM are similar to sulfuric acid. Sulfuric acid is detected at maximum intensity (collision-limited charging), and therefore determined HOM concentrations are lower bound limits of concentrations. This method has mainly been used with the CI-APi-TOF instrument, but it could be adapted to similar MS instruments using nitrate-based CIMS. The concentrations of HOM are determined using the ratio of HOM containing ions to reagent ions with a calibration coefficient C, equation 2.13:[63,64]

$$[\mathrm{HOM}] = C \times ln(1 + \frac{\sum \mathrm{HOM}(\mathrm{NO_3^-})}{\sum_{i=0}^{2}(\mathrm{HNO_3})_i(\mathrm{NO_3^-})}) \tag{2.13}$$

This simplifies to equation 2.14 under normal conditions where ∑reagent ions » ∑HOM-containing ions:

$$[\mathrm{HOM}] = C \times \frac{\sum \mathrm{HOM}(\mathrm{NO_3^-})}{\sum_{i=0}^{2}(\mathrm{HNO_3})_i(\mathrm{NO_3^-})} \tag{2.14}$$

Equation 2.14 describes the normalization of a detected ion peak, in which the signal

ion intensity is divided by the sum of the signal intensities of the ionization reagent cluster, in other words, the available charge. The concentration of HOM can then be obtained by multiplying the normalized signal intensity by the calibration coefficient C. Ideally, the calibration coefficient should be measured specifically for the instrument being used. The C values for sulfuric acid and NO_3 have usually been around 10^9 and 2×10^{10} molecules cm^{-3}. Using this method gives a crude estimate of the concentrations of HOM at best. The assumption that sulfuric acid is ionized/clustered with nitrate at similar efficiency as HOM is not exactly a very realistic assumption. It has been found that HOM cluster with nitrate at different efficiency, and the presence of hydroperoxide group (OOH) as a hydrogen bond donating group strengthens the charging.[65] It is safe to say that sulfuric acid does not cluster with nitrate at the same efficiency as all HOM.

In this thesis, the detected HOM signal intensities are normalized with respect to the ionization reagent signal intensities instead of determining the concentrations of individual HOM. The normalized intensity of a peak can be obtained from eq. 2.15, which is the equation 2.14 without the calibration coefficient C.

$$\mathrm{HOM_{NI}} = \frac{\sum \mathrm{HOM}(\mathrm{NO_3^-})}{\sum_{i=0}^{2}(\mathrm{HNO_3})_i(\mathrm{NO_3^-})} \tag{2.15}$$

2.3 Vapor pressure and volatility of organic compounds

The volatility of an organic compound is often described by the boiling point and saturation vapor pressure of the said compound. The high saturation vapor pressure and the low boiling point indicate high volatility of an organic compound. The IUPAC definition of saturation vapor pressure: "the pressure exerted by a pure substance (at a given temperature) in a system containing only the vapor and condensed phase (liquid or solid) of the substance".[66,67] At the saturation vapor pressure, the condensed and vapor phases are in thermodynamic equilibrium with each other. The definition of phase equilibrium includes the chemical equilibrium condition, thermal equilibrium condition and the mechanical equilibrium conditions, which means that there is no net molecular flux between the vapor and condensed phase, no temperature gradient and no net forces acting on the interface. The saturation vapor pressure depends strongly on the temperature and the molecular interactions in the condensed phase. The temperature dependence of vapor pressure p_i^0 of a substance i is described by the Clasius-Clapeyron equation:

$$\frac{dp_i^0}{dT} = \frac{\Delta H_{trs,i}}{T\Delta v_{m,i}} \tag{2.16}$$

In which T is the temperature, $\Delta H_{trs,i}$ is the molar enthalpy change upon vaporization, and $\Delta v_{m,i}$ is the molar volume change upon sublimation. The vapor pressure of

a substance can be estimated using the Antoine equation, which is derived from the Clasius-Clapeyron equation. The Antoine equation is presented in 2.17:

$$log_{10}P = A - \frac{B}{T - C} \tag{2.17}$$

In which A, B and C are experimentally determined coefficients, T is the temperature and P is the vapor pressure of a compound. The concentration of a compound in the gas phase is the vapor pressure of the compound divided by the total pressure of the gas. In a flow reactor, the reactant concentration c can be calculated with equation 2.18:

$$c = \frac{v_s}{v_{tot}} \times \frac{p_{vap}}{p_{tot}} \tag{2.18}$$

In which v_s is the gas flow of the sample, v_{tot} is the total total gas flow, p_{vap} is the vapor pressure of the reactant and p_{tot} is the total pressure.

3. Experimental

The experiments of this thesis were performed at the Molecular Sciences unit in the Radical Aerosol Physical Chemistry (RAPC) lab at the University of Helsinki (A.I. Virtasen aukio 1 (Chemicum), PL 55, 00014, University of Helsinki, Finland). This Section presents the instruments, conditions of the experiments, and the methodology of the measurements and data analysis.

3.1 Instrumental setup

Chemical ionization mass spectrometry (CIMS) was used for the experimental measurements of this thesis. Chemical ionization mass spectrometry uses suitable ionization reagents to ionize the analyte molecules by forming adduct ions, proton abstraction or addition, or charge exchange reactions. The ionization reagents used in this work were NO_3- and protonated ethylenediamine (EDA, $C_2H_9N_2$+). In the CI inlet, the reagent ion precursor is ionized by x-rays. When nitric acid is used, x-ray ionization forms nitrate ions (NO_3-), nitric acid-nitrate-"dimers" (HNO_3NO_3-), and nitric acid-nitrate-"trimers" ($(HNO_3)_2NO_3$-). Ethylenediamine forms clusters in a similar way as the nitrate ion, forming "dimer" and "trimer" clusters. Ethylenediamine has not been used before as a chemical ionization reagent in the purpose of ionization of HOM, which is why the function of this ionization reagent in this purpose is not thoroughly known. It is known that ammonia and its derivatives as chemical ionization reagents are more crude in the ionization process, possibly causing fragmentation of the analyte molecules in the ionization process.[68] The NH_4+ has a small mass to charge ratio, and suffers from poor transmission in Orbi-CIMS. This affects the reliability of the final normalized signal. This is why reagent ions with a higher mass to charge ratio such as EDA are preferred. Nitrate ions can ionize the analyte molecules by proton abstraction reaction, described by Equation 3.1, or with the clustering reactions.

$$NO_3^- + HX \rightleftharpoons HNO_3 + X^- \tag{3.1}$$

In the clustering reactions, clusters are formed through collisions with the sample molecule and nitrate ions (Equation 3.2), with nitric acid-nitrate-dimers (Equation 3.3) and with

nitric acid-nitrate-trimers (Equation 3.4).

$$NO_3^- + X \rightleftharpoons NO_3 \bullet X^- \tag{3.2}$$

$$HNO_3NO_3^- + X \rightleftharpoons HNO_3NO_3^- \bullet X \rightleftharpoons HNO_3 + NO_3 \bullet X^- \tag{3.3}$$

$$(HNO_3)_2NO_3^- + X \rightleftharpoons (HNO_3)_2NO_3^- \bullet X \rightleftharpoons 2\ HNO_3 + NO_3 \bullet X^- \tag{3.4}$$

The chemical ionization process occurs in a device called the chemical ionization inlet. In the instrumental setup used in these experiments, the Multi-scheme chemical IONization inlet (MION) was used, which is presented shortly in the next Section.

3.1.1 Multi-scheme chemical IONization inlet

The Multi-scheme chemical IONization inlet (MION), developed by Karsa Ltd, Helsinki, Finland, allows for fast switching of chemical ionization mode for MS. Using the MION inlet for the detection of HOM can be highly advantageous, because there often is a large range of different HOM formed in the autoxidation process, all of which cannot easily be detected by a single ionization reagent, like the most frequently used NO_3- ion. The less oxidized products in particular are not as easily detected with NO_3-. The original MION has been specified in depth by Rissanen et. al.[69] The upgraded MION2 inlet was used in this thesis, which has been described by He et. al.[70] The MION2 has improvements, such as an additional purge flow to prevent the sample flow from entering the ion source and to prevent the neutral reagent ion precursor from perturbing the gas sample. In the MION2, sample contamination, and the water vapor oxidizing the electrodes are more efficiently prevented, and increased stability of the instrument is achieved. Only a short description of the MION2 is given here.

A schematic Figure of the MION2 is presented in Figure 3.1, taken from He et. al.[70] The inlet consists of a electrically grounded inlet 24 mm i.d flow tube, with multiple ion sources. The reagent precursor is fed into the system with N_2 or air by flowing it through a saturator, or directly flowing the precursor from a gas cylinder. The reagents are then directed to their respective x-ray sources and ionized with soft x-rays (Hamamatsu L12535). After ionized, the reagent ion flows are accelerated and focused through the 5 mm orifices into the laminar sample flow by electric fields.

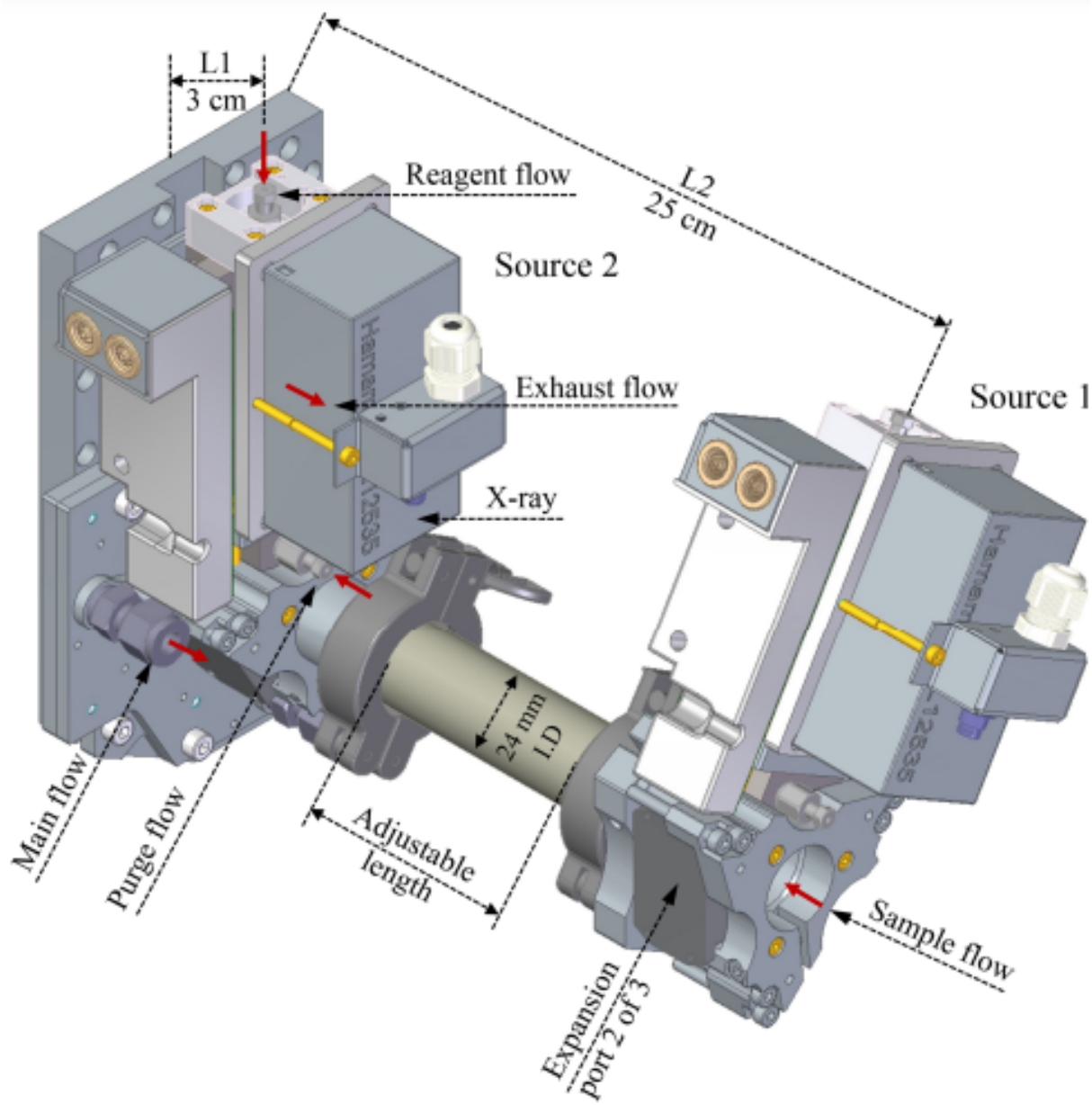

Figure 3.1: A schematic Figure of the MION2 inlet. In the inlet used in this thesis, the ion sources were positioned in the same plane, instead of being separately positioned as in this figure.

3.1.2 Flow reactor

A gas flow reactor system was connected to the mass spectrometer. The gas flows were controlled by Alicat Scientific mass flow controllers. A schematic figure of the flow reactor setup is presented in Figure 3.2. Two different volume quartz flow tube reactors were used. The larger reactor tube had an internal diameter of $\sim$ 6 cm and $\sim$ 1 meter in length. The volume of the larger reactor was 1900 sccm, while the volume of the smaller reactor was 120 sccm. In addition to the high resolution achieved by the Orbitrap mass analyzer, an additional benefit of using Orbitrap is that the fast switching of ionization

polarity is achieved when combined with the MION(2),[69,70] which was utilized in these experiments. The precursor was delivered to the reactor by bubbling N_2 gas through the liquid precursor at room temperature. The vapor pressures in 25 °C for cyclooctene and 1,5-cyclooctadiene are 864 Pa and 732 Pa respectively, calculated with the Antoine equation.[71] The reactant was allowed to react in the presence of O_3 and O_2 in the quartz reactor tube. Ozone was generated by flowing synthetic air through an ozone generator fitted with an UV lamp (UVP Ozone Generator, Analytik Jena US). The production of ozone occurs by the photolysis of oxygen which produces oxygen radicals. The oxygen radicals react with O_2 to produce O_3. The reaction time was regulated by changing the inlet flow through the reactor. The change in the inlet flow likely alters the amount of wall reactions occurring during the experiments, but the effect has previously been observed to be minor. The volumetric flow rates in the reactor were measured with a TSI 5200 model flow meter. The reaction time in the reactor was calculated by dividing the inlet flow (volumetric flow) by the reactor volume.

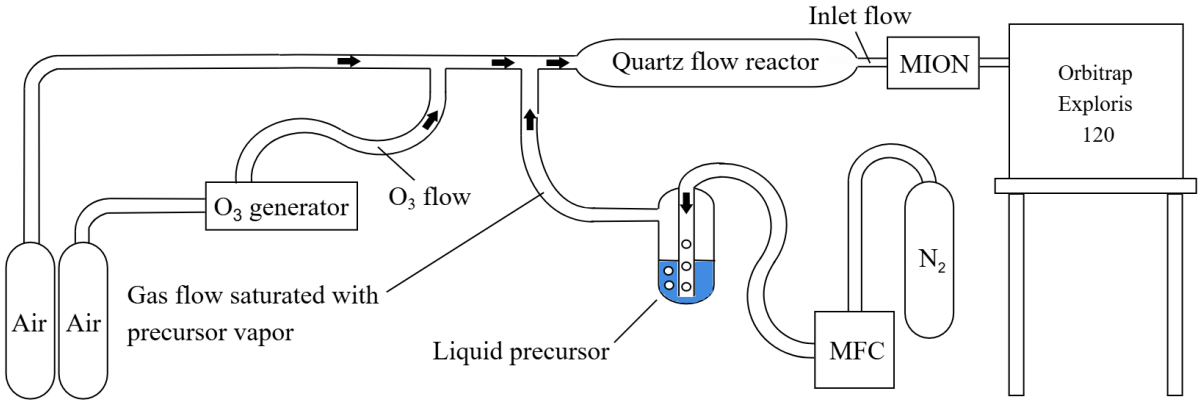

Figure 3.2: An illustration of the flow reactor setup connected to the Orbitrap Exploris 120 via the MION2 inlet (MFC = mass flow controller).

3.2 Orbitrap Exploris 120

A Thermo Fisher Scientific Orbitrap Exploris 120 mass spectrometer was used for the detection of the product ions. The Orbitrap Exploris 120 is presented in Figure 3.3, from Denisov et. al.[72] In the experimental setup used in this instance, the electrospray ion source is replaced by the MION2 chemical ionization inlet, which allows for fast switching of chemical ionization reagents with either negative or positive-polarity. Recently, Orbitrap mass spectrometers have evolved a lot, and the recent instruments have very high resolution. Orbitrap Exploris has a maximum resolution of 120000 at M/Z 200.

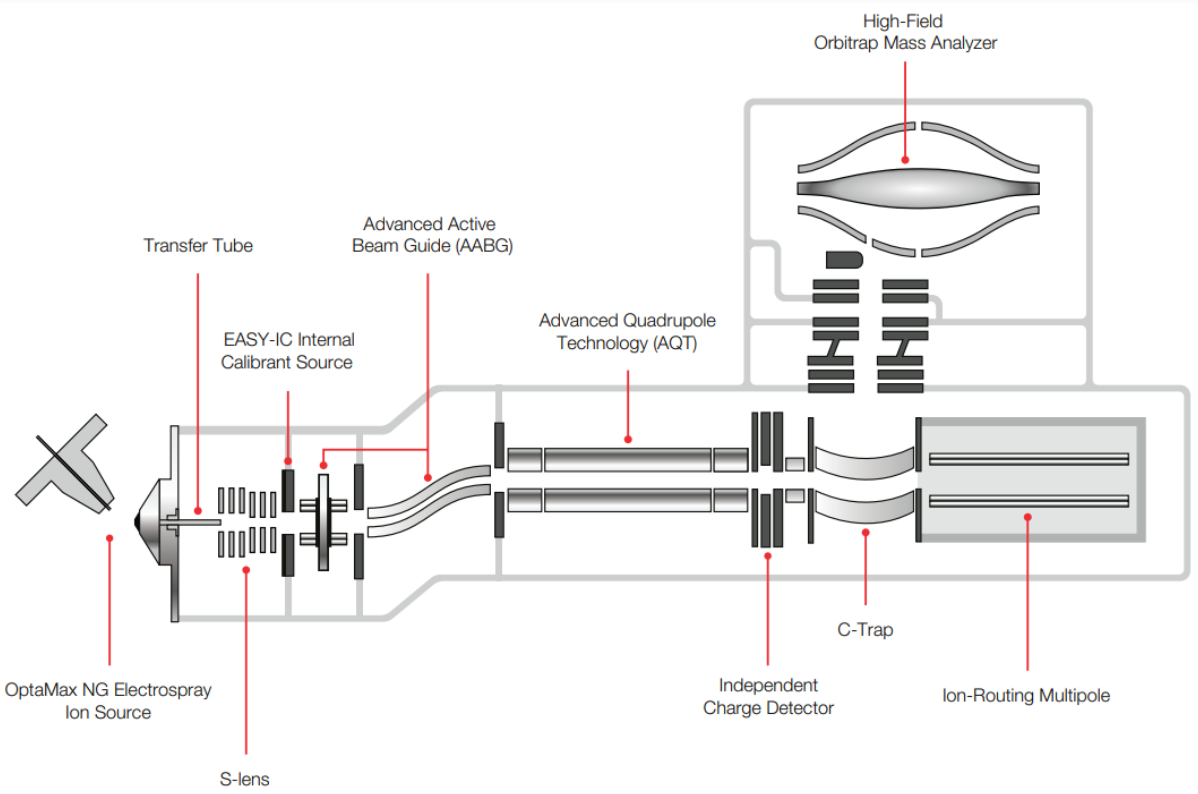

Figure 3.3: Schematic of the Orbitrap Exploris 120. Instead of the electrospray ionization, chemical ionization was used. As the ions enter the mass spectrometer, they are first directed through the Stacked-ring ion guide (S-lens), a type of ion lens which focuses the ions into a tight beam. The Advanced Active Beam Guide (AABG) further refines the incoming beam of ions. After passing the AABG, the beam of ions enters a quadrupole, which is the final filtering element before the ions reach the C-trap and the Orbitrap. The atmospheric pressure interface requires a very efficient pressure reducing system. The pumping system of Orbitrap Exploris 120 consists of a six-stage TurboVac HexaInlet turbomolecular pump and a single-stage rotary vane pump Sogevac SV65BI (both from Leybold GmbH, Cologne, Germany).[73]

3.2.1 Orbitrap mass analyzer

The orbitrap mass analyzer is a spindle-shaped ion trap, consisting of outer and inner electrodes. The orbitrap uses orbital trapping in an electrostatic potential distribution, equation 3.5, as described by Makarov:[74]

$$U(r,z) = \frac{k}{2}(z^2 - \frac{r^2}{2}) + \frac{k}{2}(R_m)^2 ln(\frac{r}{R_m}) + C \tag{3.5}$$

Where r and z are cylindrical coordinates, with (z_0) being the plane of the symmetry, C is a constant, k is field curvature and R_m is the characteristic radius. Initially, the ions are guided towards the C-trap through ion lenses and a quadrupole. The C-trap can be described as a bent quadrupole ion trap. A Figure of the orbitrap mass analyzer and the C-trap is presented in Figure 3.4. The ions are first trapped in the C-trap, and cooled with gas leaking in from the internal routing multipole (IRM). The ions are released from

the C-trap in packets to the orbitrap mass analyzer, by increasing voltage. The voltage applied between the inner and outer electrodes of the orbitrap causes the ions to begin oscillating around the orbitrap central electrode, which induces a current detected by split electrodes and amplified by a differential amplifier. The mass to charge ratio of a ion determines at which frequency the ion oscillates around the inner orbitrap electrode.

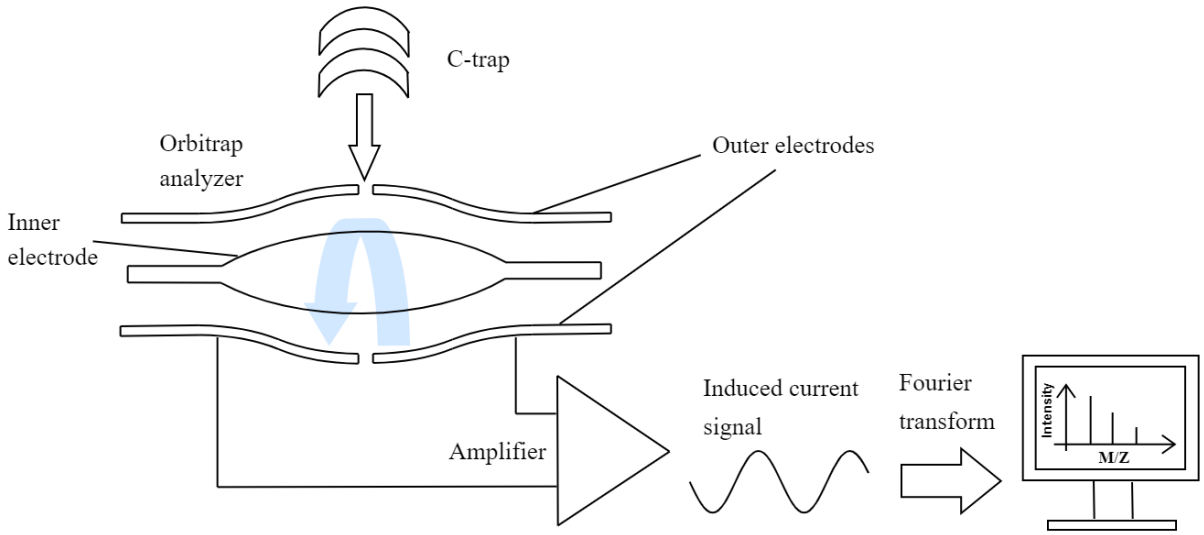

Figure 3.4: The C-trap and the orbitrap mass analyzer.

The frequency of oscillation is described mathematically the equations of motion of the ions, which are obtained from equation 3.5. The equations of motion and the solution to the axial component of motion are presented below.[74] The equations of motion in polar coordinates (r, φ, z) for ions with mass-to-charge ratio m/q, equations 3.6:

$$\begin{aligned} (a) \quad & \ddot{r} - r\dot{\varphi}^2 = -\frac{q}{m}\frac{k}{2}[\frac{(R_m)^2}{r} - r] \\ (b) \quad & \frac{d}{dt}(r^2)\dot{\varphi} = 0 \\ (c) \quad & \ddot{z} = -\frac{q}{m}kz \end{aligned} \tag{3.6}$$

With initial conditions at t = 0, eq. 3.7:

$$\begin{aligned} r(0) = r_0 \quad & \dot{r}(0) = \dot{r}_0 \\ \varphi(0) = \varphi_0 \quad & \dot{\varphi}(0) = \dot{\varphi}_0 \\ z(0) = z_0 \quad & \dot{z}(0) = \dot{z}_0 \end{aligned} \tag{3.7}$$

The motion in polar plane (r, φ) is independent of motion in axial plane z. Also, φ could be excluded from 3.6 (a) using 3.6 (b). Therefore it is useful to express the energies in

separate directions, eq. 3.8:

$$\begin{aligned} (r) \quad & qE_r = (m/2)(\dot{r}_0)^2 \\ (\varphi) \quad & qE_\varphi = (m/2)(r_0\dot{\varphi}_0)^2 \\ (z) \quad & qE_z = (m/2)(\dot{z}_0)^2 \end{aligned} \tag{3.8}$$

In the axial direction z, the equation of motion is described by a simple harmonic oscillator, and the solution is:

$$z(t) = z_0 cos(\omega t) + \sqrt{(2E_z/k)} sin(\omega t) \tag{3.9}$$

In which:

$$\omega = \sqrt{(q/m)k} \tag{3.10}$$

In equation 3.10, ω is the frequency of axial oscillations. This frequency is used for the detection of ions, as it is independent of the energy and the position of ions. As one can see, the equation describing the frequency of axial oscillation contains the familiar mass to charge ratio M/Z (m/q) of detected ions. The solutions for the equations of motion in the other planes (r, φ) give conditions for stable oscillation, and are not further discussed here. The signal voltage induced by ion oscillations to the split outer electrodes and amplified by the differential amplifier may be obtained using Green's reciprocity theorem. Fourier transform is used to convert the induced current from the time dimension to the frequency dimension, and ultimately to the mass to charge ratios of ions. Enhanced Fourier transform (eFT) algorithm is used in the Orbitrap Exploris instruments.

3.3 Data analysis and peak identification

The raw data was processed using the Orbitool program,[75] and the identification of the peaks in the mass spectra were done using Orbitool and Thermo Fisher Scientific -Freestyle software. Orbitool was used for the averaging of the data by the number of spectra (10). The Orbitrap exploris 120 uses fluoranthene as an internal calibrant, a special design of the instrument. The mass calibration of the spectra was not done in the Orbitool, because of an internal mass calibrant used in the Orbitrap Exploris 120 instrument, although with calibration a higher mass accuracy could have been achieved. After the raw data is processed with orbitool, custom Python programs, modified from the initially written codes by Netta Vinkvist, were used to sort the data further, normalize the intensity of detected peaks relative to the ionization reagent signal, and sort the data. The final mass spectra and time series were produced with the Origin program by OriginLab Corporation. The amount of data obtained in the measurements was very large, which is why Python was required for further data processing. For instance, one measurement which was 1

hour 30 minutes long resulted in $\sim$ 800 spectra, even after data averaging. The Python codes are presented in appendix E.

To identify which peaks were formed from the precursor by oxidation, background was measured without the precursor at the start of each measurement to see if the signal was present before the precursor was added to the reactor. The identification of compounds was done using the mass calculator of the Freestyle program, and the accurate mass of molecular formulae suggested by Freestyle were calculated using Orbitool. The mass difference between the peak and the calculated mass was compared to the measured and calculated mass of the chemical ionization reagent NO_3-, to verify if an offset was present or not.

3.4 Measurement conditions

The ozonolysis-initiated autoxidation products of cyclooctene and 1,5-cyclooctadiene were measured with the orbitrap mass spectrometer with negative or positive chemical ionization scheme under varying concentrations and reaction times. The chemical ionization reagent ions were NO_3- for the negative polarity ionization and $C_2H_9N_2$+ for the positive-polarity ionization experiments. The inlet flows were 10 - 25 l per minute, which means that the reaction time in the reactor when using cyclooctene or 1,5-cyclooctadiene as the precursor were between 0.33-10.75 s. All experiments were done in room temperature and atmospheric pressure. The O_3 concentrations were measured at constant O_3 flow rates with a commercial Model 205 Dual Beam Ozone Monitor by 2B technologies.

In the higher reaction time experiments, the concentration of the precursor was decreased over time, whereas with the lower reaction time experiments the precursor concentration was increased during the measurement. Because of wall adsorption reactions, it is better to increase the concentration during the measurement as opposed to decreasing the concentration starting from higher concentrations. This is because the precursor is absorbed to the reactor walls when using a high precursor concentration. The precursor is then released from the walls after decreasing the concentration in the gas phase, causing a higher precursor concentration than desired. The reason that the concentration was decreased during the measurement in the higher reaction time measurements is that the reactor volume is so large that the measurement would have taken too long. This is discussed more in depth in the error sources Section in the next chapter. The experimental conditions used for individual measurements are presented in Table 3.1.

Table 3.1: Conditions of the experiments. The volumetric flow rates are given in square cubic centrimeters per minute (sccm).

Precursor	Precursor flow	Inlet flow	O_3	Tube volume	Reaction time	Ionization reagent
	[*sccm*]	[*sccm*]	[ppb]	[*sccm*]	[*s*]	
Cyclooctene	0.1, 0.5, 1, 5, 10	21650	37	120	0.33	NO_3-
Cyclooctene	0.1, 0.5, 1, 5, 10	21650	37	120	0.33	EDA(H+)
Cyclooctene	0.1, 0.5, 1, 5, 10	12210	66	120	0.59	NO_3-
Cyclooctene	0.1, 0.5, 1, 5, 10	12210	66	120	0.59	EDA(H+)
Cyclooctene	0.1, 0.5, 1, 5, 10	20800	42	1900	5.48	NO_3-
Cyclooctene	0.1, 0.5, 1, 5, 10	10600	82	1900	10.75	NO_3-
1,5-Cyclooctadiene	0.1, 0.5, 1, 5, 10	21550	38	120	0.33	EDA(H+)
1,5-Cyclooctadiene	0.1, 0.5, 1, 5, 10	20700	41	120	0.35	NO_3-
1,5-Cyclooctadiene	0.1, 0.5, 1, 5, 10	11460	72	120	0.63	NO_3-
1,5-Cyclooctadiene	0.1, 0.5, 1, 5, 10	11460	72	120	0.63	EDA(H+)
1,5-Cyclooctadiene	0.1, 0.5, 1, 4.5, 9, 18	21550	40	1900	5.29	NO_3-
1,5-Cyclooctadiene	0.1, 0.5, 1, 4.5, 9, 18	10650	80	1900	10.70	NO_3-

4. Results

The results are presented in this chapter, mainly as mass spectra and time series of the measurement data. In the mass spectra presented hereafter, all products were measured as adducts of the chemical ionization reagent ions (NO_3- or $C_2H_9N_2$+). The molecular formulae of the chemical ionization reagents are left out of the molecular formulae of the products for the sake of clarity, but the mass to charge (M/Z) ratios include the chemical ionization reagent. The data is first presented in two Sections, one for both cyclooctene and 1,5-cyclooctadiene, and in the third Section, the results are discussed in more detail, and the results obtained using both precursors are compared. Finally, sources of error are briefly discussed. In all of the mass spectra and time series presented in this thesis, signal intensities were normalized with respect to the reagent ion intensities using equation 2.15, and therefore normalized signal intensities therefore usually appear in the scale of <1. During data analysis, an attempt was made to avoid the C^{13} isotope peaks, which is why peaks without a sufficiently high intensity, and which appear after major peaks, are usually not labeled in the mass spectra or included in the time series. Some of the identified products are likely isotopes, because the C^{13} isotope had an overlapping molecular weight as the proposed species, although the calculated mass of the proposed species fit with the experimental peaks. For example, the peaks that were $\sim$ 1 M/Z higher and with an intensity of $\sim$ 1/10, and were non accretion product peaks are likely isomers, because of the natural abundance of C^{13}, which is $\sim$1%. An 8 carbon molecule has a C^{13} peak of $\sim$ 8% intensity of the main peak at M/Z + 1. For the accretion products, the C^{13} isomer peaks appear at higher intensity because of higher amount of carbon.

4.1 Cyclooctene as the precursor

The molecular formulae of the most abundant species detected in the cyclooctene experiments using negative polarity ionization are shown in Table 4.1, along with the signal intensities at different reaction time measurements. All of the proposed molecular formulae for detected ions in the cyclooctene experiments using negative-polarity ionization at the highest and lowest reaction times are tabulated in the Appendix, if one is curious about some unlabeled peaks in the mass spectra presented in the following.

Table 4.1: Major HOM detected using cyclooctene at varying reaction times. All peaks are clusters of NO_3-, and the experimental mass-to-charge ratios (M/Z) include NO_3-. Monomer and accretion product relative intensities are given for the high concentration of precursor, and the radical signal intensities are given at low concentration of precursor. (Except for the m/z 225 radical, which had a medium intensity at high concentration and low intensity at low concentration.) The relative intensities were obtained as comparison to the highest signal intensity HOM: High = >20%, Medium = 10%-20%, Low = <10%. The measurements were also carried out at a reaction time of 5.48 s, although the relative intensities are not included here.

Molecular formula	M/Z ratio	Int. at 0.33 s	Int. at 0.59 s	Int. at 10.75 s	Molecular formula	M/Z ratio	Int. at 0.33 s	Int. at 0.59 s	Int. at 10.75 s
Monomers/ Radicals					Accretion products				
$C_6H_{11}O_5$	225.0495	-	Low	Medium	$C_{16}H_{28}O_5$	362.1831	-	Low	Low
$C_8H_{13}O_4$	235.0703	Low	Low	Low	$C_{16}H_{28}O_6$	378.1779	-	Low	Low
$C_8H_{14}O_4$	236.0799	Low	Low	Low	$C_{16}H_{28}O_7$	394.1729	-	Low	High
$C_8H_{12}O_5$	250.0574	Low	Low	Low	$C_{16}H_{26}O_8$	408.1522	-	Low	Medium
$C_8H_{14}O_5$	252.0730	Low	Low	Low	$C_{15}H_{26}O_9$	412.1472	-	Low	Medium
$C_7H_{11}O_6$	253.0446	-	-	Low	$C_{16}H_{28}O_9$	426.1629	-	Low	High
$C_7H_{12}O_6$	254.0526	-	Low	Low	$C_{16}H_{26}O_{10}$	440.1422	-	Low	High
$C_7H_{13}O_6$	255.0606	-	Low	Low	$C_{16}H_{26}O_{10}$	442.1584	-	-	Medium
$C_7H_{14}O_6$	256.0682	-	-	Low	$C_{16}H_{26}O_{11}$	456.1371	-	-	Medium
$C_8H_{13}O_6$	267.0619	High	Medium	Low	$C_{16}H_{26}O_{11}$	458.1536	-	-	Low
$C_8H_{12}O_7$	282.0494	Low	Medium	High	$C_{15}H_{26}O_{12}$	460.1320	-	-	Low
$C_8H_{13}O_7$	283.0567	Low	Low	Low	$C_{16}H_{26}O_{12}$	472.1320	-	Low	Medium
$C_8H_{14}O_7$	284.0646	Low	Medium	High	$C_{16}H_{26}O_{13}$	488.1268	-	-	Low
$C_8H_{12}O_8$	298.0423	-	Low	Medium	$C_{16}H_{26}O_{14}$	504.1219	-	-	Low
$C_8H_{13}O_8$	299.0503	High	High	High	$C_{16}H_{26}O_{15}$	520.1168	-	-	Low
$C_8H_{14}O_8$	300.0579	Low	Low	Medium	$C_{16}H_{26}O_{16}$	536.1118	-	-	Low
$C_8H_{12}O_9$	314.0372	-	Low	High					
$C_8H_{13}O_9$	315.0453	Low	Low	Low					
$C_8H_{14}O_9$	316.0528	-	Low	Medium					
$C_8H_{12}O_{10}$	330.0324	-	-	Low					
$C_8H_{13}O_{10}$	331.0401	Low	Low	Low					
$C_8H_{14}O_{10}$	332.0479	-	Low	Low					
$C_8H_{12}O_{11}$	346.0254	-	-	Low					

4.1.1 Long reaction time

In the experiments done with the large reactor, there was a rich variety of oxidation products in the reactor with the largest concentrations used, as expected. The long reaction time allows for the autoxidation reaction to proceed for a longer time, also allowing bimolecular reactions to occur, which results in a large amount of different HOM formed. Mass spectra at a reaction time of 5.48 s for the largest and the smallest reactant concentration are presented in Figures 4.1 and 4.2 respectively. The O_3 concentrations were 82 and 42 ppb for the 10.75 s and 5.48 s reaction time measurements respectively.

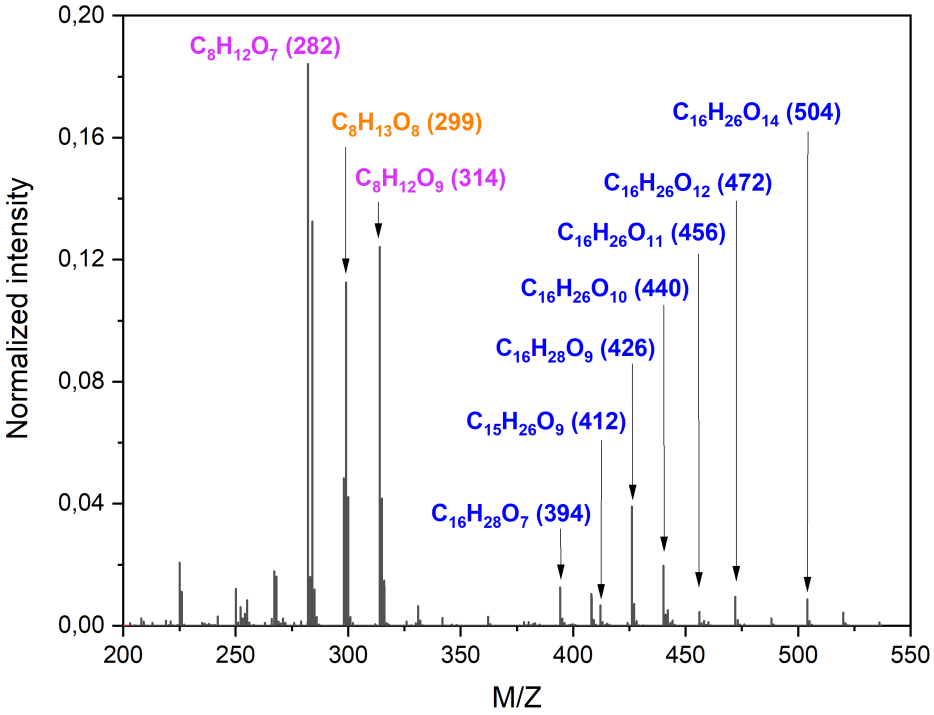

Figure 4.1: Negative mode chemical ionization mass spectrum of ozonolysis-initiated autoxidation products measured at a high concentration of cyclooctene (4.1 ppm) and a reaction time of 5.48 s. Colors of the molecular formulae are: purple = closed-shell monomer, orange = radical, blue = accretion product.

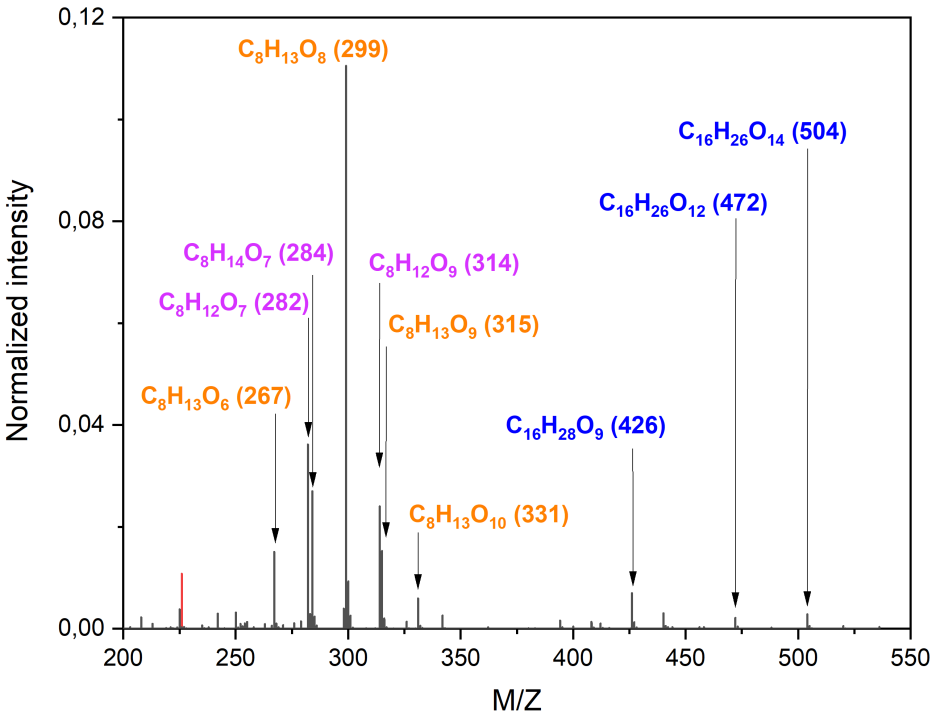

Figure 4.2: Negative mode chemical ionization mass spectrum of ozonolysis-initiated autoxidation products measured using cyclooctene. A reaction time of 5.48 s and a low concentration of cyclooctene (0.041 ppm) were used. Colors of the molecular formulae are: purple = closed-shell monomer, orange = radical, blue = accretion product. Red peaks indicate background peaks.

Corresponding high and low concentration mass spectra for the longest reaction time used, 10.75 s are shown in Figures 4.3 and 4.4. Molecular formulae of most of the high intensity peaks are marked in the mass spectra. Red peaks in the spectra are background peaks. There is a larger amount of HOM found at the higher reaction time of 10.75 than at a reaction time of 5.48 s, due to the increased time available for reactions. The increased product formation at the higher reaction times can be seen when comparing the intensity scale of Figures 4.3 and 4.1. At lower concentrations, the radical species (with odd mass number, orange color) are more abundant, while at the higher concentrations the closed-shell species (purple color) and the accretion products (blue color) are more abundant.

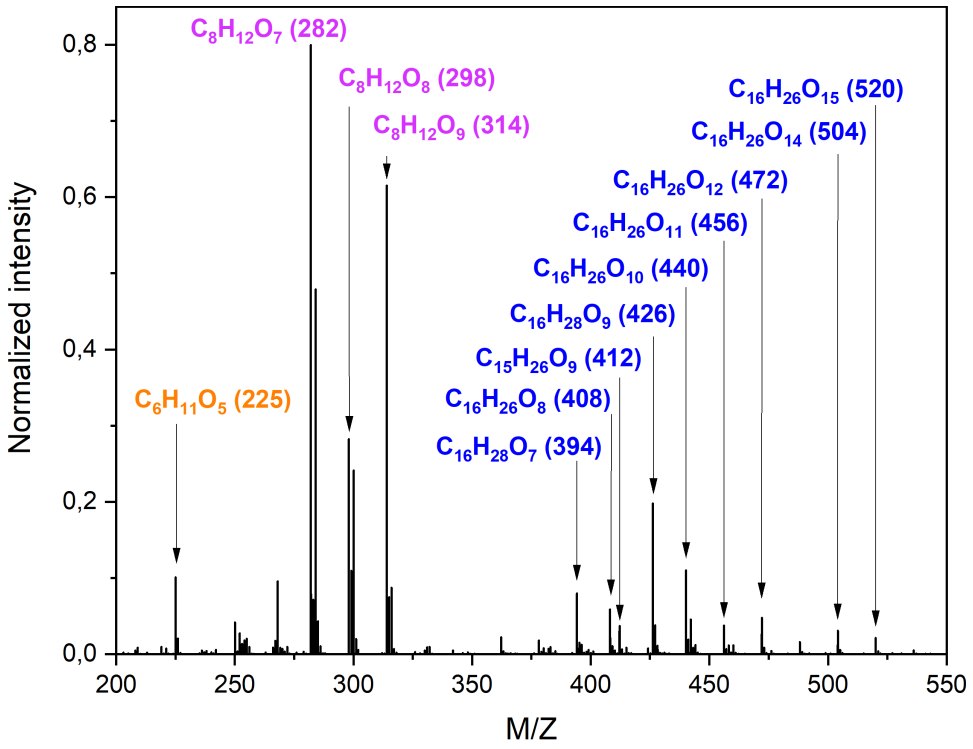

Figure 4.3: A chemical ionization mass spectrum of ozonolysis-initiated autoxidation products measured using cyclooctene as the precursor and NO_3- as the reagent ion. A reaction time of 10.75 s and a low concentration of cyclooctene (4.02 ppm) were used. The colors of the molecular formulae are the following: purple = closed-shell monomer, orange = radical, blue = accretion product. Red peaks indicate background peaks.

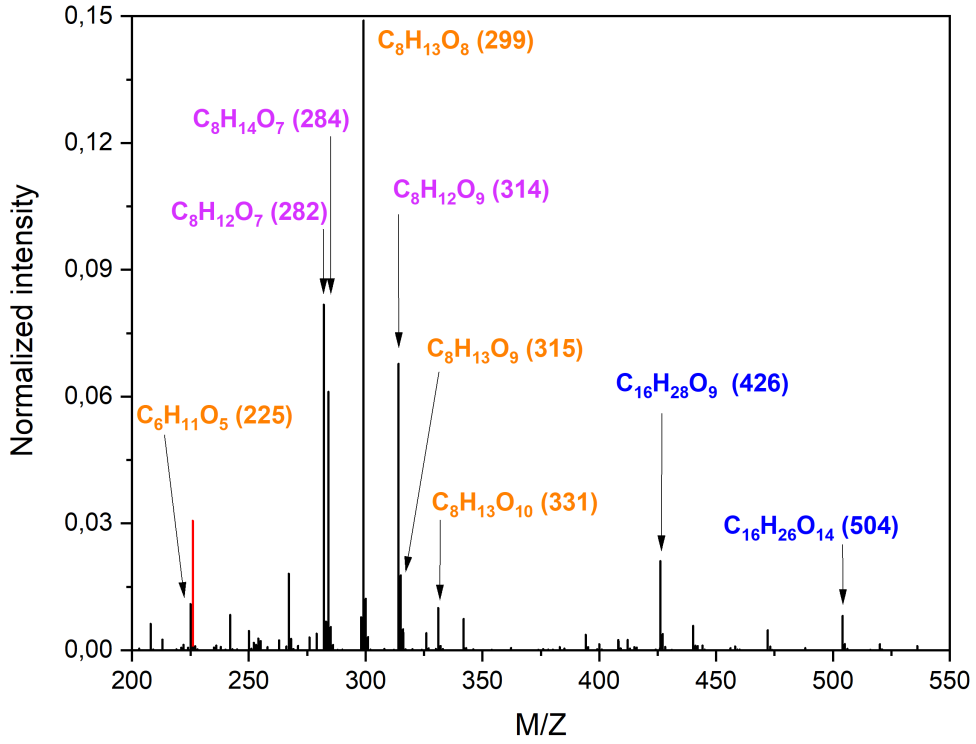

Figure 4.4: A chemical ionization mass spectrum of ozonolysis-initiated autoxidation products measured using a low concentration of cyclooctene (0.0805 ppm) and a reaction time of 10.75 s. The colors of the molecular formulae are the following: purple = closed-shell monomer, orange = radical, blue = accretion product. Red peaks indicate background peaks.

The abundance of closed-shell species and accretion products increases at higher precursor concentrations. At lower precursor concentration there are relatively more radical species because there are less species which radicals can react with, and less time for collisions. A time series including some of the most abundant product ions found is presented in Figure 4.5. Another time series including closed-shell species, radicals and accretion products in a reaction time of 10.75 s is presented in Figure 4.6. Higher relative abundance of radicals at lower precursor concentrations is visible in Figure 4.5 when looking at radical $C_8H_{13}O_8$ (M/Z 299), which is the highest abundance species at lower precursor concentrations. This radical stays at almost constant intensity at all concentrations of precursor.

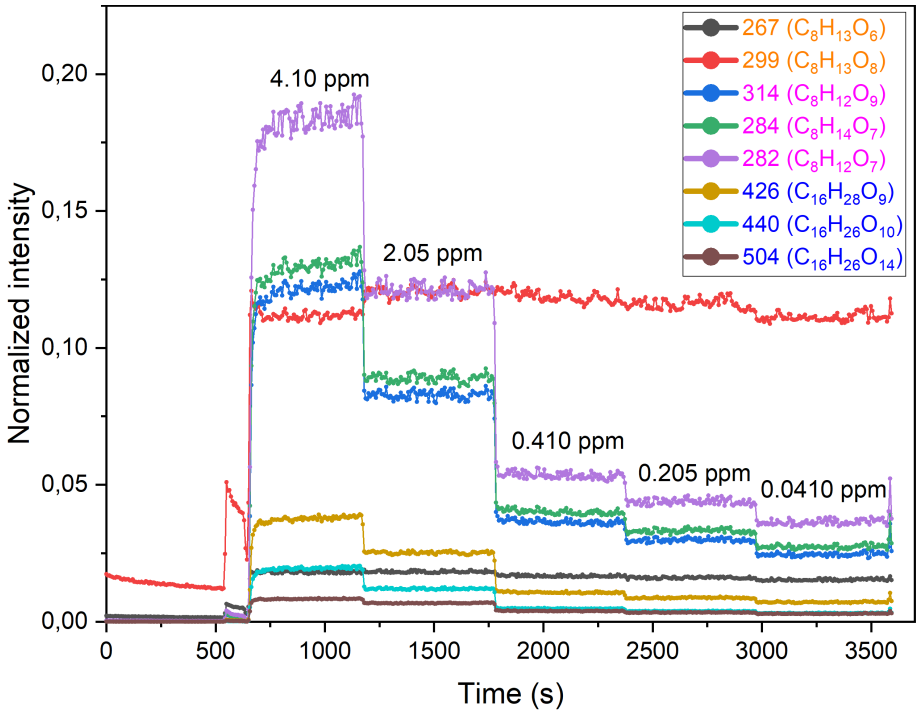

Figure 4.5: A time series of the normalized signal intensities of the most abundant radicals (orange color), closed-shell species (purple color) and accretion product (blue color) of ozonolysis-initiated autoxidation products using a reaction time of 5.48 s and measured as adducts of NO_3-. The M/Z includes NO_3-, but NO_3- is left out of molecular formulae for clarity. The concentration of cyclooctene during the measurement is written on the Figure.

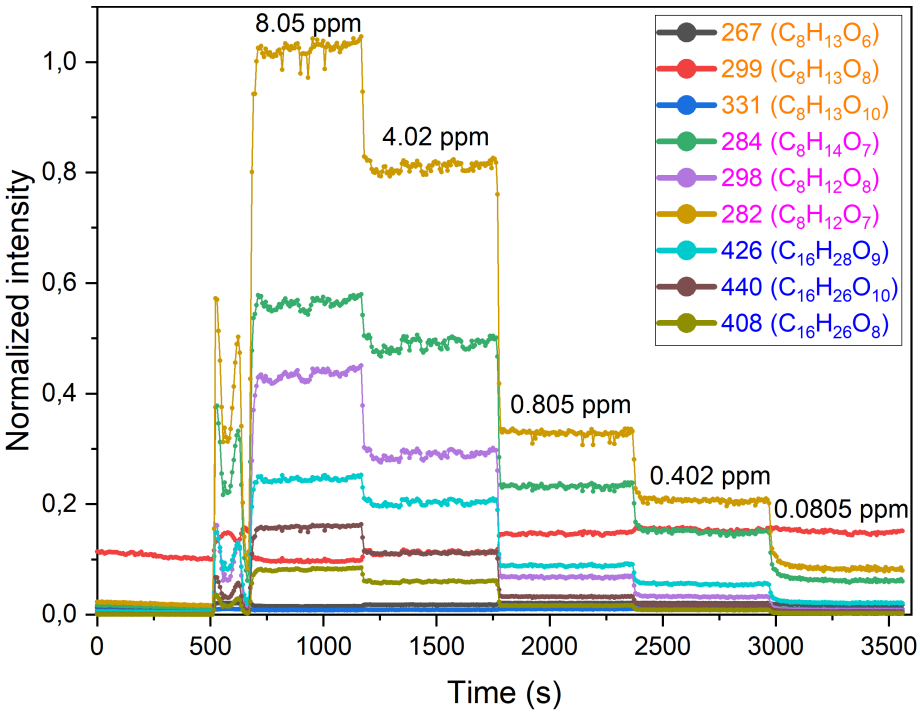

Figure 4.6: A time series of the normalized signal intensities of the most abundant ozonolysis-initiated autoxidation products of cyclooctene at a higher reaction time of 10.75 s (measured as adducts of NO_3-).

4.1.2 Short reaction time

At a reaction time of 0.33 s, accretion products were not found in the reactor. Figures 4.7 and 4.8 present the mass spectra of the high and low concentrations measured using negative polarity ionization. Ozone concentration used for the 0.59 s and 0.33 s reaction time experiments were 66 and 33 ppb respectively. The main products seen at the lower reaction time using negative polarity ionization were the radicals $C_8H_{13}O_6$ and $C_8H_{13}O_8$. The spectra measured with positive-polarity ionization at the same concentrations are presented in Figures 4.9 and 4.10. This can easily be seen when comparing the intensity scales of the negative and positive-polarity ionization spectra. The positive-polarity ionization spectra (in which also low oxygen content HOM are detected) have much higher intensity scales than the negative polarity ionization spectra, due to the biased detection efficiency of NO_3- towards more oxidized products, which is in contrast to the EDA(H+) detection, which seems to be more efficient in detecting less oxidized products. In the positive-polarity spectra, the most abundant species were the closed-shell species $C_8H_{14}O_3$ and $C_8H_{14}O_2$. Product $C_8H_{13}O_2$ could be originating from $C_8H_{13}O_4$ via O_2 cleavage. Product $C_8H_{13}O_4$ could be the first RO_2 formed via ozonolysis of cyclooctene.

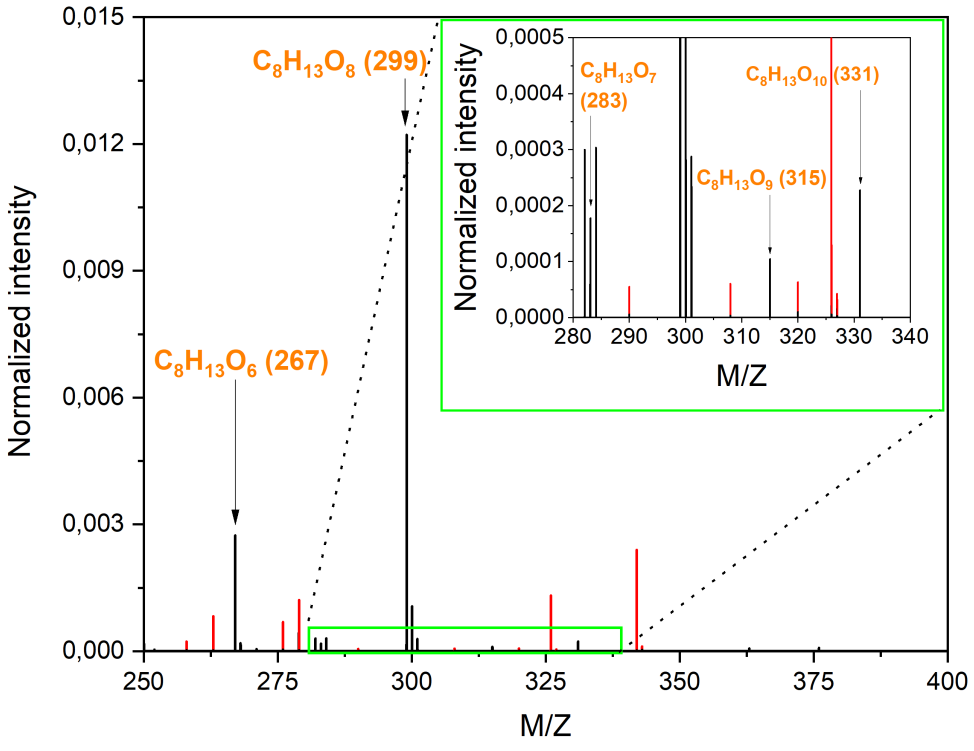

Figure 4.7: Mass spectrum of ozonolysis-initiated autoxidation products using a reaction time of 0.33 s and negative polarity ionization and a high concentration (3.94 ppm) of cyclooctene. A zoom into the M/Z 280 - 340 area of the spectrum is shown in the inset. The reaction time is sufficiently low so that only radicals are detected in notable intensities. Background peaks are marked with red color.

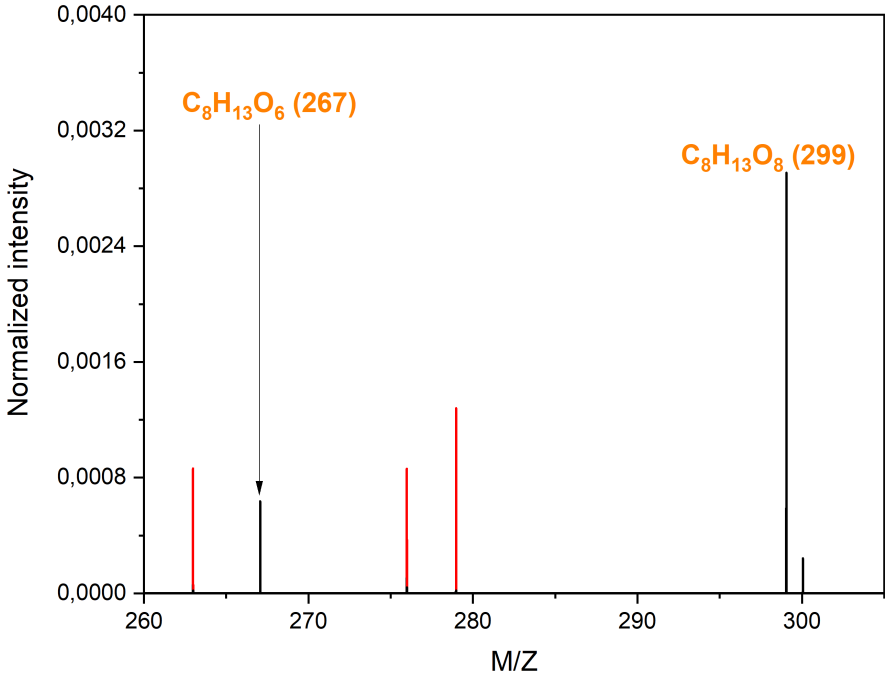

Figure 4.8: Mass spectrum of ozonolysis-initiated autoxidation products using a reaction time of 0.33 s and negative polarity ionization and a low concentration (0.039 ppm) of cyclooctene. Only $C_8H_{13}O_6$ and $C_8H_{13}O_8$ are detected at an appreciable intensity.

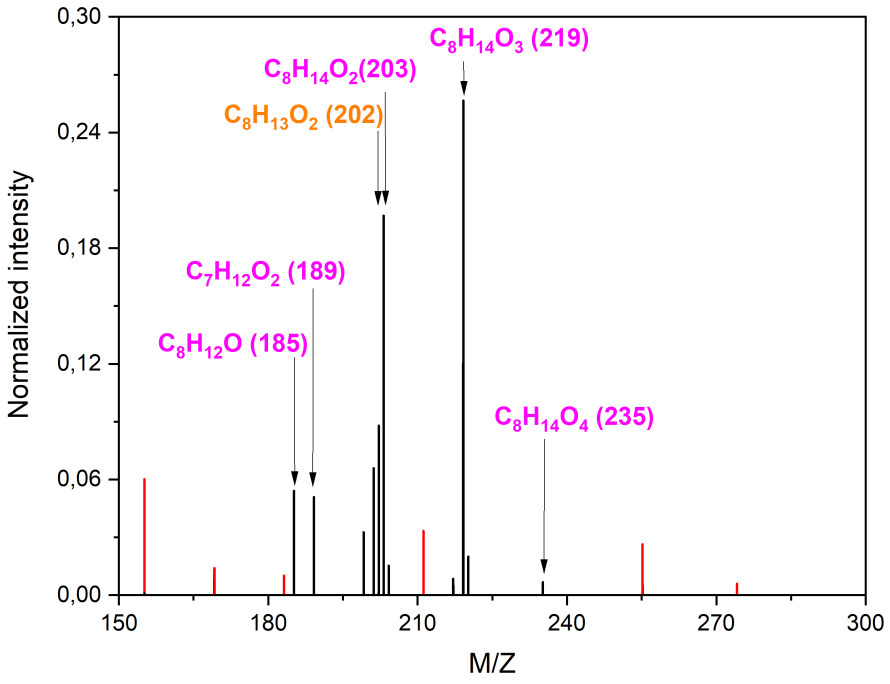

Figure 4.9: Chemical ionization mass spectrum of ozonolysis-initiated autoxidation products of cyclooctene measured using positive-polarity ionization and a reaction time of 0.33 s, and a high concentration of cyclooctene (3.94 ppm). Orange color = radical, purple = closed-shell monomer. Background peaks are marked with red color. All species were detected as clusters of EDA(H+) ($C_2H_9N_2$+), and this is included in the M/Z ratios, but left out of molecular formulae for clarity.

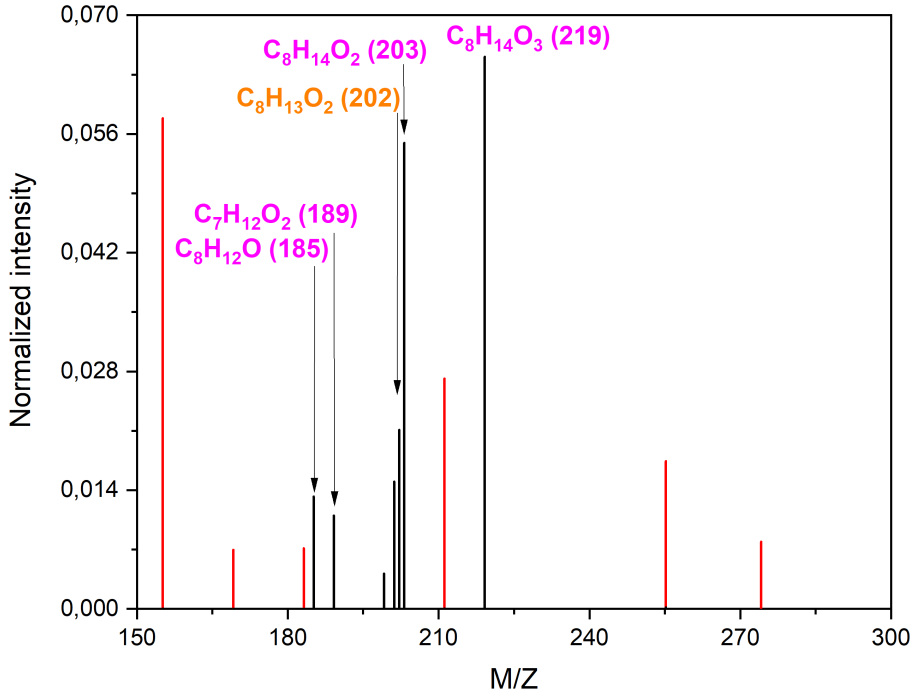

Figure 4.10: Chemical ionization mass spectrum of ozonolysis-initiated autoxidation products of cyclooctene measured using positive-polarity ionization and a reaction time of 0.33 s, and a high concentration of cyclooctene (0.039 ppm). Orange color = radical, purple color = closed-shell monomer. Background peaks are marked with red color. All species were detected as clusters of EDA(H+) ($C_2H_9N_2+$), and this is included in the M/Z ratios of peaks, but left out of molecular formulae for clarity.

Accretion products are formed in the reactor as precursor concentration is increased at a reaction time of 0.59 s. A time series of the highest intensity accretion product $C_{16}H_{26}O_{10}$ and the highest intensity radicals for comparison of intensities is shown in Figure 4.11. The accretion product $C_{16}H_{26}O_{10}$ could be formed by the self-reaction of $C_8H_{13}O_6$ or the cross-reactions between $C_8H_{13}O_8$ and $C_8H_{13}O_4$ for example. The time series shows that the accretion product is at a very low relative intensity at all precursor concentrations. The signal intensities of radicals $C_8H_{13}O_6$ and $C_8H_{13}O_8$ increase strongly as the precursor concentration is increased. This behavior is different than in the time series of larger reaction time data, 4.5, 4.6 in which the normalized signal intensities stay at close to constant intensity.

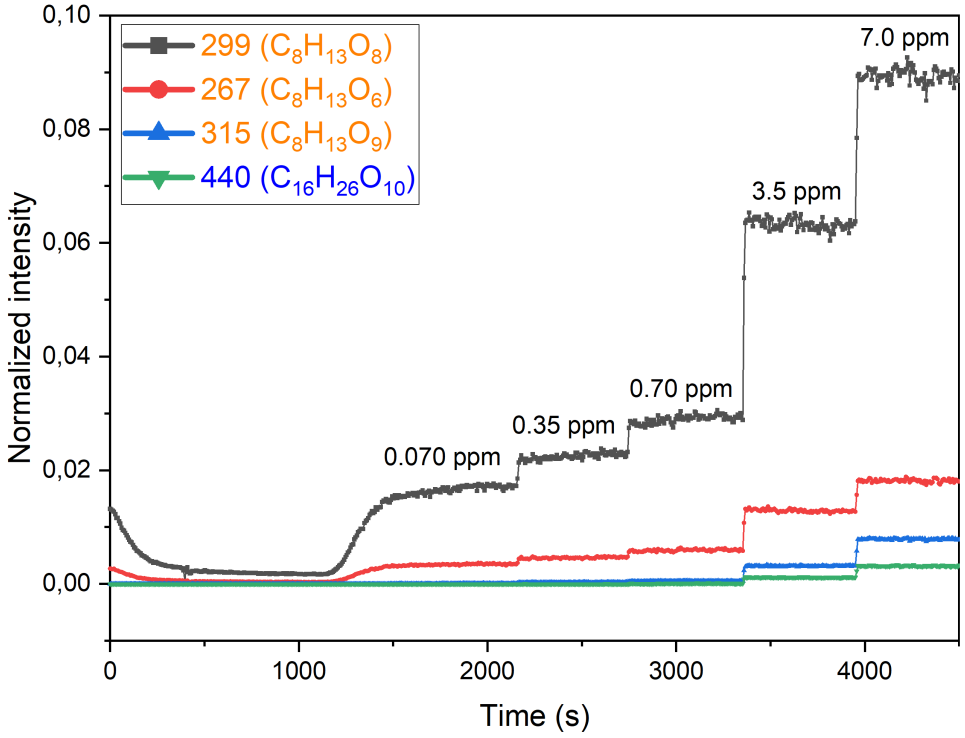

Figure 4.11: A time series of normalized signal intensities of the three highest intensity radical species (orange color) and the signal intensity of the most abundant accretion product (blue color) formed via ozonolysis-initiated autoxidation detected using positive-polarity chemical ionization mass spectrometry. A reaction time of 0.59 s was used. The concentration of cyclooctene is written on the spectrum. All species were detected as clusters of NO_3-, and this is included in the M/Z ratios of peaks, but left out of molecular formulae for clarity.

4.2 1,5-cyclooctadiene as the precursor

A broad list of HOM detected at high reaction time using 1,5-cyclooctadiene shown presented in Table 4.2. In general, more accretion products are found in the experiments using 1,5-cyclooctadiene when compared with cyclooctene. Especially with longer reaction times, the amount of accretion products was very high, and the most abundant species in the mass spectra was an accretion product in some cases. The results at high reaction time are presented first, and the results at the lower reaction time are presented afterwards.

4.2.1 Long reaction time

All identified products are tabulated in the appendix, and the proposed molecular formulae of the major peaks are presented in Table 4.2. As explained in 4.1.1, some of the proposed peaks are likely just isotopic peaks, or at least the intensities of the peaks are affected by the isotopic peaks. The mass spectra with concentrations of 6.10 ppm and

Table 4.2: Major HOM peaks detected using 1,5-cyclooctadiene and varying reaction time. All peaks are clusters of NO_3-, and the experimental mass-to-charge ratios (M/Z) include NO_3-. The molecular formulae are presented without NO_3- for clarity. Monomer and accretion product relative intensities are given for the high concentration of precursor, and the radical signal intensities are given at low precursor concentration. The relative intensities are as comparison to the highest signal intensity HOM: High = >20%, Medium = 10%-20%, Low = <10%. The measurements were also carried out at a reaction time of 5.29 s, although the relative intensities are not included here.

Molecular formula	M/Z ratio	Int. at 0.35 s	Int. at 0.63 s	Int. at 10.70 s	Molecular formula	M/Z ratio	Int. at 0.35 s	Int. at 0.63 s	Int. at 10.70 s
Monomers/ Radicals					Accretion products				
$C_8H_{12}O_5$	250.0571	Low	Low	Low	$C_{15}H_{24}O_7$	394.1360	-	Low	Low
$C_7H_{10}O_6$	252.0365	Low	Low	Low	$C_{16}H_{26}O_8$	408.1522	-	-	Low
$C_7H_{12}O_6$	254.0523	Low	Low	Low	$C_{14}H_{20}O_{10}$	410.0946	-	Low	Low
$C_8H_{11}O_6$	265.0445	Low	Low	Low	$C_{16}H_{24}O_9$	422.1310	-	Medium	High
$C_8H_{12}O_6$	266.0520	Low	Low	Low	$C_{15}H_{24}O_{10}$	426.1260	-	-	Low
$C_8H_{13}O_6$	267.0596	-	-	Low	$C_{16}H_{22}O_{10}$	436.1103	-	Low	Low
$C_7H_{10}O_7$	268.0313	-	Low	Low	$C_{16}H_{24}O_{10}$	438.1264	-	-	Low
$C_8H_{14}O_6$	268.0677	-	Low	Low	$C_{15}H_{22}O_{11}$	440.1053	-	Low	Low
$C_7H_{11}O_7$	269.0393	Low	Low	Low	$C_{14}H_{22}O_{12}$	444.1002	-	-	Low
$C_7H_{12}O_7$	270.0474	-	-	Low	$C_{16}H_{24}O_{11}$	454.1209	-	Low	Medium
$C_6H_{11}O_8$	273.0341	Low	Low	Low	$C_{16}H_{22}O_{12}$	468.1002	-	Low	Medium
$C_8H_{10}O_7$	280.0315	-	Low	Medium	$C_{16}H_{24}O_{12}$	470.1164	-	-	Low
$C_8H_{11}O_7$	281.0414	Low	Low	Low	$C_{15}H_{22}O_{13}$	472.1320	-	Low	High
$C_8H_{12}O_7$	282.0471	Low	High	High	$C_{16}H_{24}O_{13}$	486.1110	-	-	Low
$C_7H_{10}O_8$	284.0264	-	Low	Medium	$C_{15}H_{22}O_{14}$	488.0904	-	-	Low
$C_7H_{11}O_8$	285.0362	Low	Low	Low	$C_{16}H_{22}O_{14}$	500.0900	Low	Medium	High
$C_7H_{12}O_8$	286.0421	-	Low	Medium	$C_{12}H_{24}O_{17}$	502.0938	-	Low	Low
$C_8H_{11}O_8$	297.0343	High	High	High	$C_{15}H_{22}O_{15}$	504.0847	-	Low	Low
$C_8H_{12}O_8$	298.0420	Low	Low	Medium	$C_{16}H_{22}O_{16}$	532.0797	-	Low	Low
$C_7H_{11}O_9$	301.0291	Medium	Medium	Medium					
$C_8H_{10}O_9$	312.0213	-	Low	High					
$C_8H_{12}O_9$	314.0369	-	Low	High					
$C_8H_{11}O_{10}$	329.0242	Medium	Medium	Low					
$C_8H_{12}O_{10}$	330.0318	-	Low	Low					
$C_8H_{14}O_{10}$	332.0479	-	-	Low					
$C_8H_{10}O_{11}$	344.0112	-	-	Low					
$C_8H_{12}O_{11}$	346.0269	-	-	Low					
$C_8H_{11}O_{12}$	361.0127	-	-	Low					

0.00678 ppm are shown in Figures 4.12 and 4.13.

The reaction time in the experiments of Figures 4.12 and 4.13 was 10.70 s. The lower reaction time used was 5.29 s, and the mass spectra for the high and low concentrations are presented in Figures 4.14 and 4.15. The O_3 concentration at reaction times of 10.7 s and 5.29 s were 80 and 40 ppb respectively. In all the mass spectra presented here the same colors apply as for the first spectra presented in 4.1 (purple = closed-shell product, orange = radical, blue = accretion product). There is a very large amount of an accretion product with 14 oxygen, $C_{16}H_{22}O_{14}$, at M/Z 500. This product is likely formed in large

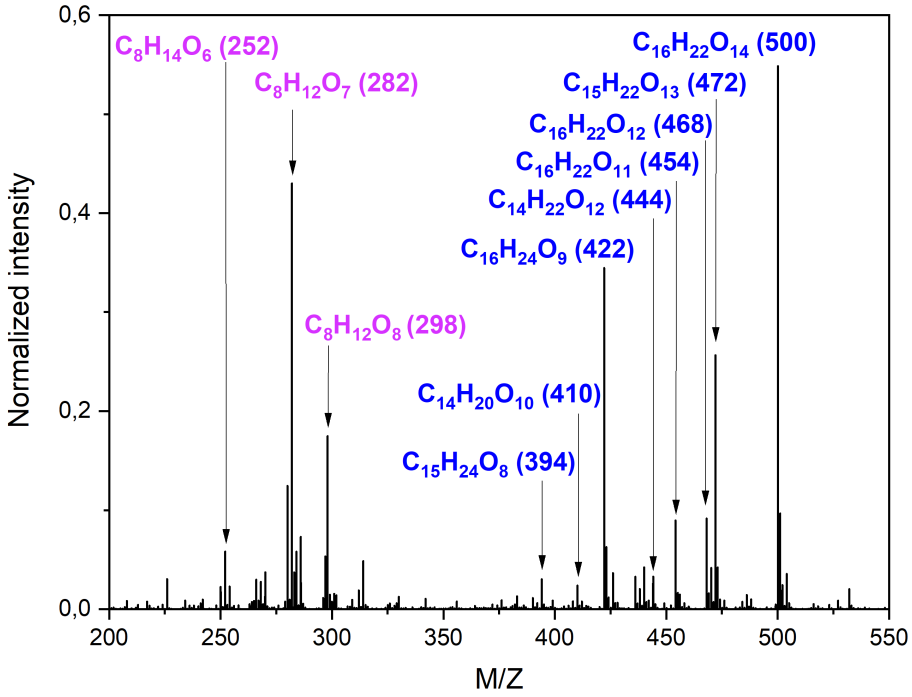

Figure 4.12: Mass spectrum of ozonolysis-initiated autoxidation products using negative polarity chemical ionization and a high concentration (6.1 ppm) of 1,5-cyclooctadiene at a reaction time of 10.70 s. closed-shell monomer products = purple color, accretion products = blue color.

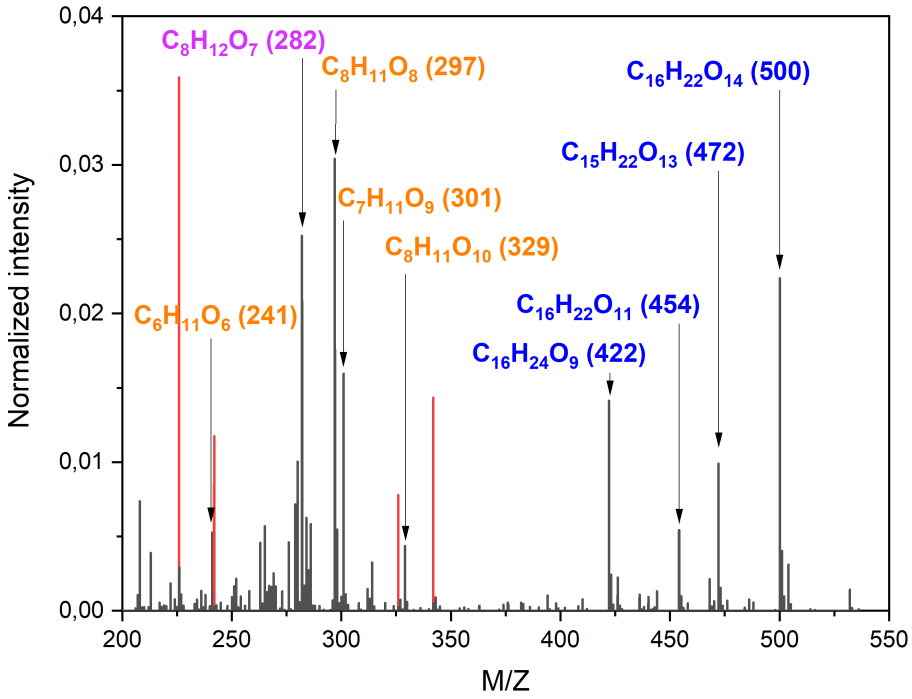

Figure 4.13: Mass spectrum of ozonolysis-initiated autoxidation products measured using NO_3- ionization and a low concentration (0.0678 ppm) of 1,5-cyclooctadiene at a reaction time of 10.70 s. Red color marks background peaks. Purple color = closed-shell monomer product, blue color = accretion product and orange color = radical.

amounts from radical $C_8H_{11}O_8\bullet$ the reaction channel 2.12,

$$C_8H_{11}O_8 \bullet + C_8H_{11}O_8\bullet \rightarrow C_{16}H_{22}O_{14} + O_2$$

given that there is a large amount of $C_8H_{11}O_8$ radical found in the reactor at high and low concentrations of 1,5-cyclooctadiene. This product can also be formed from other radicals such as from $C_8H_{11}O_{10}$ and $C_8H_{11}O_6$ through 2.12, but these other radicals are found in smaller quantities than $C_8H_{11}O_8$ in the mass spectra. The closed-shell product $C_8H_{12}O_7$ (M/Z 282) is detected at a strong signal, which could be formed through the same cross-reaction of $C_8H_{11}O_8$ which forms $C_{16}H_{22}O_{14}$, but a different branching channel:

$$C_8H_{11}O_8 \bullet + C_8H_{11}O_8\bullet \rightarrow C_8H_{12}O_8 + C_8H_{10}O_8$$

This channel should form $C_8H_{10}O_7$ in equal amounts as $C_8H_{12}O_7$, but surprisingly $C_8H_{10}O_7$ is detected at a much lower intensity. In the cyclooctene spectra, the corresponding radical $C_8H_{13}O_8$ with 2 more hydrogen is detected in large amounts, and closed-shell products $C_8H_{12}O_7$ and $C_8H_{14}O_7$ formed through the same supposed cross-reaction channel are detected at similar intensities. Perhaps $C_8H_{12}O_7$ is formed through another mechanism, or by the same cross-reaction channel with other radical species in addition to the above-mentioned self-reaction channel in the case of 1,5-cyclooctadiene. Product $C_{15}H_{22}O_{13}$ is also notable because when cyclooctene was used, no accretion products with 15 carbon were detected at appreciable intensities. The $C_{15}H_{22}O_{13}$ is potentially formed through the cross-reaction of C_7 and C_8 radicals. In the spectra measured using 1,5-cyclooctadiene, more C_7 radical products were detected than using cyclooctene.

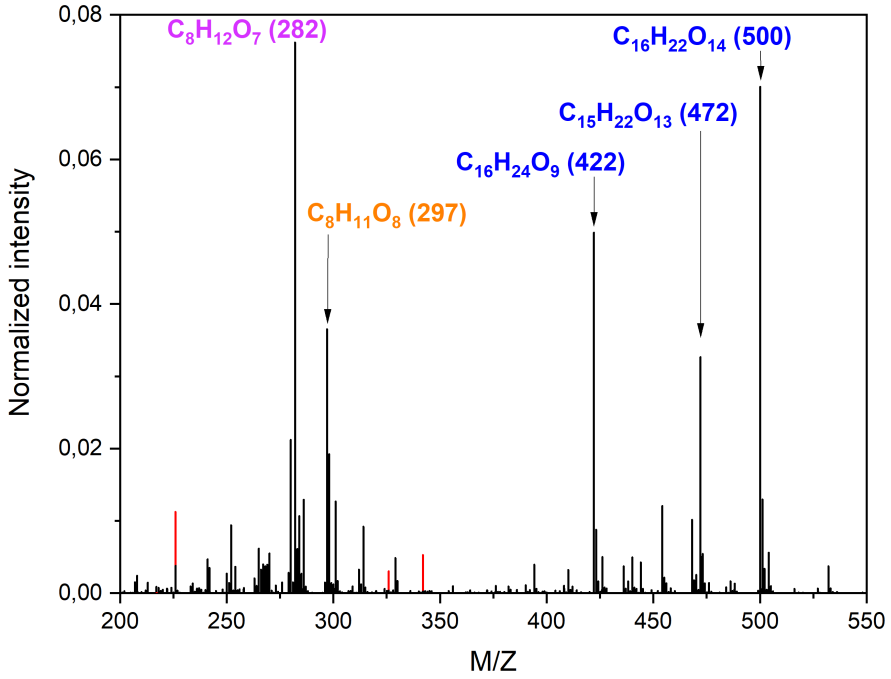

Figure 4.14: Mass spectrum of ozonolysis-initiated autoxidation products measured using NO_3- ionization and a high concentration (6.03 ppm) of 1,5-cyclooctadiene at a reaction time of 5.29 s. Red color marks background peaks. Orange color = radical, purple color = closed-shell monomer product, and blue color = accretion product.

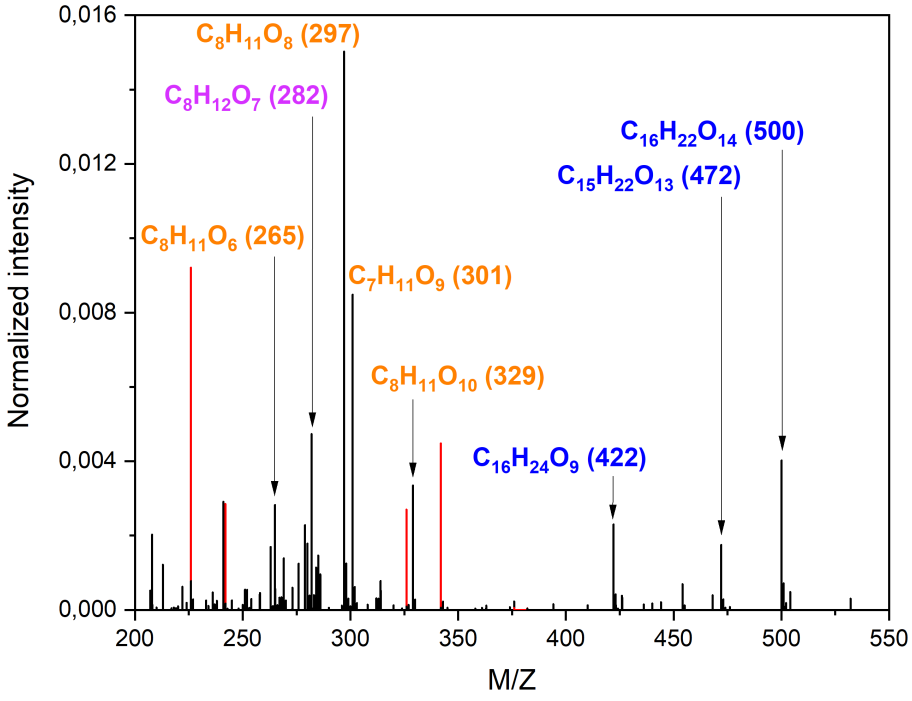

Figure 4.15: A chemical ionization Mass spectrum of ozonolysis-initiated autoxidation products using NO_3- ionization and a low concentration (0.0352 ppm) of 1,5-cyclooctadiene and a reaction time of 5.29 s. Red color = background peaks. Orange color = radical, purple color = closed-shell monomer, and blue color = accretion product.

Time series of product ions at both reaction times are shown in Figures 4.16 and 4.17. Especially in Fig. 4.17 the dominance of radicals $C_8H_{11}O_8$ and $C_7H_{11}O_9$ at lower concentrations is clear, because the reaction time is 5.48 s, which is lower than the reaction time of 10.7 s in Figure 4.16. At lower reaction times, radicals are observed at higher relative intensities, as already seen in the spectra measured using cyclooctene. The accretion product $C_{15}H_{22}O_{13}$ which is detected at high intensities relative to other accretion products, could potentially be formed through the cross-reaction of $C_7H_{11}O_9$ and $C_8H_{11}O_6$, both of which are clearly seen especially at lower precursor concentrations.

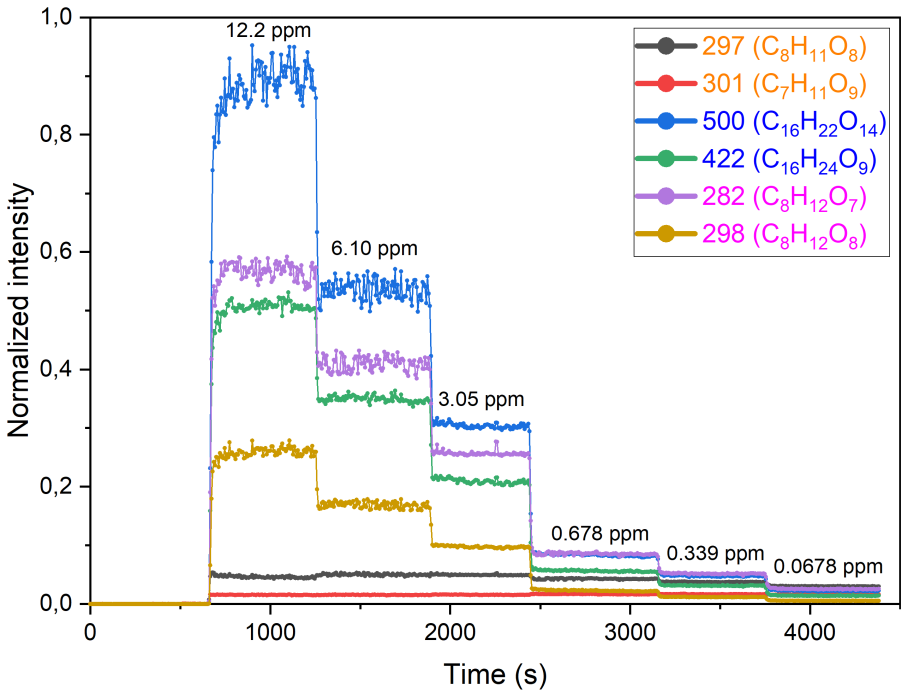

Figure 4.16: A time series of normalized signal intensities of two highest intensity radical species (orange color), closed-shell species (purple color) and accretion product (blue color) formed via ozonolysis-initiated autoxidation at a high reaction time (10.75 s) detected as adducts of NO_3-. The NO_3- is left out of the molecular formulae but included in the M/Z. The concentration of 1,5-cyclooctadiene during a time period is marked on the spectra.

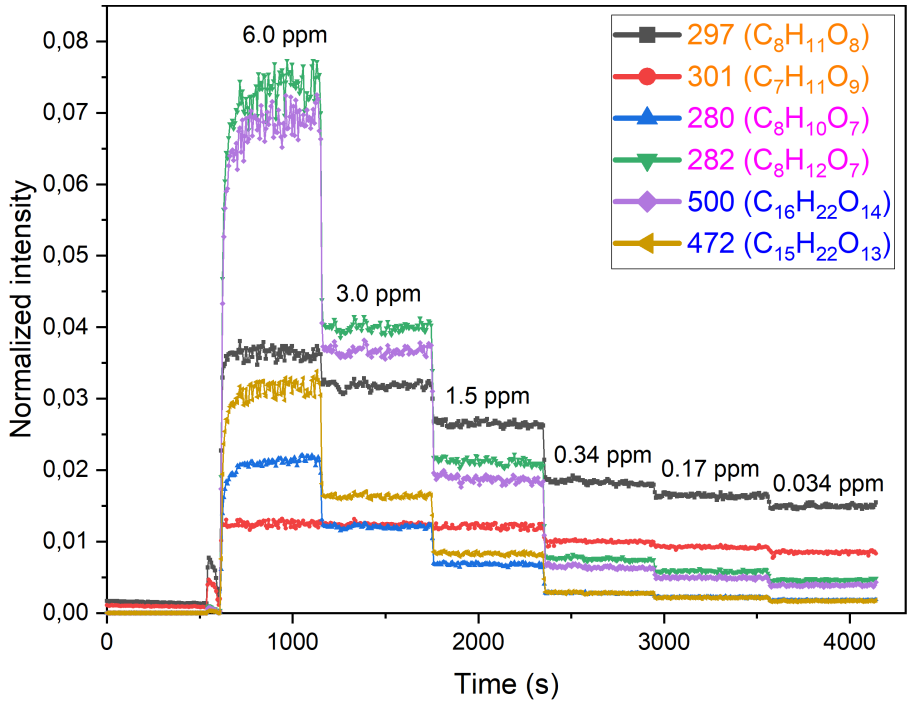

Figure 4.17: A time series of two high intensity radicals, closed-shell monomer and accretion products measured under otherwise same conditions as in Figure 4.16, but a lower reaction time (5.29 s).

4.2.2 Short reaction time

In the short reaction time experiments using negative polarity ionization, the reaction times were 0.63 s and 0.35 s for 1,5-cyclooctadiene. The mass spectra measured using reaction times of 0.63 s and 0.35 s at high and low concentrations of precursor are presented in Figures 4.18, 4.19 and 4.20, 4.21, respectively. The O_3 concentrations were 41 ppb at 0.35 s reaction time and 72 ppb at 0.63 s reaction time. The most abundant accretion product at M/Z of 500 can still barely be seen from the spectrum with the highest concentration at a reaction of 0.35 s, Figure 4.20. At lower concentrations, no accretion products were detected at the lower reaction time of 0.35 s. With a higher reaction time of 0.63 s, accretion products are still found at all concentrations except the lowest concentration measured, which is shown in 4.19. The $C_8H_{11}O_8$ radical at M/Z 297 is very dominant in all low reaction time spectra.

In the positive-polarity ionization experiments, much less identifiable product ions were found in the spectra. This is because EDA is less efficient as a chemical ionization reagent for more oxidized products. Only product ions with relatively small amounts of oxygen atoms are observed when using EDA compared to NO_3-, because EDA selectively forms clusters with different species than the species, which NO_3- forms clusters with. The main ions found in the spectra of cyclooctene and 1,5-cyclooctadiene using positive-polarity ionization were with 1-4 oxygen atoms. Some of these species were perhaps

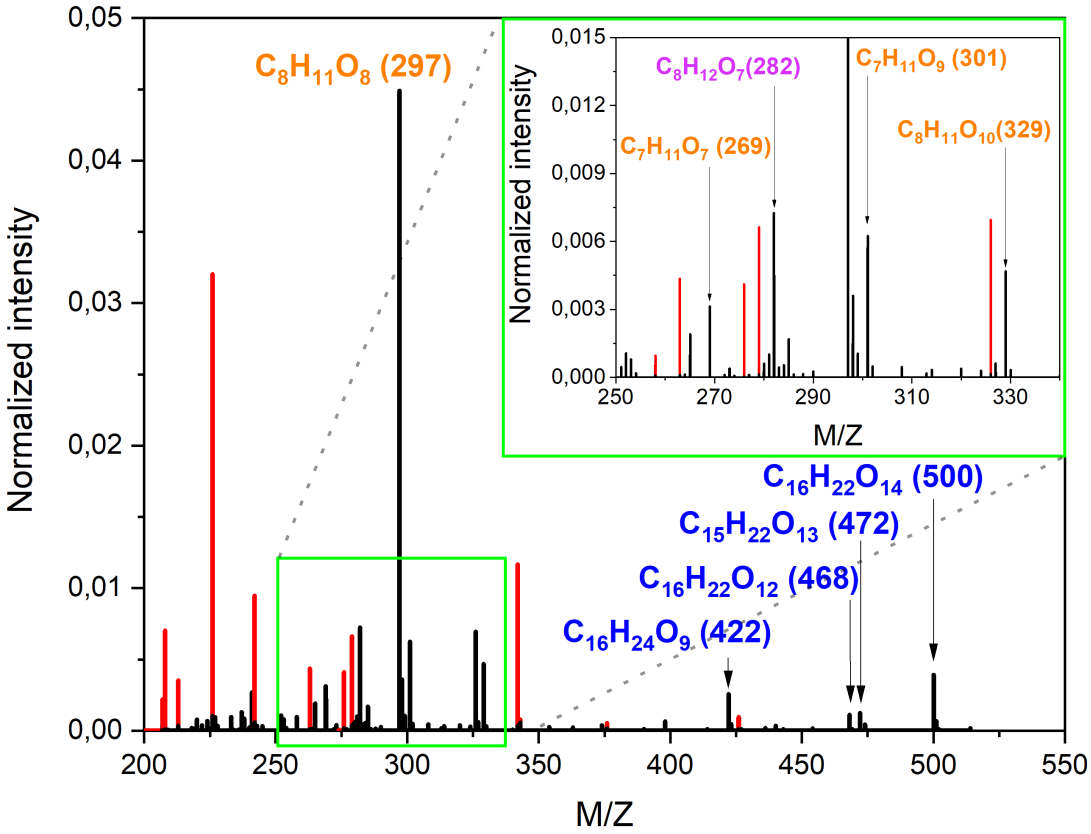

Figure 4.18: Chemical ionization mass spectrum of ozonolysis-initiated autoxidation products using 1,5-cyclooctadiene as the precursor at a high concentration of 3.15 ppm, and a reaction time of 0.63 s. All products were detected as clusters as NO_3-, and the M/Z ratios include NO_3, but NO_3- is removed from the molecular formulae for clarity.

formed from species with more oxygen atoms by fragmentation or OH radical chemistry, meaning the decomposition of VHP forms OH radicals, which are mostly scavenged by the precursor molecules, potentially forming the detected low oxygen content species. The VHP and other intermediates formed in the ozonolysis of cyclooctene have 2-3 oxygen atoms, and the lowest amount of oxygen atoms found in the products was 1 oxygen, which is 2 oxygen less. The intermediates of the ozonolysis reaction are assumed too short lived to be detected in these experiments, and therefore the low oxygen species detected here are likely fragments. Similar spectra although at lower intensities of the normalized signals were obtained when using positive-polarity ionization with a lower reaction time of 0.33 s. Only one positive-polarity ionization mass spectrum is presented here in Figure 4.22, because there was no other difference than the larger signal intensity of the detected species between the spectra measured at other concentrations.

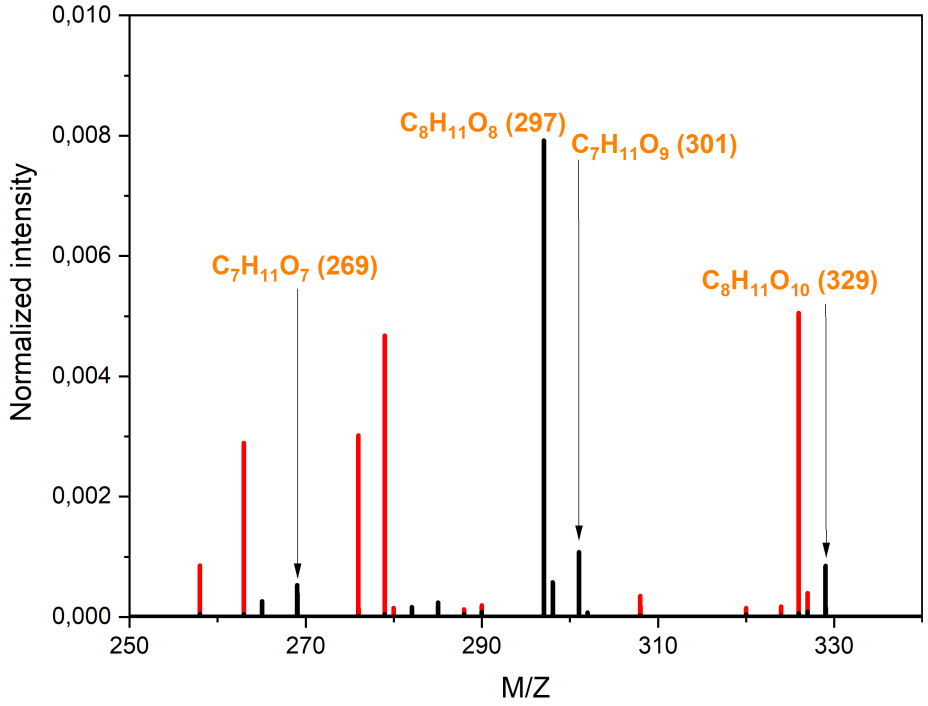

Figure 4.19: Nitrate chemical ionization mass spectrum of ozonolysis-initiated autoxidation products using 1,5-cyclooctadiene as the precursor at a low concentration of 0.063 ppm, and a reaction time of 0.63 s.

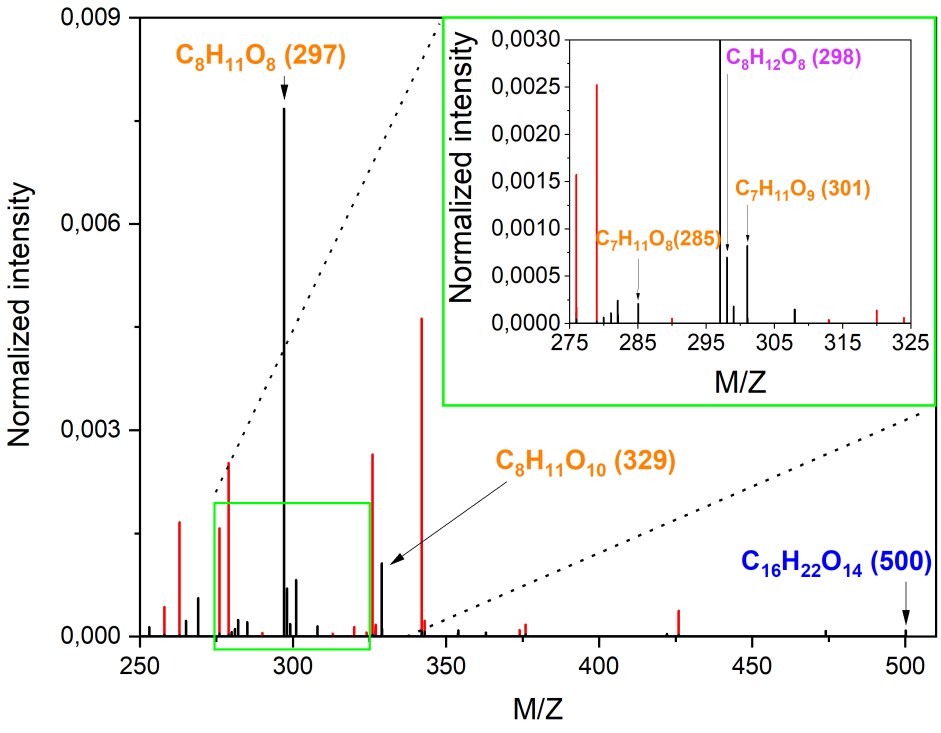

Figure 4.20: Nitrate chemical ionization mass spectrum of ozonolysis-initiated autoxidation products using 1,5-cyclooctadiene as the precursor at a reaction time of 0.35 s and a high concentration (3.49 ppm) of 1,5-cyclooctadiene.

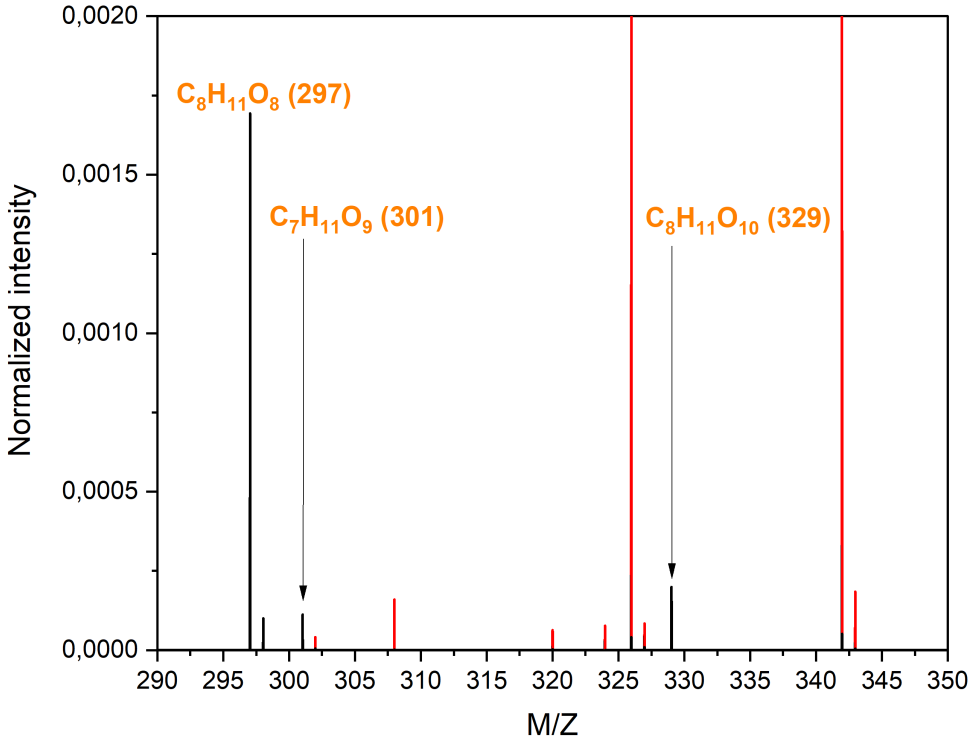

Figure 4.21: Nitrate chemical ionization mass spectrum of ozonolysis-initiated autoxidation products using 1,5-cyclooctadiene at a low concentration of 0.0349 ppm of 1,5-cyclooctadiene and a reaction time of 0.35 s

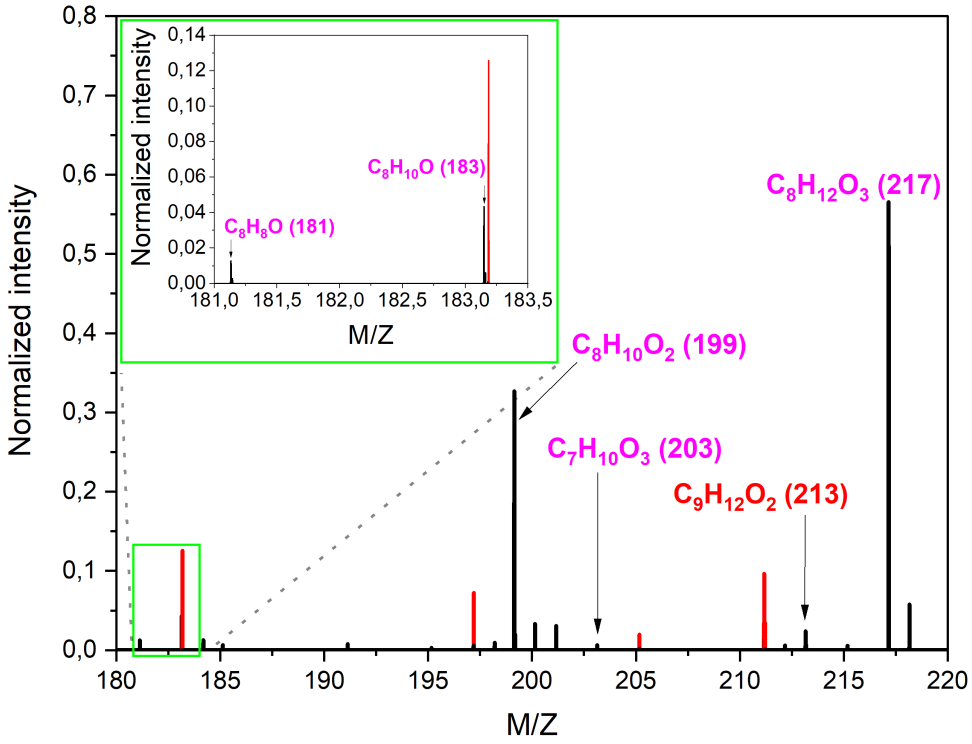

Figure 4.22: A positive-polarity chemical ionization mass spectrum measured using a 1,5-cyclooctadiene concentration of 0.63 ppm and reaction time of 0.63 s. All peaks were detected as clusters of $C_2H_9N_2+$, which is included in the M/Z ratios of peaks, but is removed from the molecular formulae for clarity. The peak which is marked with red color $C_9H_{12}O_2$ at M/Z 213 is possibly a background peak, even though the peak signal wasn't present when measuring the background.

When comparing the molecular formulae of the highest intensity peaks $C_8H_{12}O_3$ at m/z 217 and $C_8H_{10}O_2$ at m/z 199, There is exactly 2 H and 1 O missing from 217, which would indicate that 199 could have been formed from 217 by cleavage of H_2O, although this has not been suggested in previous studies with regard to HOM. Suprisingly, no radical products were detected using positive ionization and 1,5-cyclooctadiene as the precursor. This could be due to very rapid first steps of 1,5-cyclooctadiene autoxidation.

4.3 Summary and discussion of the results

4.3.1 Comparison of the products formed using both precursors

The amount of accretion products detected in the experiments using 1,5-cyclooctadiene is much higher than when cyclooctene was used, as already mentioned. Because the only difference between cyclooctane and 1,5-cyclooctadiene is the extra double bond that 1,5-cyclooctadiene has, the first assumption is that the high amount of accretion products is linked to this extra double bond. An extra double bond is known to stabilize radicals by resonance. Earlier computational predictions have pointed that H-shift rates can be significantly increased by the chemical environment of the carbon atom from which the hydrogen is abstracted, as already discussed in Section 2.1.3. Already at a low reaction time of $\sim$ 0.6 seconds, there is a large difference in the amount of accretion products found in the experiments using both precursors by looking at mass spectra measured from cyclooctene and 1,5-cyclooctadiene at almost the same reaction time and precursor concentration, figs 4.23 and 4.24.

Possible reasons for the increased amount of accretion product formation from 1,5-cyclooctadiene that the extra double bond 1,5-cyclooctadiene either speeds up the autoxidation chain in general, which would also explain why there are accretion products detected earlier, or that the extra double bond increases the reaction 2.12 branching ratio. When comparing the positive-polarity ionization spectra at $\sim$ 0.3 s reaction time measured using both precursors, (spectrum of 1,5-cyclooctadiene is included in the appendix D, D.5) there is no noticeable difference between the intensity scales of the HOM signals, which indicates that the autoxidation is proceeding at nearly the same pace, at least up until to the formation of the products measured using positive-polarity ionization. As already mentioned earlier, the accretion product $C_{16}H_{22}O_{14}NO_3$-, M/Z 500 that is the most abundant product formed from 1,5-cyclooctadiene is likely formed by the cross-reaction of two of the radical $C_8H_{11}O_8NO_3$-. The corresponding radical $C_8H_{13}O_8NO_3$- with 2 more hydrogen is detected in large amount from cyclooctene, but a much smaller amount of the accretion product $C_{16}H_{26}O_{14}NO_3$-, M/Z 504 is detected in the mass spectra. It could be that the RO_2 formed from 1,5-cyclooctadiene have a higher branching ratio of reaction

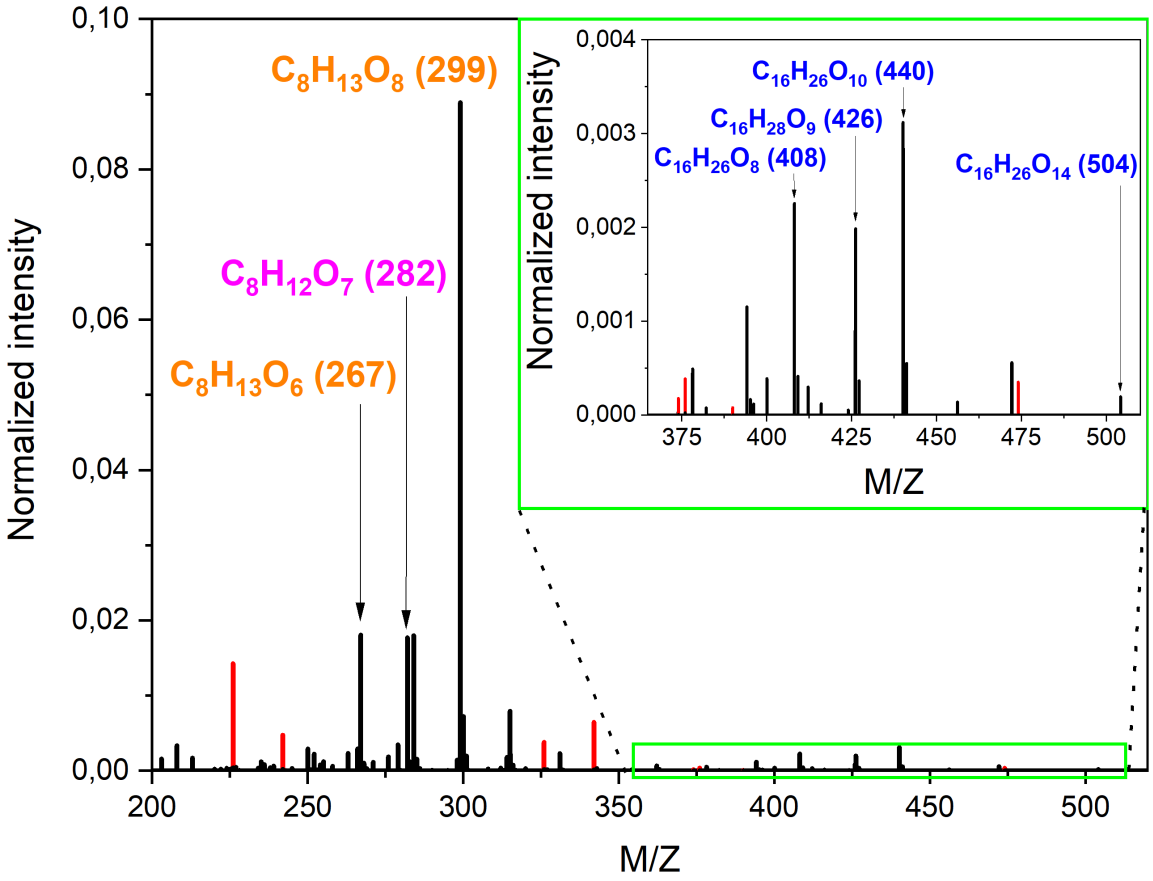

Figure 4.23: Nitrate mode chemical ionization mass spectrum of ozonolysis-initiated autoxidation products measured using a high concentration of cyclooctene (7 ppm) and a reaction time of 0.59 s. Background peaks are marked with red color.

RO_2 + R'O_2 → ROOR' + O_2, when comparing to reactions RO_2 + R'O_2 → RO + R'O + O_2 and RO_2 + R'O_2 → ROH + R'C=O + O_2. A higher branching ratio of reaction RO_2 + R'O_2 → ROH + R'C=O + O_2 in the case of cyclooctene is possible, because there is a large amount of closed-shell monomer products detected. Earlier studies have computed the rate coefficients of the cross combination reactions of α-pinene,[52,76] and the effect of some substituent group on cross combination reactions,[77] but the results of those studies do not provide a clear explanation for an increased branching ratio of RO_2 + R'O_2 → ROOR' + O_2 for the RO_2 formed from 1,5-cyclooctadiene. The increased formation of accretion products from 1,5-cyclooctadiene could also be explained by an alternative pathway of accretion product formation. Recently, Pasik et. al.[78] found that RO_2 can react with a double bond of another isoprene, monoterpenes, and tetramethylethylene, forming accretion products. In the case of 1,5-cyclooctadiene, this could possibly occur between RO_2 radicals or between a RO_2 and the precursor, 1,5-cyclooctadiene, or alternatively between RO_2 and a closed-shell monomer species. Because there is a much higher amount of 1,5-cyclooctadiene in the reactor than HOM species, it is more likely that the

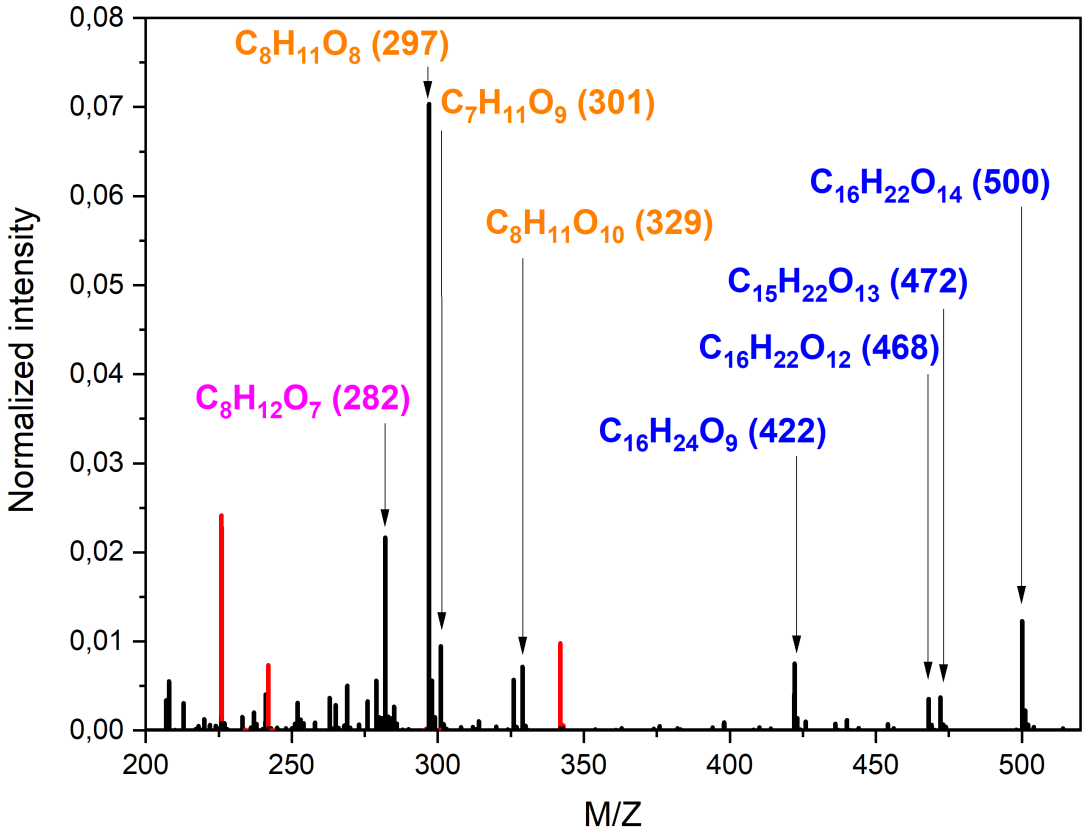

Figure 4.24: Nitrate mode chemical ionization mass spectrum of ozonolysis-initiated autoxidation products measured using a similar reaction time (0.63 s) and a similar concentration of 1,5-cyclooctadiene (6.3 ppm) as in the previous Figure 4.23. Background peaks are marked with red color.

RO_2 would react with 1,5-cyclooctadiene. These reactions are presented in Figure 4.25.

Reaction c) is likely not favourable because the product has 2 radical centers. If reactions a and b are occurring in the 1,5-cyclooctadiene experiments, the accretion products formed in these reactions could in principle further oxidize, because these reactions do not terminate the autoxidation chain. This would also explain the higher abundance of the higher oxygen containing accretion products found in the experimental results of 1,5-cyclooctadiene.

Closed-shell HOM species seem to be more dominant in the spectra of cyclooctene than 1,5-cyclooctadiene. This can also be seen from the mass spectra presented above, Figures 4.23 and 4.24, although not as clearly as the difference in the amounts of accretion products. The difference in the amount of closed-shell monomers between experiments using cyclooctene and 1,5-cyclooctadiene is more clearly seen when comparing the mass spectra measured at a higher reaction time. In Figures 4.23 and 4.24, the difference in the closed-shell HOM products can be seen when looking at the peaks 282 and 284. Peak 282 is seen in both spectra at nearly the same intensity, but peaks 284 and 280 are virtually absent in the spectrum measured using 1,5-cyclooctadiene. Because 1,5-cyclooctadiene

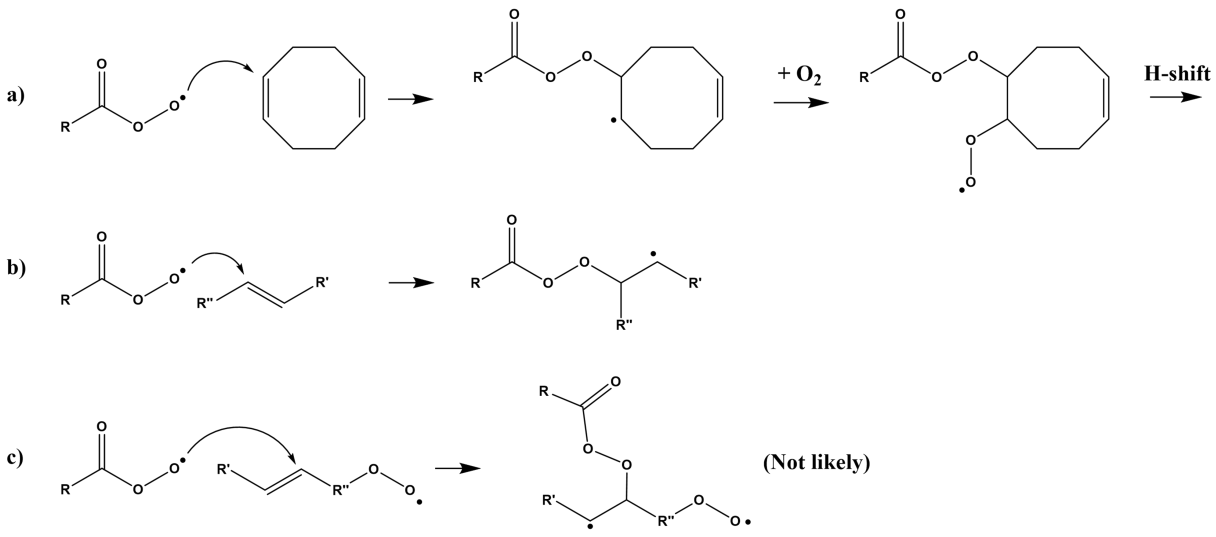

Figure 4.25: An acylperoxyradical could potentially react with a C=C bond, which could reside on: **a)** precursor molecule, **b)** closed-shell HOM, or **c)** another RO_2 radical. The precursor has much higher concentration than the other targets of this reaction, which is why the precursor molecule would be the most likely target of this reaction. It should be noted that this reaction could potentially occur between acylperoxy radicals and the precursor molecule when using cyclooctene as the precursor as well.

has 2 hydrogen initially so $C_8H_{14}O_7$ M/Z 284 in the spectra of 1,5-cyclooctadiene would correspond to $C_8H_{12}O_7$ or M/Z 282 in the spectra of cyclooctene, and $C_8H_{10}O_7$ or M/Z 280 in the spectra of 1,5-cyclooctadiene would correspond to $C_8H_{12}O_7$ or M/Z 282 in the spectra of cyclooctene. For cyclooctene closed-shell products, H12 products are clearly more abundant than H10 products, which is opposite of what is observed for cyclooctene. This is unxpected because H10 products can also be formed through unimolecular OH cleavage in addition to reaction $RO_2 + R'O_2 \rightarrow ROH + R'C{=}O + O_2$. It also looks like there are slightly more radicals in the spectrum of cyclooctene autoxidation products. According to current knowledge, closed-shell HOM are formed at least through the cross-reaction $RO_2 + R'O_2 \rightarrow ROH + R'C{=}O + O_2$. It would seem that either this reaction channel has a higher yield for the RO_2 formed from cyclooctene and smaller yield for RO_2 formed from 1,5-cyclooctadiene, or closed-shell monomer species are being removed from the 1,5-cyclooctadiene system, possibly by the formation of accretion product through bimolecular reaction of RO_2 with a double bond of another species.

One of the aspects motivating these experiments was to find specifically at what concentration of precursor and reaction time HOM are formed. In the autoxidation of both precursors, rapid formation of the 8 oxygen radical, $C_8H_{13}O_8$ from cyclooctene and $C_8H_{11}O_8$ from 1,5-cyclooctadiene, is observed. This agrees with the results of Berndt et. al.,[37] who observed fast formation of $C_8H_{13}O_8$ from cyclooctene using higher reaction times of 1.5-7.9 s with a jet-flow reactor combined with the Atmospheric Pressure interface Time of Flight Mass Spectrometry (APi-ToF-MS). The short time scale experiments

found that the accretion products are already detected at a reaction time of 0.35 seconds when the precursor was 1,5-cyclooctadiene (Figure 4.20) at a concentration of 3.49 ppm. Accretion products were not found when the precursor was cyclooctene at a similar reaction time (0.33 s) and concentration of precursor, (3.94 ppm) Figure 4.7. This again indicates that the accretion product formation is more efficient for the RO_2 formed from 1,5-cyclooctadiene than for the RO_2 formed from cyclooctene.

4.3.2 The autoxidation mechanisms

Similar molecular formulae were identified for the HOM formed from cyclooctene as in the proposed autoxidation mechanism of cyclooctene,[34,37,38] shown in Figure 2.4. Because molecular structures cannot be determined with the methods used in this thesis, it is uncertain if the molecular formulae determined in these experiments match with the structures presented in the mechanism. Some species were found in the measurements with cyclooctene which were not included in the mechanism. One example is the radical $C_6H_{11}O_5$ at M/Z $\sim$ 225. Mostly the difference between the molecular formulae in the mechanism and the detected species is a missing hydrogen, or an extra hydrogen. Closed-shell monomer species are formed by the cross combination reaction 2.10, which results in either R=O or ROH groups, with ± 1 hydrogen than the RO_2 in the autoxidation mechanism. This explains the missing or extra hydrogens in most cases. A suggested autoxidation mechanism of 1,5-cyclooctadiene is presented in Figure 4.26. A more thorough autoxidation mechanism of 1,5-cyclooctadiene could be obtained with computational rates of individual steps. As an example, it is uncertain if the 1,9 H-shift which the RO_2 labeled 1. can undergo occurs at competitive rate. Usually, RO_2 H-shifts have the highest rate for 1,5 - 1,7 H-shifts due to favorable transition state geometry. An 1,4 H-shift, could also occur for species 1, and it is uncertain which is faster, the 1,4 H-shift or the 1,9 H-shift.

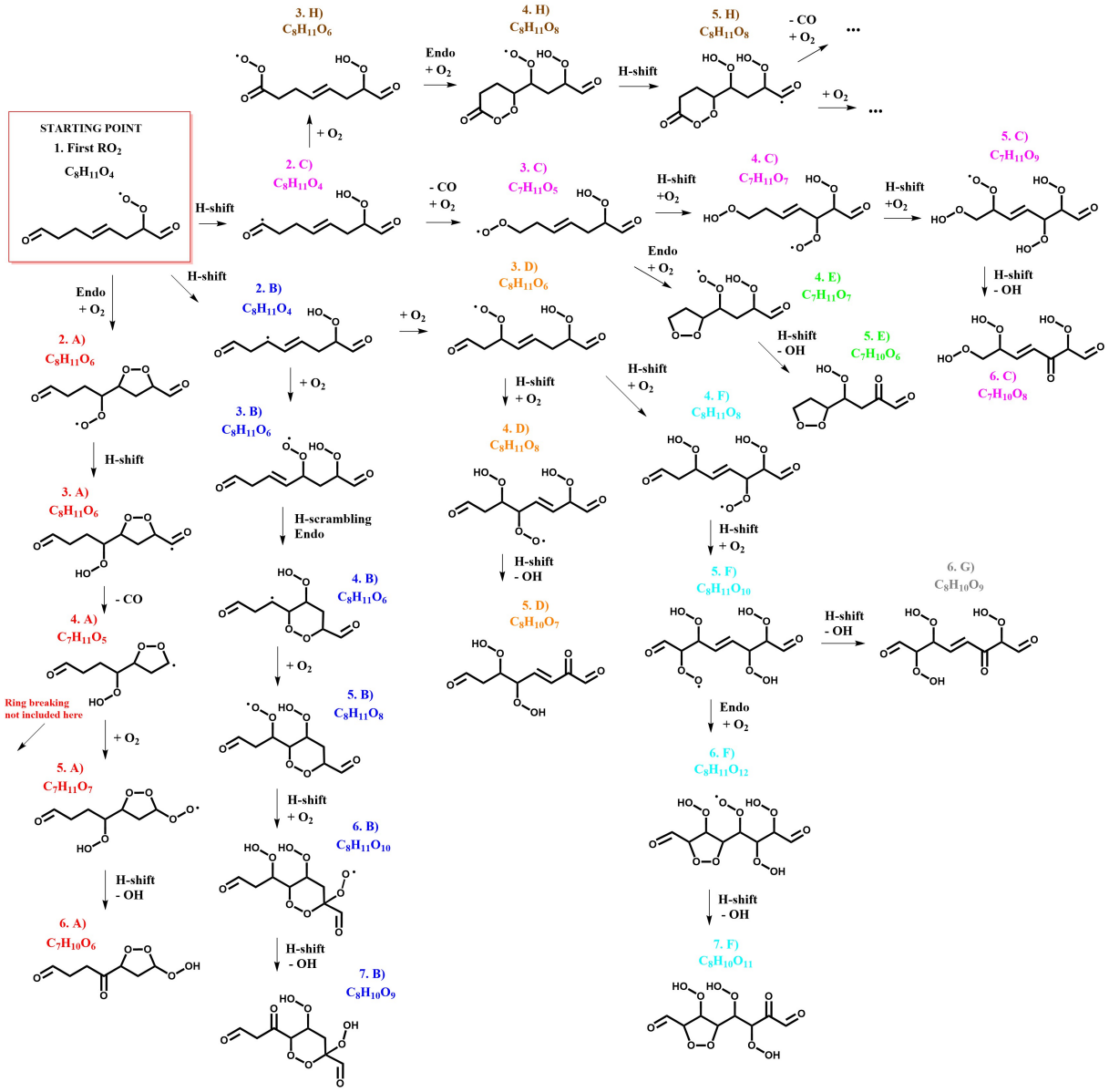

Figure 4.26: A suggested autoxidation mechanism of 1,5-cyclooctadiene. According to Vereecken et. al.,[43] endo cyclization to a β-substituted unsaturated RO_2 is not favorable, forming either 4-membered rings, or 5-membered ring structures with the radical center inside the structure. Based on the same results, the formation of 6-membered rings in which the radical center is left inside the ring is also assumed not competitive. However, when the ring structures reach the size of 7-8 membered, the ring formation with the radical center left inside the ring can become competitive. The additional double bond seems to ease further oxygen additions after CO cleavage reaction, providing more possibilities for H-shifts, and decreasing the odds of termination through OH cleavage reaction. This agrees with experimental results, as higher oxygen content C7 species were detected in the experiments using 1,5-cyclooctadiene. Reaction paths A, B, C, D, E, F, G, H are represented by colors: A: Red, B: Blue, C: Purple, D: Orange, E: Green, F: Cyan, G: Gray, H: Brown.

The individual steps of the autoxidation mechanism of 1,5-cyclooctadiene are as follows: The ozonolysis of 1,5-cyclooctadiene is assumed to proceed in the analogous way as

the ozonolysis of cyclooctene, producing the first RO_2: **1.** It is possible that the ozonolysis produces RO_2 with a different structure, if endoperoxidation and/or epoxidation occurs during ozonolysis. After formation, **1.** can either react in endoperoxidation and rapidly add O_2 to produce **2. A)**, or H-shift can occur to 2 most probable locations, forming **2. B)** or **2. C)**. Products **2. A)** as well as **2. B)** and **2. C)** further react in reaction paths A, B, C, and the intermediate products also react in alternative paths D, E, F, G and H. **Reaction path A**: Product **2. A)** most likely reacts in a H-shift to either of the CO groups at the opposing sides of the molecule, but the option where H-shift occurs to the endoperoxide ring side of the molecule is shown here. Product **3. A)** is formed, which further reacts by the cleavage of CO forming **4. A)** and a subsequent rapid addition of O_2 forming **5. A)**, or alternatively **4. A)** could react by ring breaking. Species **3. A)** likely also reacts with O_2 to some degree, forming an alternative reaction path, which is not included here. Product **5. A)** react by a H-shift at the OOH group, followed by an OH cleavage to produce **6. A)**. **Reaction path B: 2. B)** adds oxygen to either of the 2 locations due to the resonance structures formed by the double bond, forming either **3. B)** or **3. D)**, which continues in path D. **3. B)** likely reacts by H-scrambling and a rapid endoperoxidation follow up reaction, forming **4. B)**. **3. B)** also likely reacts by a H-shift to the CO group next to the OOH group, forming an additional reaction path, which is not included here. **4. B)** rapidly adds oxygen, forming **5. B)**, which reacts in a H-shift to another location, likely towards the CO-group near the endoperoxide ring structure. If **5. B)** H-shifts next to the CO-group, it likely rapidly adds oxygen afterwards forming **6. B)**, which further reacts in a H-shift near the OOH group on the other end of the molecule, and a rapid cleavage of OH occurs, forming **7. B)**. **6. B)** could also H-shift from the CO-group directly, which is not included in the mechanism. **Reaction path C:** Species **2. c)** either adds O_2 forming **3. H)**, which continues in path H, or **2. c)** reacts by the cleavage of CO and a rapid addition of O_2, forming **3. c)**, which likely reacts in endoperoxidation and an rapid addition of O_2, forming **4. E)**, which continues in path E. **3. c)** also likely reacts by H-shift between the double bond and the OOH group, rapidly adding O_2, forming **4. c)**. The double bond causes resonance, forming a product where the O_2 adds to another location, but this is not included in the mechanism. **4. c)** likely reacts by a H-shift next to the double bond, and adds O_2 rapidly, forming **5. c)**. Another product likely is again formed due to the resonance of the double bond, but is not included in the mechanism. **5. c)** likely reacts in a rapid H-shift from the OOH group next to the double bond, and a rapid OH cleavage occurs, forming **6. c)**. **Reaction path D:** Species **3. D)** reacts with a H-shift between the double bond and the OOH group, and due to the resonance structures of the double bond, either **4. D)** or **4. F)** is formed, of which **4. F)** continues in path F. **4. D)** likely reacts with a H-shift to the OOH group next to the double bond, and OH is rapidly cleaved, forming **5. D)**. **Reaction path E:** Species **4.**

E) most likely reacts by an H-shift from the carbon connected to the OOH group, followed by cleavage of OH, forming **5. E)**. Species **4. E)** could also H-shift from the CO group, and the product formed through this reaction could then add O_2 forming $C_7H_{11}O_9$, or CO cleavage could occur, forming $C_6H_{11}O_6$, which could react further. **Reaction path F:** Species **4. F)** Likely reacts by a H-shift from next to the CO group at the opposite end of the molecule, and quickly adds O_2 to form **5. F)**, which can then either react with an endocyclization, followed by an rapid O_2 addition forming **6. F)**, or another H-shift reaction from the OOH group next to the double bond. This is then followed by a OH cleavage, which forms **6. G)**, terminating the chain. Species **6. F)** likely reacts by a H-shift from OH group position, followed by an OH cleavage forming **7. F)**. Species **6. F)** could also react by H-shift at the CO group, but this would ultimately form products with molecular formulas of C_7O_{10} or C_8O_{14}, which were not detected. **Reaction path H:** Species **3. H)** most likely reacts by endo cyclization, and rapidly adds O_2 to form **4. H)**, which reacts with H-shift at the CO group on the opposite side of the molecule looking at the endocyclic ring structure, forming **5. H)**, which can further autoxidize.

The mechanism is branched to multiple paths already from the first H-shift after the formation of the initial RO_2 in the ozonolysis, as already shown in Figure 2.5. Even though the autoxidation mechanisms of the precursors are different, many products with similar molecular formulae were detected except for the 2 less hydrogens that 1,5-cyclooctadiene has because of the extra double bond. Products with the same molecular formulae can have very different chemical structures, even though one might assume otherwise based on the molecular formulae. The suggested autoxidation mechanism of 1,5-cyclooctadiene leans on the computational results of Richters et. al.[15] on the autoxidation mechanism of 1,4-cyclohexadiene. It is assumed that the ozonolysis of 1,5-cyclooctadiene forms the first RO_2 in the analogous way as for cyclooctene, but the ozonolysis mechanism of 1,5-cyclooctadiene could be slightly different than the ozonolysis mechanism of cyclooctene, because of the double bond that could potentially cause endoperoxidation during ozonolysis or other reactions. Richters et. al. suggested that the formation of a 5-membered or larger endoperoxide ring structures are feasible, and smaller rings such as 4-membered rings are not formed. In addition, no endoperoxide ring structures were formed such that the radical center is left inside the ring structure. No computations were performed at this time to confirm the rates of these reaction steps, and therefore the autoxidation mechanism presented here is speculative. Additional autoxidation pathways exist in addition to the pathways presented here. Species with identical molecular formulae as presented in the proposed autoxidation mechanism of 1,5-cyclooctadiene were detected in the experiments using 1,5-cyclooctadiene. The double bond of 1,5-cyclooctadiene allows for pathways not likely for cyclooctene, leading to higher oxygen content C_7 HOM species detected in the experiments using 1,5-cyclooctadiene. To summarize the difference between the

autoxidation mechanisms of cyclooctene and 1,5-cyclooctadiene, the extra double bond of 1,5-cyclooctadiene can alter the autoxidation mechanism quite significantly, although the autoxidation of 1,5-cyclooctadiene still leads to products with similar chemical formulae as the autoxidation of cyclooctene, which agrees with experimental results, although the chemical structures of products with similar molecular formulae can differ greatly.

4.3.3 The results of the positive-polarity ionization experiments

In the positive-polarity ionization experiments, species with oxygen content of 1-3 for 1,5-cyclooctadiene and cyclooctene were detected and these species are not found in the proposed autoxidation mechanisms. The intermediates in the ozonolysis reaction are most likely too short-lived to be measured in these experiments, although Berndt et. al. have previously claimed that they achieved direct detection of Criegee intermediates formed in cyclohexene ozonolysis using CI-APi-TOF with n- and tert-butylamine and diethylamine.[79] A possible explanation for the detection of the low oxygen products is that they were formed from higher oxygen products by cleavage of oxygen atoms in some manner, possibly during the chemical ionization. As already mentioned earlier, ammonia and amine chemical ionization reagents have been found to cause fragmentation during the chemical ionization process sometimes, and thus it is possible that EDA causes fragmentation of HOM during chemical ionization. Product $C_8H_{13}O_2$ was also measured from cyclooctene, which could be formed from $C_8H_{13}O_4$ via cleavage of O_2. A very large amount of $C_8H_{14}O_3$ detected of was detected using cyclooctene and $C_8H_{12}O_3$ correspondingly when using 1,5-cyclooctadiene. These HOM could be intact, because there is a similar amount of hydrogen in the molecular formula as detected with many of the HOM using negative polarity ionization, or if they were formed by fragmentation, only oxygen was cleaved. The detected species with 2-1 oxygens could have been formed from the 3 oxygen bearing high intensity species via fragmentation, as there seems to be high amounts of the 3 oxygen species present in the reactor. Some of the low oxygen species detected also have a low amount of hydrogen, which could mean that oxygen and hydrogen containing moiety was fragmented from the original HOM species, such as H_2O. Although the cleavage of H_2O from hydroperoxide groups has been observed to occur in MS-MS experiments,[80,81] it is unknown if this can occur under the conditions of one-dimensional MS, and under the experimental conditions used in this thesis. Berndt[82] used protonated ethylamine to detect the ozonolysis-initiated autoxidation products of α-pinene, and suggested that a 2 oxygen-bearing HOM species detected of α-pinene was formed via cleavage of O_2 during or after ionization with aminium ions. In an earlier study, Berndt et. al.[59] used protonated n-propylamine to detect HOM formed of α-pinene, and observed the formation of the same 2 oxygen-bearing HOM species as in the later study. Berndt[82] also pointed that

the chemical nature of the detected species is highly speculative at the moment, which also holds for the statements about the HOM detected using positive-polarity ionization mode in this thesis.

It could be that also the 3 oxygen atom species were formed from higher oxygen content species through dissociation reactions, but probably not, because there are no higher oxygen content species detected, and it is unlikely that cleavage would occur for all of the original species. Computational methods could be used to find more information about the possibility of fragmentation reactions. If the 3 oxygen atom species were not a result of oxygen dissociating from these structures, perhaps it could be some species formed through OH-roaming reactions from VHP similar to the ones presented by Klippenstein et. al.[35] Another possibility is that the detected species is a secondary ozonide. The formation of secondary ozonides in the ozonolysis of α-pinene has been suggested. Another interesting observation was that for cyclooctene, there was a weak signal of $C_8H_{14}O_4$ at a reaction time of 0.33 s and concentration of 3.94 ppm. In the experiments using 1,5-cyclooctadiene, a 4 oxygen species was not detected in the positive-polarity ionization experiments.

In the ozonolysis reactions of cyclooctene and 1,5-cyclooctadiene, OH radicals are formed each time the VHP decomposes, and therefore OH is present in the reactor. The precursor molecule acts as an OH scavenger, immediately consuming nearly all OH after formation. The reactions of OH with the precursor can form species with 1-4 oxygen atoms, and therefore it is possible that at least some of the species detected using positive-polarity ionization were formed via OH-reactions. The OH-initiated autoxidation of 1,5-cyclooctadiene does not require the formation of alkoxy radicals due to the second double bond allowing for fast follow-up unimolecular H-shift reactions of RO_2, which is why the accumulation of low oxygenated closed-shell products is unexpected for 1,5-cyclooctadiene, although the OH-initiated autoxidation of 1,5-cyclooctadiene was not thoroughly examined.

4.3.4 The effect of precursor concentration and the reaction time on the product distribution

In the experiments using both precursors, it was generally observed that the concentrations of closed-shell monomer HOM and accretion product HOM are decreasing as the concentration of precursor is decreased. The concentrations of radicals have varying dependence on the concentration of precursor. Some radicals seem to have little correlation to the precursor concentration, having almost constant normalized signal intensity during changing of the precursor concentration. An example of this can be seen in Figure 4.27, a time series of radical HOM measured using 1,5-cyclooctadiene as the precursor.

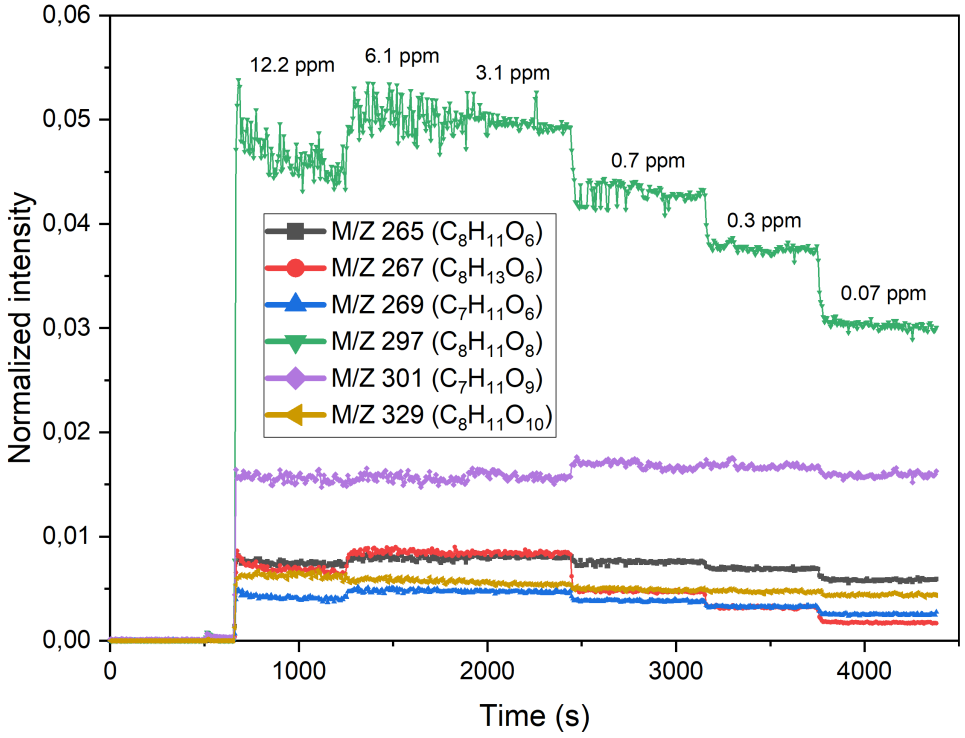

Figure 4.27: A time series of radical signal intensities of the ozonolysis-initiated autoxidation products measured using chemical ionization mass spectrometry with a reaction time of 10.7 s, and a varying concentration of 1,5-cyclooctadiene. All products were detected as adducts of NO_3-, which is included in M/Z ratios, but left out of the molecular formulae for clarity.

The $C_8H_{11}O_6$ radical normalized signal intensity decreases more significantly than radical $C_7H_{11}O_9$ as the precursor concentration is decreased. Radical $C_7H_{11}O_9$ normalized signal intensity remains constant at all of the precursor concentrations. The normalized signal intensities of the radicals which remain at almost constant intensity resembles a steady-state behavior of some intermediates in a chemical reaction. In lower reaction times, the normalized signal intensities of radicals $C_8H_{13}O_6$ and $C_8H_{11}O_8$ increase strongly as the precursor concentration is increased, as seen in 4.11. It would appear that in higher reaction times, the signal intensities of the radicals are less affected by the concentration of the precursor, eventually reaching constant signal intensities. This could be due to rapid bimolecular reactions consuming radicals at the rate of formation. At lower reaction time the radical HOM signal intensities grow as the precursor concentration is increased.

4.4 Sources of error

There are only a few sources of error worth mentioning with the results. The limitations of using mass spectrometry have already been discussed earlier (mainly the inability to accurately define the structure of analytes), which is why they are not discussed here.

First, the error of vapor pressures of cyclooctene and 1,5-cyclooctadiene determined with the Antoine equation, using Yaws Handbook of Vapor Pressure.[71] Obtained values from the Yaws Handbook were experimental values, and this is why these values were chosen over the alternative source for the vapor pressures, the ChemSpider website, which provides computationally obtained values on the vapor pressures of cyclooctene and 1,5-cyclooctadiene. The vapor pressures obtained from both sources had (minor) differences. From Yaws, obtained values were 0.0085 atm at 25 °C for cyclooctene, and 0.0072 atm at 25 °C for 1,5-cyclooctadiene. From the ChemSpider website, corresponding values were 0.0079 atm at 25 °C for cyclooctene and 0.0057 atm at 25 °C for 1,5-cyclooctadiene. The difference between the vapor pressures of 1,5-cyclooctadiene obtained from these sources is larger than the difference between the vapor pressures of cyclooctene. Using the vapor pressure values obtained from ChemSpider would yield lower calculated concentrations of 1,5-cyclooctadiene in the measurements. This would result in even larger differences in the formation of accretion products between 1,5-cyclooctadiene and cyclooctene. The possible error that results from this is not a major error, because the vapor pressures are still quite similar.

The second potential source of error is caused by the surface adsorption/desorption effects, often called wall reactions, which can cause the precursor concentration to be underestimated in the lower concentration measurements. The precursor can be adsorbed on the tube and reactor walls, and then released as the concentration is lowered, causing a larger concentration of precursor in the measurement. The concentration difference between the lowest and highest concentrations measured during a single measurement is about 100 times in most measurements, which is quite large. The effect of this is not seen very clearly in the measurement data, and therefore the effect is likely minor. For larger reaction time experiments, the smallest concentrations used would have taken a very long time for the concentration to stabilize in the reactor, if the measurement was started with the lowest precursor concentration used. For the smaller reactor, at the beginning of the measurement it took close to 30 minutes for the precursor concentration to stabilize in the reactor. The smaller reactor volume is about 1/16 of the volume of the larger reactor, which means that it would have taken roughly 8 hours for the concentration to stabilize in the reactor at the same flow rate, obtained by simple extrapolation. Therefore, it was not feasible to start at the lower precursor concentration when using the large reactor.

Finally, the usage of mass flow controllers always introduces uncertainties in the flow rates of gases, resulting in errors in reactant concentration and reaction time. Although the mass flow controllers are calibrated, there is always inevitably at least a small error in the flow rate. Using multiple mass flow controllers can stack error, especially if the errors of the mass flow controllers are in the same direction, although the errors of calibrated mass flow controllers are individually minor.

5. Conclusions and outlook

In the experiments using 1,5-cyclooctadiene, it was immediately found that a relatively high amount of accretion products was formed. The reason for the increased formation of the accretion products can stem from at least 2 possible scenarios, 1: the extra double bond causes the RO_2 formed from 1,5-cyclooctadiene to have a higher RO_2 cross-reaction branching ratio in channel leading to accretion products, or 2: there is an alternative route of formation for the accretion products for 1,5-cyclooctadiene. New mechanisms for the formation of HOM are frequently found, and in this case there could be some unknown mechanism forming accretion products. A possible alternative route is the reaction proposed recently by Pasik et. al.,[78] in which an acylperoxy radical reacts with the double bond of a precursor molecule, another RO_2 or a closed-shell monomer species (the reaction with the precursor is the most probable due to the large amount of precursor in the reactor), forming an accretion product that can further autoxidize. Both of these scenarios are possible, and the high amount of accretion products found in the 1,5-cyclooctadiene experiments could be due to both an increased branching ratio in 2.12 and an additional mechanism of accretion product formation. The rates of the acylperoxy radical addition reaction to the double bond of another species computed by Pasik et. al.[78] were relatively low overall, with the highest rates being in the order of 10^{-15} cm^3 s^{-1}. This would suggest that an increased rate of cross-reaction in 2.12 is the main contributor to the accumulation of accretion products in the 1,5-cyclooctadiene experiments (scenario 1). Fewer closed-shell monomer species are found in the 1,5-cyclooctadiene spectra, especially in the higher reaction time experiments, suggesting that these could be consumed in the alternative RO_2 cross-reaction. However, if there is a higher yield of the branching channel leading to accretion products, this also leads to a smaller amount of closed-shell products formed through the other branching channel by which closed-shell products are formed, which is why no conclusions can be made that the closed-shell products are formed through the alternative RO_2 cross-reaction. It is not possible to determine with more precision which scenario causes the increase in the amount of accretion product formation from 1,5-cyclooctadiene using the methods of this thesis, because the HOM structures cannot be determined with these methods. To determine the reason for the increased accretion product formation in the autoxidation of 1,5-cyclooctadiene, further

studies should computationally find the overall reaction rate of RO_2 cross-reaction, and perhaps the branching ratio in 2.12, as well as the rate of reaction a) in Figure 4.25 for at least some of the acylperoxy radicals formed in the autoxidation of 1,5-cyclooctadiene. All things considered, it most likely is the increased branching ratio in 2.12, which causes the large amount of accretion product formation observed in the experiments using 1,5-cyclooctadiene.

The results of the positive-polarity ionization-mode experiments also need further clarification. The low amount of oxygen detected in some of the products detected using EDA(H+) as the ionization reagent could be due to fragmentation reactions. Some of the species with low oxygen content appear to have exactly 2 H and 1 O less than a higher m/z peak, which could potentially indicate fragmentation of H_2O, or something else such as O_2, as already suggested by Berndt,[82] although he studied autoxidation of α-pinene, and used a slightly different positive-polarity ionization reagent: protonated ethylamine. The possibility of fragmentation during the chemical ionization process should therefore be investigated computationally. Further experiments and computational studies on the use of EDA(H+) as the ionization reagent for the detection of HOM could provide more information about the ionization process of HOM with this reagent. Other chemical ionization reagents should also be tested to see if they are suitable for the ionization of HOM (As a side note, many promising chemical ionization reagents have been experimented on recently, such as urea, although yet unpublished). Other amine derivatives are promising for the ionization of low-oxygen-content HOM. If one were to add a known amount of some HOM model compound to the reactor and attempt to ionize this using a chemical ionization reagent of interest, one could in principle easily see if the reagent in question would be a good choice as a chemical ionization reagent. The problem with this approach is that there are no commercial standards of HOM available.

Only one previous study about the autoxidation of cyclic dienes was found, and therefore more experiments using cyclic dienes could be done in the future. Generally speaking, future research into the formation of HOM through autoxidation could experiment with more precursors. A recent study by Barua et. al.[83] found that hexanal can autoxidize in atmospheric conditions, and longer chain aldehydes and ketones were found to autoxidize efficiently in atmospheric conditions by Wang et al.[11] An interesting possibility to experiment with could, for example, be benzaldehyde, since the autoxidation of aromatics has already been observed in atmospheric conditions. A recent study found that benzaldehyde had significant emissions in china.[84]

Furthermore, similar cross-reactions as the acylperoxy radical reaction with the double bond of another species, recently studied by Pasik et. al.[78] could be interesting to study, since so far most experiments have studied the autoxidation of individual compounds, and the possibility of combination reactions between other species has not

generally been studied. Experiments in which two (or more) compounds are mixed in a reactor and allowed to autoxidize could be interesting and could possibly reveal new reaction types. However, the results of such measurements would probably be difficult to interpret, since the autoxidation of only individual compounds can be very complex at times. In polluted areas, there could be various VOCs in the atmosphere, which, in principle, could react with each other during the autoxidation process. Field measurements already provide information on this part, but require considerable effort in planning and moving the equipment. The conditions in different environments could be simulated in experiments if accurate emission and air quality data is available.

One of the largest obstacles to HOM research is the inability to accurately define the chemical structures of HOM using mass spectrometry. Other methods for HOM detection are not available, and common analytical methods for obtaining structural information such as chromatography and spectroscopy, are difficult to use for numerous reasons, previously discussed in 2.2. Alternative methods should still be thought of, such as (gas-phase) NMR spectroscopy (just an example, as gas-phase NMR probably is not a very feasible method in reality).

As for the robustness of the experiments in this thesis, there were no major problems with the experiments, and the error sources discussed in Section 4.4 are minor. The experiments of this thesis were therefore successful. Positive-polarity chemical ionization experiments were planned for the higher reaction times, but there was no time for this. Further studies should measure autoxidation products using positive mode at the higher reaction times, and this would show how much of the lower oxygen content HOM are present at longer reaction times. The results of these experiments broaden our knowledge about the autoxidation reactions of VOCs, especially the effect of the chemical structure on efficient autoxidation. To complement these results, one could use computational methods to find the reaction rates of bimolecular reactions, as well as the H-shift and endoperoxidation reactions shown in the suggested autoxidation mechanism of 1,5-cyclooctadiene.

To conclude, there is still a lot of work to understand the autoxidation mechanisms of VOCs in the atmosphere. The total contribution of HOM to the amount of secondary organic aerosol in the atmosphere is still largely unknown, which is why further research is certainly required.

Bibliography

[1] J. Lelieveld, A. Pozzer, U. Pöschl, M. Fnais, A. Haines, and T. Münzel. Loss of life expectancy from air pollution compared to other risk factors: a worldwide perspective. *Cardiovascular research*, 116(11):1910–1917, 2020.

[2] Y. Liu, S. Yang, C. Li, Q. Fang, C. Han, C. Cheng, Y. Cao, F. Cui, and X. Li. Changes in years of life lost and life expectancy by reducing air pollution. *Air Quality, Atmosphere & Health*, 17(1):89–102, 2024.

[3] H. Zhao, G. Geng, Y. Liu, Y. Liu, Y. Zheng, T. Xue, H. Tian, K. He, and Q. Zhang. Reduction of global life expectancy driven by trade-related transboundary air pollution. *Environmental Science & Technology Letters*, 9(3):212–218, 2022.

[4] M. Shiraiwa, K. Ueda, A. Pozzer, G. Lammel, C. J. Kampf, A. Fushimi, S. Enami, A. M. Arangio, J. FroÌhlich-Nowoisky, Y. Fujitani, et al. Aerosol health effects from molecular to global scales. *Environmental science & technology*, 51(23):13545–13567, 2017.

[5] J. L. Jimenez, MR Canagaratna, NM Donahue, ASH Prevot, Q. Zhang, J. H Kroll, P. F. DeCarlo, J. D. Allan, H. Coe, NL. Ng, et al. Evolution of organic aerosols in the atmosphere. *science*, 326(5959):1525–1529, 2009.

[6] S. Iyer, A. Kumar, A. Savolainen, S. Barua, C. Daub, L. Pichelstorfer, P. Roldin, O. Garmash, P. Seal, T. Kurtén, et al. Molecular rearrangement of bicyclic peroxy radicals is a key route to aerosol from aromatics. *nature communications*, 14(1):4984, 2023.

[7] M. Claeys, B. Graham, W. Vas, G.and Wang, R. Vermeylen, V. Pashynska, J. Cafmeyer, P. Guyon, M. O. Andreae, P. Artaxo, et al. Formation of secondary organic aerosols through photooxidation of isoprene. *Science*, 303(5661):1173–1176, 2004.

[8] J. Helberg and D. A. Pratt. Autoxidation vs. antioxidants–the fight for forever. *Chemical Society Reviews*, 50(13):7343–7358, 2021.

[9] C. E. Frank. Hydrocarbon autoxidation. *Chemical reviews*, 46(1):155–169, 1950.

[10] M. Ehn, J. A Thornton, E. Kleist, M. Sipilä, H. Junninen, I. Pullinen, M. Springer, F. Rubach, R. Tillmann, B. Lee, et al. A large source of low-volatility secondary organic aerosol. *Nature*, 506(7489):476–479, 2014.

[11] Z. Wang, M. Ehn, M. P. Rissanen, O. Garmash, L. Quéléver, L. Xing, M. Monge-Palacios, P. Rantala, N. M. Donahue, T. Berndt, et al. Efficient alkane oxidation under combustion engine and atmospheric conditions. *Communications chemistry*, 4(1):18, 2021.

[12] F. Bianchi, T. Kurtén, M. Riva, C. Mohr, M. P. Rissanen, P. Roldin, T. Berndt, J. D. Crounse, P. O. Wennberg, T. F. Mentel, J. Wildt, H. Junninen, T. Jokinen, M. Kulmala, D. R. Worsnop, J. A. Thornton, N. Donahue, H. G. Kjaergaard, and M. Ehn. Highly oxygenated organic molecules (HOM) from gas-phase autoxidation involving peroxy radicals: A key contributor to atmospheric aerosol. *Chemical Reviews*, 119(6):3472–3509, 2019.

[13] M. Ehn, E. Kleist, H. Junninen, T. Petäjä, G. Lönn, S. Schobesberger, M. Dal Maso, A. Trimborn, M. Kulmala, D. R. Worsnop, A. Wahner, J. Wildt, and Th. F. Mentel. Gas phase formation of extremely oxidized pinene reaction products in chamber and ambient air. *Atmospheric Chemistry and Physics*, 12(11):5113–5127, 2012.

[14] M. Ehn, H. Junninen, T. Petäjä, T. Kurtén, V.-M. Kerminen, S. Schobesberger, H. E. Manninen, I. K. Ortega, H. Vehkamäki, M. Kulmala, and D. R. Worsnop. Composition and temporal behavior of ambient ions in the boreal forest. *Atmospheric Chemistry and Physics*, 10(17):8513–8530, 2010.

[15] Stefanie Richters, Mark Pfeifle, Matthias Olzmann, and Torsten Berndt. endo-cyclization of unsaturated ro_2 radicals from the gas-phase ozonolysis of cyclohexadienes. *Chemical Communications*, 53(29):4132–4135, 2017.

[16] T. Jokinen, O. Kausiala, O. Garmash, O. Peräkylä, H. Junninen, S. Schobesberger, C. Yan, M. Sipilä, and M. P. Rissanen. Production of highly oxidized organic compounds from ozonolysis of β-caryophyllene: laboratory and field measurements. *Boreal Environment Research*, 21(3-4):262, 2016.

[17] S. Richters, H. Herrmann, and T. Berndt. Highly oxidized RO2 radicals and consecutive products from the ozonolysis of three sesquiterpenes. *Environmental science & technology*, 50(5):2354–2362, 2016.

[18] V. F. McNeill. Atmospheric aerosols: clouds, chemistry, and climate. *Annual review of chemical and biomolecular engineering*, 8(1):427–444, 2017.

[19] N. M. Donahue, A. L. Robinson, and S. N. Pandis. Atmospheric organic particulate matter: From smoke to secondary organic aerosol. *Atmospheric Environment*, 43(1):94–106, 2009.

[20] M. Hallquist, J. C. Wenger, U. Baltensperger, Y. Rudich, D. Simpson, M. Claeys, J. Dommen, N. M. Donahue, C. George, A. H. Goldstein, J. F. Hamilton, H. Herrmann, T. Hoffmann, Y. Iinuma, M. Jang, M. E. Jenkin, J. L. Jimenez, A. Kiendler-Scharr, W. Maenhaut, G. McFiggans, Th. F. Mentel, A. Monod, A. S. H. Prévôt, J. H. Seinfeld, J. D. Surratt, R. Szmigielski, and J. Wildt. The formation, properties and impact of secondary organic aerosol: current and emerging issues. *Atmospheric Chemistry and Physics*, 9(14):5155–5236, 2009.

[21] Duseong S. Jo, Benjamin A. Nault, Simone Tilmes, Andrew Gettelman, Christina S. McCluskey, Alma Hodzic, Daven K. Henze, Muhammad Omar Nawaz, Ka Ming Fung, and Jose L. Jimenez. Global health and climate effects of organic aerosols from different sources. *Environmental Science & Technology*, 57(37):13793–13807, 2023.

[22] R. Atkinson and J. Arey. Atmospheric degradation of volatile organic compounds. *Chemical Reviews*, 103(12):4605–4638, 2003.

[23] P. J Ziemann and R. Atkinson. Kinetics, products, and mechanisms of secondary organic aerosol formation. *Chemical Society Reviews*, 41(19):6582–6605, 2012.

[24] L. J. Beck, N. Sarnela, H. Junninen, C. JM Hoppe, O. Garmash, F. Bianchi, M. Riva, C. Rose, O. Peräkylä, D. Wimmer, et al. Differing mechanisms of new particle formation at two arctic sites. *Geophysical Research Letters*, 48(4):e2020GL091334, 2021.

[25] T. Jokinen, M. Sipilä, J. Kontkanen, V. Vakkari, P. Tisler, E.-M. Duplissy, H. Junninen, J. Kangasluoma, H. E. Manninen, T. Petäjä, et al. Ion-induced sulfuric acid–ammonia nucleation drives particle formation in coastal antarctica. *Science Advances*, 4(11):eaat9744, 2018.

[26] V.-M. Kerminen, X. Chen, V. Vakkari, T. Petäjä, M. Kulmala, and F. Bianchi. Atmospheric new particle formation and growth: review of field observations. *Environmental Research Letters*, 13(10):103003, 2018.

[27] F. Bianchi, J. Tröstl, H. Junninen, C. Frege, S. Henne, C. R. Hoyle, U. Molteni, E. Herrmann, A. Adamov, N. Bukowiecki, et al. New particle formation in the free troposphere: A question of chemistry and timing. *Science*, 352(6289):1109–1112, 2016.

[28] HE Manninen, T. Nieminen, E. Asmi, S. Gagné, S. Häkkinen, K. Lehtipalo, P. Aalto, M. Vana, A. Mirme, S. Mirme, et al. EUCAARI ion spectrometer measurements at 12

european sites–analysis of new particle formation events. *Atmospheric Chemistry and Physics*, 10(16):7907–7927, 2010.

[29] S. Schobesberger, H. Junninen, F. Bianchi, G. Lönn, M. Ehn, K. Lehtipalo, J. Dommen, S. Ehrhart, I. K. Ortega, A. Franchin, et al. Molecular understanding of atmospheric particle formation from sulfuric acid and large oxidized organic molecules. *Proceedings of the National Academy of Sciences*, 110(43):17223–17228, 2013.

[30] F. Riccobono, S. Schobesberger, C. E. Scott, J. Dommen, I. K. Ortega, L. Rondo, J. Almeida, A. Amorim, F. Bianchi, M. Breitenlechner, et al. Oxidation products of biogenic emissions contribute to nucleation of atmospheric particles. *Science*, 344(6185):717–721, 2014.

[31] F. Bianchi, O. Garmash, X. He, C. Yan, S. Iyer, I. Rosendahl, Z. Xu, M. P. Rissanen, M. Riva, R. Taipale, et al. The role of highly oxygenated molecules (HOMs) in determining the composition of ambient ions in the boreal forest. *Atmospheric Chemistry and Physics*, 17(22):13819–13831, 2017.

[32] J. Kirkby, J. Duplissy, K. Sengupta, C. Frege, H. Gordon, C. Williamson, M. Heinritzi, M. Simon, C. Yan, J. Almeida, et al. Ion-induced nucleation of pure biogenic particles. *Nature*, 533(7604):521–526, 2016.

[33] J. Tröstl, W. K. Chuang, H. Gordon, M. Heinritzi, C. Yan, U. Molteni, L. Ahlm, C. Frege, F. Bianchi, R. Wagner, et al. The role of low-volatility organic compounds in initial particle growth in the atmosphere. *Nature*, 533(7604):527–531, 2016.

[34] M. P. Rissanen, T. Kurtén, M. Sipilä, J. A. Thornton, J. Kangasluoma, N. Sarnela, H. Junninen, S. JÃžrgensen, S. Schallhart, M. K. Kajos, R. Taipale, M. Springer, T. F. Mentel, T. Ruuskanen, T. Petäjä, D. R. Worsnop, H. G. Kjaergaard, and M. Ehn. The formation of highly oxidized multifunctional products in the ozonolysis of cyclohexene. *Journal of the American Chemical Society*, 136(44):15596–15606, 2014.

[35] S. J. Klippenstein and Sarah N. Elliott. OH roaming during the ozonolysis of α-pinene: A new route to highly oxygenated molecules? *The Journal of Physical Chemistry A*, 127(50):10647–10662, 2023.

[36] A. Sharma, M. Walavalkar, A. Kumar, S. Dhanya, and P. D. Naik. Reactions of tropospheric oxidants-Cl, OH and O3 with cyclic hydrocarbons with eight carbon atoms at 298 k. *Atmospheric environment*, 213:433–443, 2019.

[37] T. Berndt, S. Richters, R. Kaethner, J. VoigtlaÌnder, F. Stratmann, M. SipilaÌ, M. Kulmala, and H. Herrmann. Gas-phase ozonolysis of cycloalkenes: formation of highly

oxidized RO2 radicals and their reactions with NO, NO2, SO2, and other RO2 radicals. *The Journal of Physical Chemistry A*, 119(41):10336–10348, 2015.

[38] N. Hyttinen, H. C. Knap, M. P Rissanen, S. Jørgensen, H. G. Kjaergaard, and T. Kurten. Unimolecular HO2 loss from peroxy radicals formed in autoxidation is unlikely under atmospheric conditions. *The Journal of Physical Chemistry A*, 120(20):3588–3595, 2016.

[39] J. D. Crounse, L. B. Nielsen, S. Jørgensen, H. G. Kjaergaard, and P. O. Wennberg. Autoxidation of organic compounds in the atmosphere. *The Journal of Physical Chemistry Letters*, 4(20):3513–3520, 2013.

[40] R. V. Otkjær, H. H. Jakobsen, C. M. Tram, and H. G. Kjaergaard. Calculated hydrogen shift rate constants in substituted alkyl peroxy radicals. *The Journal of Physical Chemistry A*, 122(43):8665–8673, 2018.

[41] S. Jørgensen, H. C. Knap, R. V. Otkjær, A. M. Jensen, M. LH. Kjeldsen, P. O. Wennberg, and H. G. Kjaergaard. Rapid hydrogen shift scrambling in hydroperoxy-substituted organic peroxy radicals. *The Journal of Physical Chemistry A*, 120(2):266–275, 2016.

[42] K. H. Møller, R. V. Otkjær, J. Chen, and H. G. Kjaergaard. Double bonds are key to fast unimolecular reactivity in first-generation monoterpene hydroxy peroxy radicals. *The Journal of Physical Chemistry A*, 124(14):2885–2896, 2020.

[43] L Vereecken, G Vu, A Wahner, A Kiendler-Scharr, and HMT Nguyen. A structure activity relationship for ring closure reactions in unsaturated alkylperoxy radicals. *Physical Chemistry Chemical Physics*, 23(31):16564–16576, 2021.

[44] J. Chen, K. H. Møller, P. O. Wennberg, and H. G. Kjaergaard. Unimolecular reactions following indoor and outdoor limonene ozonolysis. *The Journal of Physical Chemistry A*, 125(2):669–680, 2021.

[45] S. Iyer, M. P. Rissanen, R. Valiev, S. Barua, J. E. Krechmer, J. Thornton, M. Ehn, and T. Kurtén. Molecular mechanism for rapid autoxidation in α-pinene ozonolysis. *Nature communications*, 12(1):878, 2021.

[46] J. J. Orlando and G. S. Tyndall. Laboratory studies of organic peroxy radical chemistry: an overview with emphasis on recent issues of atmospheric significance. *Chemical Society Reviews*, 41(19):6294–6317, 2012.

[47] R. Atkinson. Kinetics and mechanisms of the gas-phase reactions of the hydroxyl radical with organic compounds under atmospheric conditions. *Chemical Reviews*, 86(1):69–201, 1986.

[48] P. D. Lightfoot, RA Cox, JN. Crowley, M. Destriau, GD. Hayman, ME. Jenkin, GK. Moortgat, and F. Zabel. Organic peroxy radicals: kinetics, spectroscopy and tropospheric chemistry. *Atmospheric Environment. Part A. General Topics*, 26(10):1805–1961, 1992.

[49] R. Atkinson. Gas-phase tropospheric chemistry of organic compounds: a review. *Atmospheric Environment. Part A. General Topics*, 24(1):1–41, 1990.

[50] W. Nie, C. Yan, L. Yang, P. Roldin, Y. Liu, A. L. Vogel, U. Molteni, D. Stolzenburg, H. Finkenzeller, A. Amorim, et al. NO at low concentration can enhance the formation of highly oxygenated biogenic molecules in the atmosphere. *Nature Communications*, 14(1):3347, 2023.

[51] Galib Hasan, Vili-Taneli Salo, Rashid R Valiev, Jakub Kubecka, and Theo Kurten. Comparing reaction routes for ^{3}(RO...OR') intermediates formed in peroxy radical self- and cross-reactions. *The Journal of Physical Chemistry A*, 124(40):8305–8320, 2020.

[52] R. R. Valiev, G. Hasan, V.-T. Salo, J. Kubecka, and T. Kurten. Intersystem crossings drive atmospheric gas-phase dimer formation. *The Journal of Physical Chemistry A*, 123(30):6596–6604, 2019.

[53] G Moortgat, B Veyret, and R Lesclaux. Absorption spectrum and kinetics of reactions of the acetylperoxy radical. *The Journal of Physical Chemistry*, 93(6):2362–2368, 1989.

[54] Dudley E Shallcross, M Teresa Raventos-Duran, Max W Bardwell, Asan Bacak, Zachary Solman, and Carl J Percival. A semi-empirical correlation for the rate coefficients for cross-and self-reactions of peroxy radicals in the gas-phase. *Atmospheric Environment*, 39(4):763–771, 2005.

[55] Eric Villenave and Robert Lesclaux. Kinetics of the cross reactions of CH3O2 and C2H5O2 radicals with selected peroxy radicals. *The Journal of Physical Chemistry*, 100(34):14372–14382, 1996.

[56] Otso Perakyla, Torsten Berndt, Lauri Franzon, Galib Hasan, Melissa Meder, Rashid R Valiev, Christopher David Daub, Jonathan G Varelas, Franz M Geiger, Regan J Thomson, et al. Large gas-phase source of esters and other accretion products in the atmosphere. *Journal of the American Chemical Society*, 145(14):7780–7790, 2023.

[57] T. Berndt, S. Richters, T. Jokinen, N. Hyttinen, T. Kurtén, R. V. Otkjær, H. G. Kjaergaard, F. Stratmann, H. Herrmann, M. Sipilä, et al. Hydroxyl radical-induced formation of highly oxidized organic compounds. *Nature communications*, 7(1):13677, 2016.

[58] S. Richters, H. Herrmann, and T. Berndt. Different pathways of the formation of highly oxidized multifunctional organic compounds (HOMs) from the gas-phase ozonolysis of β-caryophyllene. *Atmospheric Chemistry and Physics*, 16(15):9831–9845, 2016.

[59] T. Berndt, W. Scholz, B. Mentler, L. Fischer, H. Herrmann, M. Kulmala, and A. Hansel. Accretion product formation from self-and cross-reactions of RO2 radicals in the atmosphere. *Angewandte Chemie International Edition*, 57(14):3820–3824, 2018.

[60] J. E. Krechmer, M. Groessl, X. Zhang, H. Junninen, P. Massoli, A. T. Lambe, J. R. Kimmel, M. J. Cubison, S. Graf, Y-H. Lin, et al. Ion mobility spectrometry–mass spectrometry (IMS–MS) for on-and offline analysis of atmospheric gas and aerosol species. *Atmospheric Measurement Techniques*, 9(7):3245–3262, 2016.

[61] M. Rissanen. Anthropogenic volatile organic compound (AVOC) autoxidation as a source of highly oxygenated organic molecules (HOM). *The Journal of Physical Chemistry A*, 125(41):9027–9039, 2021.

[62] A. Kürten, L. Rondo, S. Ehrhart, and J. Curtius. Calibration of a chemical ionization mass spectrometer for the measurement of gaseous sulfuric acid. *The Journal of Physical Chemistry A*, 116(24):6375–6386, 2012.

[63] A. Kürten, A. Bergen, M. Heinritzi, M. Leiminger, V. Lorenz, F. Piel, M. Simon, R. Sitals, A. C. Wagner, and J. Curtius. Observation of new particle formation and measurement of sulfuric acid, ammonia, amines and highly oxidized organic molecules at a rural site in central germany. *Atmospheric Chemistry and Physics*, 16(19):12793–12813, 2016.

[64] T. Jokinen, M. Sipilä, H. Junninen, M. Ehn, G. Lönn, J. Hakala, T. Petäjä, RL. Mauldin III, M. Kulmala, and DR Worsnop. Atmospheric sulphuric acid and neutral cluster measurements using CI-APi-TOF. *Atmospheric Chemistry and Physics*, 12(9):4117–4125, 2012.

[65] N. Hyttinen, O. Kupiainen-M., M. P. Rissanen, M. Muuronen, M. Ehn, and T. Kurtén. Modeling the charging of highly oxidized cyclohexene ozonolysis products using nitrate-based chemical ionization. *The Journal of Physical Chemistry A*, 119(24):6339–6345, 2015.

[66] M. Bilde, K. Barsanti, M. Booth, C. D. Cappa, N. M. Donahue, E. U. Emanuelsson, G. McFiggans, U. K. Krieger, C. Marcolli, D. Topping, P. Ziemann, M. Barley, S. Clegg, B. Dennis-Smither, M. Hallquist, Ã. M. Hallquist, A. Khlystov, M. Kulmala, D. Mogensen, C. J. Percival, F. Pope, J. P. Reid, M. A. V. Ribeiro da S., T. Rosenoern, K. Salo, V. P. Soonsin, T. Yli-Juuti, N. L. Prisle, J. Pagels, J. Rarey, A. A. Zardini, and I. Riipinen. Saturation vapor pressures and transition enthalpies of low-volatility organic molecules of atmospheric relevance: From dicarboxylic acids to complex mixtures. *Chemical Reviews*, 115(10):4115–4156, 2015.

[67] J. G. Calvert. Glossary of atmospheric chemistry terms (Recommendations 1990). *Pure and Applied Chemistry*, 62(11):2167–2219, 1990.

[68] J. L. Little and A. S. Howard. Qualitative gas chromatography–mass spectrometry analyses using amines as chemical ionization reagent gases. *Journal of The American Society for Mass Spectrometry*, 24(12):1913–1918, 2013.

[69] M. P. Rissanen, J. Mikkilä, S. Iyer, and J. Hakala. Multi-scheme chemical ionization inlet (MION) for fast switching of reagent ion chemistry in atmospheric pressure chemical ionization mass spectrometry (CIMS) applications. *Atmospheric Measurement Techniques*, 12(12):6635–6646, 2019.

[70] Xu-C. He, J. Shen, S. Iyer, P. Juuti, J. Zhang, M. Koirala, M. M. Kytökari, D. R. Worsnop, M. Rissanen, M. Kulmala, et al. Characterisation of gaseous iodine species detection using the multi-scheme chemical ionisation inlet 2 with bromide and nitrate chemical ionisation methods. *Atmospheric Measurement Techniques*, 16(19):4461–4487, 2023.

[71] C. L. Yaws. *The Yaws handbook of vapor pressure: Antoine coefficients*. Gulf Professional Publishing, 2015.

[72] E. Denisov, E. Damoc, and A. Makarov. Exploring frontiers of orbitrap performance for long transients. *International Journal of Mass Spectrometry*, 466:116607, 2021.

[73] J-P. Hauschild, A. C. Peterson, E. Couzijn, E. Denisov, D. Chernyshev, C. Hock, H. Stewart, R. Hartmer, D. Grinfeld, C. Thoeing, et al. A novel family of quadrupole-orbitrap mass spectrometers for a broad range of analytical applications. 2020.

[74] A. Makarov. Electrostatic axially harmonic orbital trapping: a high-performance technique of mass analysis. *Analytical chemistry*, 72(6):1156–1162, 2000.

[75] R. Cai, Y. Li, Y. Clément, D. Li, C. Dubois, M. Fabre, L. Besson, S. Perrier, C. George, M. Ehn, et al. Orbitool: a software tool for analyzing online orbitrap mass spectrometry data. *Atmospheric Measurement Techniques Discussions*, 2020:1–23, 2020.

[76] G. Hasan, R. R. Valiev, V.-T. Salo, and T. Kurtén. Computational investigation of the formation of peroxide (ROOR) accretion products in the OH-and NO3-initiated oxidation of α-pinene. *The Journal of Physical Chemistry A*, 125(50):10632–10639, 2021.

[77] G. Hasan, V.-T. Salo, T. Golin A., R. R. Valiev, and T. Kurtén. Computational investigation of substituent effects on the alcohol + carbonyl channel of peroxy radical self-and cross-reactions. *The Journal of Physical Chemistry A*, 127(7):1686–1696, 2023.

[78] D. Pasik, B. N. Frandsen, M. Meder, S. Iyer, T. Kurtén, and N. Myllys. Gas-phase oxidation of atmospherically relevant unsaturated hydrocarbons by acyl peroxy radicals. *Journal of the American Chemical Society*, 146(19):13427–13437, 2024.

[79] Torsten Berndt, Hartmut Herrmann, and Theo Kurten. Direct probing of criegee intermediates from gas-phase ozonolysis using chemical ionization mass spectrometry. *Journal of the American Chemical Society*, 139(38):13387–13392, 2017.

[80] Marc-Christopher Reinnig, Jörg Warnke, and Thorsten Hoffmann. Identification of organic hydroperoxides and hydroperoxy acids in secondary organic aerosol formed during the ozonolysis of different monoterpenes and sesquiterpenes by on-line analysis using atmospheric pressure chemical ionization ion trap mass spectrometry. *Rapid Communications in Mass Spectrometry: An International Journal Devoted to the Rapid Dissemination of Up-to-the-Minute Research in Mass Spectrometry*, 23(11):1735–1741, 2009.

[81] Michal Holčapek, Robert Jirásko, and Miroslav Lísa. Basic rules for the interpretation of atmospheric pressure ionization mass spectra of small molecules. *Journal of Chromatography A*, 1217(25):3908–3921, 2010.

[82] Torsten Berndt. Peroxy radical and product formation in the gas-phase ozonolysis of α-pinene under near-atmospheric conditions: Occurrence of an additional series of peroxy radicals O, O–C10H15O (O2) y O2 with y= 1–3. *The Journal of Physical Chemistry A*, 126(37):6526–6537, 2022.

[83] Shawon Barua, Siddharth Iyer, Avinash Kumar, Prasenjit Seal, and Matti Rissanen. An aldehyde as a rapid source of secondary aerosol precursors: theoretical and experimental study of hexanal autoxidation. *Atmospheric Chemistry and Physics*, 23(18):10517–10532, 2023.

[84] Ziwei Mo, Min Shao, and Sihua Lu. Compilation of a source profile database for hydrocarbon and OVOC emissions in china. *Atmospheric Environment*, 143:209–217, 2016.

Appendix A. Proposed molecular formulae of ions detected in the cyclooctene experiments using negative polarity ionization.

A.1 Proposed molecular formulae of ions detected in the oxidation of cyclooctene at a reaction time of 10.75 s.

Table A.1: Molecular formulae in the range of M/Z 193 - 350 using negative polarity ionization with high reaction time.

Molecular formula	Theoretical M/Z	Experimental M/Z	Molecular formula	Theoretical M/Z	Experimental M/Z
$C_6H_{11}O_3NO_3$-	193.0592	193.0596	$C_7H_{13}O_7NO_3$-	271.0545	271.0558
$C_6H_{11}O_4NO_3$-	209.0541	209.0547	$C_7H_{14}O_7NO_3$-	272.0623	272.0630
$C_7H_{11}O_4NO_3$-	221.0541	221.0546	$C_7H_{15}O_7NO_3$-	273.0701	272.0666
$C_6H_{10}O_5NO_3$-	224.0412	224.0421	$C_8H_{10}O_7NO_3$-	280.0310	280.0319
$C_6H_{11}O_5NO_3$-	225.0490	225.0496	$C_8H_{12}O_7NO_3$-	282.0467	282.0474
$C_8H_{13}O_4NO_3$-	235.0698	235.0708	$C_8H_{13}O_7NO_3$-	283.0545	283.0508
$C_8H_{14}O_4NO_3$-	236.0776	236.0782	$C_8H_{14}O_7NO_3$-	284.0623	284.0629
$C_7H_{11}O_5NO_3$-	237.0490	237.0496	$C_8H_{14}O_8NO_3$-	285.0701	285.0665
$C_7H_{12}O_5NO_3$-	238.0568	238.0574	$C_7H_{15}O_7NO_3$-	288.0572	288.0586
$C_7H_{13}O_5NO_3$-	239.0647	239.0600	$C_8H_{10}O_8NO_3$-	296.0259	296.0266
$C_7H_{14}O_5NO_3$-	240.0725	240.0732	$C_8H_{12}O_8NO_3$-	298.0416	298.0424
$C_6H_{11}O_6NO_3$-	241.0439	241.0446	$C_8H_{13}O_8NO_3$-	299.0494	299.0503
$C_8H_{12}O_5NO_3$-	250.0568	250.0587	$C_8H_{14}O_8NO_3$-	300.0572	300.0580
$C_8H_{13}O_5NO_3$-	251.0647	251.0609	$C_8H_{15}O_8NO_3$-	301.0651	301.0618
$C_8H_{14}O_5NO_3$-	252.0725	252.0731	$C_8H_{11}O_9NO_3$-	313.0287	313.0306
$C_7H_{11}O_6NO_3$-	253.0439	253.0446	$C_8H_{12}O_9NO_3$-	314.0365	314.0374
$C_7H_{12}O_6NO_3$-	254.0518	254.0526	$C_8H_{13}O_9NO_3$-	315.0443	315.0431
$C_7H_{13}O_6NO_3$-	255.0596	255.0605	$C_8H_{14}O_9NO_3$-	316.0521	316.0529
$C_7H_{14}O_6NO_3$-	256.0674	256.0683	$C_8H_{15}O_9NO_3$-	317.0600	317.0572
$C_7H_{15}O_6NO_3$-	257.0752	257.0718	$C_8H_{12}O_{10}NO_3$-	330.0314	330.0324
$C_8H_{12}O_6NO_3$-	266.0518	266.0525	$C_8H_{13}O_{10}NO_3$-	331.0392	331.0402
$C_8H_{13}O_6NO_3$-	267.0596	267.0604	$C_8H_{14}O_{10}NO_3$-	332.0471	332.0480
$C_8H_{14}O_6NO_3$-	268.0674	268.0681	$C_8H_{15}O_{10}NO_3$-	333.0549	333.0522
$C_8H_{15}O_6NO_3$-	269.0752	269.0716	$C_8H_{12}O_{11}NO_3$-	346.0263	346.0271
$C_7H_{12}O_7NO_3$-	270.0467	270.0474	$C_8H_{14}O_{11}NO_3$-	348.0420	348.0424

Table A.2: Molecular formulae in the range of M/Z 360 - 540 using negative polarity ionization and high reaction time.

Molecular formula	Theoretical M/Z	Experimental M/Z	Molecular formula	Theoretical M/Z	Experimental M/Z
$C_{16}H_{30}O_5NO_3$-	348.2028	348.2042	$C_{16}H_{26}O_9NO_3$-	424.1460	424.1472
$C_{16}H_{26}O_5NO_3$-	360.1664	360.1673	$C_{16}H_{28}O_9NO_3$-	426.1617	426.1628
$C_{16}H_{28}O_5NO_3$-	362.1820	362.1831	$C_{15}H_{26}O_{10}NO_3$-	428.1410	428.1422
$C_{15}H_{26}O_6NO_3$-	364.1602	364.1621	$C_{14}H_{24}O_{11}NO_3$-	430.1202	430.1209
$C_{16}H_{30}O_5NO_3$-	364.1977	364.1990	$C_{16}H_{26}O_{10}NO_3$-	440.1410	440.1421
$C_8H_{15}O_{12}NO_3$-	365.0447	365.0499	$C_{16}H_{28}O_{10}NO_3$-	442.1566	442.1583
$C_{15}H_{28}O_6NO_3$-	366.1770	366.1792	$C_{15}H_{26}O_{11}NO_3$-	444.1359	444.1372
$C_{14}H_{26}O_7NO_3$-	368.1562	368.1575	$C_{16}H_{30}O_{10}NO_3$-	444.1723	444.1625
$C_{16}H_{26}O_6NO_3$-	376.1613	376.1621	$C_{15}H_{28}O_{11}NO_3$-	446.1515	446.1418
$C_{16}H_{28}O_6NO_3$-	378.1770	378.1780	$C_{16}H_{24}O_{11}NO_3$-	454.1202	454.1212
$C_{15}H_{26}O_7NO_3$-	380.1562	380.1573	$C_{16}H_{26}O_{11}NO_3$-	456.1359	456.1371
$C_{15}H_{28}O_7NO_3$-	382.1719	382.1730	$C_{16}H_{28}O_{11}NO_3$-	458.1515	458.1537
$C_{14}H_{26}O_7NO_3$-	384.1511	384.1519	$C_{15}H_{26}O_{12}NO_3$-	460.1308	460.1320
$C_{16}H_{26}O_7NO_3$-	392.1562	392.1566	$C_{15}H_{28}O_{12}NO_3$-	462.1464	462.1370
$C_{16}H_{28}O_7NO_3$-	394.1708	394.1711	$C_{16}H_{26}O_{12}NO_3$-	472.1308	472.1320
$C_{15}H_{26}O_8NO_3$-	396.1511	396.1523	$C_{16}H_{28}O_{12}NO_3$-	474.1464	474.1376
$C_{15}H_{28}O_8NO_3$-	398.1668	398.1687	$C_{15}H_{26}O_{13}NO_3$-	476.1257	476.1268
$C_{14}H_{26}O_9NO_3$-	400.1460	400.1468	$C_{16}H_{26}O_{13}NO_3$-	488.1257	488.1270
$C_{16}H_{26}O_8NO_3$-	408.1511	408.1522	$C_{15}H_{24}O_{14}NO_3$-	490.1039	490.1068
$C_{16}H_{28}O_8NO_3$-	410.1668	410.1694	$C_{15}H_{26}O_{14}NO_3$-	492.1206	492.1210
$C_{15}H_{26}O_9NO_3$-	412.1460	412.1471	$C_{16}H_{26}O_{14}NO_3$-	504.1206	504.1219
$C_{15}H_{28}O_9NO_3$-	414.1617	414.1653	$C_{16}H_{26}O_{15}NO_3$-	520.1155	520.1169
$C_{15}H_{28}O_9NO_3$-	416.1035	416.1057	$C_{16}H_{26}O_{16}NO_3$-	536.1105	536.1124
$C_{14}H_{26}O_{10}NO_3$-	416.1399	416.1427			

A.2 Proposed molecular formulae of ions detected in the cyclooctene experiments with 0.33 s reaction time and negative polarity ionization.

Table A.3: Proposed molecular formulae of HOM detected from cyclooctene using negative polarity ionization with 0.33 s reaction time.

Molecular formula	Theoretical M/Z	Experimental M/Z	Molecular formula	Theoretical M/Z	Experimental M/Z
$C_8H_{13}O_4NO_3$-	235.0687	235.0719	$C_8H_{12}O_7NO_3$-	282.0456	282.0494
$C_8H_{14}O_4NO_3$-	236.0765	236.0799	$C_8H_{13}O_7NO_3$-	283.0534	283.0570
$C_7H_{13}O_5NO_3$-	239.0636	239.0667	$C_8H_{14}O_7NO_3$-	284.0612	284.0646
$C_8H_{12}O_5NO_3$-	250.0557	250.0589	$C_8H_{13}O_8NO_3$-	299.0483	299.0519
$C_8H_{13}O_6NO_3$-	267.0596	267.0619	$C_8H_{13}O_9NO_3$-	315.0432	315.0475
$C_8H_{14}O_6NO_3$-	268.0663	268.0654	$C_8H_{13}O_{10}NO_3$-	331.0381	331.0424
$C_7H_{13}O_7NO_3$-	271.0534	271.0563			

Appendix B. Proposed molecular formulae of ions detected in the 1,5-cyclooctadiene experiments with negative polarity ionization.

B.1 Proposed molecular formulae of HOM detected with negative polarity ionization and long reaction time.

Table B.1: Proposed molecular formulae of HOM formed detected with 1,5-cyclooctadiene using negative polarity ionization and reaction time of 10.70 s (up until m/z 300).

Molecular formula	Theoretical M/Z	Experimental M/Z	Molecular formula	Theoretical M/Z	Experimental M/Z
$C_8H_{12}O_3NO_3$-	218.0670	218.0676	$C_6H_{10}O_7NO_3$-	256.0310	256.0316
$C_7H_{10}O_4NO_3$-	220.0463	220.0469	$C_6H_{12}O_7NO_3$-	258.0467	258.0472
$C_6H_8O_5NO_3$-	222.0255	222.0260	$C_8H_9O_6NO_3$-	263.0283	263.0289
$C_6H_{10}O_5NO_3$-	224.0412	224.0416	$C_8H_{10}O_6NO_3$-	264.0361	264.0368
$C_6H_{11}O_5NO_3$-	225.0490	225.0453	$C_8H_{11}O_6NO_3$-	265.0439	265.0447
$C_6H_{12}O_5NO_3$-	226.0568	226.0574	$C_8H_{12}O_6NO_3$-	266.0518	266.0525
$C_8H_{10}O_4NO_3$-	232.0463	232.0467	$C_8H_{13}O_6NO_3$-	267.0596	267.0609
$C_8H_{11}O_4NO_3$-	233.0541	233.0547	$C_8H_{14}O_6NO_3$-	268.0674	268.0681
$C_8H_{12}O_4NO_3$-	234.0619	234.0625	$C_7H_{11}O_7NO_3$-	269.0388	269.0401
$C_8H_{13}O_4NO_3$-	235.0698	235.0650	$C_7H_{12}O_7NO_3$-	270.0467	270.0474
$C_7H_{10}O_5NO_3$-	236.0412	236.0418	$C_7H_{13}O_7NO_3$-	271.0545	271.0509
$C_7H_{11}O_5NO_3$-	237.0490	237.0479	$C_6H_{11}O_8NO_3$-	273.0338	273.0345
$C_7H_{12}O_5NO_3$-	238.0568	238.0574	$C_6H_{12}O_8NO_3$-	274.0416	274.0427
$C_7H_{13}O_5NO_3$-	239.0647	239.0611	$C_8H_{10}O_7NO_3$-	280.0310	280.0317
$C_6H_{10}O_6NO_3$-	240.0361	240.0367	$C_8H_{12}O_7NO_3$-	282.0467	282.0473
$C_6H_{11}O_6NO_3$-	241.0439	241.0446	$C_8H_{13}O_7NO_3$-	283.0545	283.0507
$C_8H_8O_5NO_3$-	246.0255	246.0256	$C_7H_{10}O_8NO_3$-	284.0259	284.0266
$C_8H_{10}O_5NO_3$-	248.0412	248.0419	$C_7H_{11}O_8NO_3$-	285.0338	285.0335
$C_8H_{11}O_5NO_3$-	249.0490	249.0495	$C_7H_{12}O_8NO_3$-	286.0416	286.0423
$C_8H_{12}O_5NO_3$-	250.0568	250.0575	$C_7H_{13}O_8NO_3$-	287.0494	287.0458
$C_8H_{13}O_5NO_3$-	251.0647	251.0664	$C_8H_{10}O_8NO_3$-	296.0259	296.0267
$C_7H_{10}O_6NO_3$-	252.0361	252.0367	$C_8H_{11}O_8NO_3$-	297.0338	297.0345
$C_7H_{11}O_6NO_3$-	253.0439	253.0394	$C_8H_{12}O_8NO_3$-	298.0416	298.0423
$C_7H_{12}O_6NO_3$-	254.0512	254.0524	$C_8H_{13}O_8NO_3$-	299.0494	299.0461
$C_7H_{13}O_6NO_3$-	255.0596	255.0602	$C_7H_{10}O_9NO_3$-	300.0208	300.0217

Table B.2: Proposed molecular formulae of HOM formed detected with 1,5-cyclooctadiene using negative polarity ionization and reaction time of 10.70 s (up until m/z 532).

Molecular formula	Theoretical M/Z	Experimental M/Z	Molecular formula	Theoretical M/Z	Experimental M/Z
$C_7H_{11}O_9NO_3$-	301.0287	301.0295	$C_{13}H_{20}O_9NO_3$-	382.0991	382.1003
$C_7H_{12}O_9NO_3$-	302.0365	302.0374	$C_{16}H_{24}O_7NO_3$-	390.1406	390.1417
$C_7H_{13}O_9NO_3$-	303.0443	303.0411	$C_{16}H_{26}O_7NO_3$-	392.1562	392.1576
$C_8H_{10}O_9NO_3$-	312.0208	312.0216	$C_{15}H_{24}O_8NO_3$-	394.1355	394.1364
$C_8H_{12}O_9NO_3$-	314.0365	314.0373	$C_{16}H_{26}O_8NO_3$-	408.1511	408.1523
$C_8H_{13}O_9NO_3$-	315.0443	315.0428	$C_{14}H_{20}O_{10}NO_3$-	410.0940	410.0950
$C_8H_{14}O_9NO_3$-	316.0521	316.0530	$C_{15}H_{24}O_9NO_3$-	410.1304	410.1314
$C_7H_{12}O_{10}NO_3$-	318.0314	318.0324	$C_{14}H_{20}O_{10}NO_3$-	412.1097	412.1115
$C_8H_{10}O_{10}NO_3$-	328.0158	328.0170	$C_{16}H_{24}O_9NO_3$-	422.1304	422.1315
$C_8H_{11}O_{10}NO_3$-	329.0236	329.0246	$C_{15}H_{24}O_{10}NO_3$-	426.1253	426.1265
$C_8H_{12}O_{10}NO_3$-	330.0314	330.0323	$C_{16}H_{22}O_{10}NO_3$-	436.1097	436.1108
$C_8H_{13}O_{10}NO_3$-	331.0392	331.0363	$C_{16}H_{24}O_{10}NO_3$-	438.1253	438.1267
$C_8H_{10}O_{11}NO_3$-	344.0107	344.0117	$C_{15}H_{22}O_{11}NO_3$-	440.1046	440.1057
$C_{16}H_{26}O_4NO_3$-	344.1715	344.1725	$C_{14}H_{22}O_{12}NO_3$-	444.0995	444.1007
$C_8H_{11}O_{11}NO_3$-	345.0185	345.0186	$C_{16}H_{24}O_{11}NO_3$-	454.1202	454.1214
$C_8H_{12}O_{11}NO_3$-	346.0263	346.0272	$C_{16}H_{22}O_{12}NO_3$-	468.0995	468.1007
$C_{14}H_{22}O_6NO_3$-	348.1289	348.1306	$C_{16}H_{24}O_{12}NO_3$-	470.1151	470.1169
$C_{12}H_{16}O_8NO_3$-	350.0718	350.0738	$C_{15}H_{22}O_{13}NO_3$-	472.0944	472.0956
$C_{13}H_{20}O_7NO_3$-	350.1082	350.1097	$C_{14}H_{22}O_{14}NO_3$-	476.0893	476.0905
$C_{12}H_{18}O_8NO_3$-	352.0874	352.0887	$C_{16}H_{22}O_{13}NO_3$-	484.0944	484.0955
$C_{16}H_{26}O_5NO_3$-	360.1664	360.1665	$C_{16}H_{24}O_{13}NO_3$-	486.1101	486.1115
$C_8H_{12}O_{12}NO_3$-	362.0212	362.0219	$C_{15}H_{22}O_{14}NO_3$-	488.0893	488.0908
$C_{15}H_{24}O_6NO_3$-	362.1457	362.1461	$C_{16}H_{22}O_{14}NO_3$-	500.0893	500.0905
$C_{14}H_{22}O_7NO_3$-	364.1249	364.1257	$C_{16}H_{22}O_{15}NO_3$-	516.0842	516.0862
$C_{14}H_{23}O_7NO_3$-	365.0447	365.0509	$C_{16}H_{24}O_{15}NO_3$-	518.0999	518.1022
$C_{14}H_{24}O_7NO_3$-	366.1406	366.1415	$C_{16}H_{22}O_{16}NO_3$-	532.0792	532.0806
$C_{12}H_{18}O_9NO_3$-	368.0834	368.0844			
$C_{16}H_{24}O_6NO_3$-	374.1457	374.1465			
$C_{16}H_{26}O_6NO_3$-	376.1613	376.1624			
$C_{14}H_{22}O_8NO_3$-	380.1198	380.1209			

B.2 Proposed molecular formulae of HOM detected using 1,5-cyclooctadiene with negative polarity ionization and reaction time of 0.35 s

Table B.3: Proposed molecular formulae of detected ions using negative polarity ionization with 0.35 s reaction time.

Molecular formula	Theoretical M/Z	Experimental M/Z	Molecular formula	Theoretical M/Z	Experimental M/Z
$C_6H_9O_4NO_3$-	207.0374	207.0403	$C_8H_{11}O_7NO_3$-	281.0378	281.0413
$C_7H_{10}O_4NO_3$-	220.0452	220.0479	$C_8H_{12}O_7NO_3$-	282.0456	282.0491
$C_8H_{11}O_4NO_3$-	233.0530	233.0559	$C_7H_{11}O_8NO_3$-	285.0327	285.0364
$C_7H_{11}O_5NO_3$-	237.0479	237.0511	$C_8H_{11}O_8NO_3$-	297.0327	297.0363
$C_6H_{11}O_6NO_3$-	241.0428	241.0459	$C_8H_{12}O_8NO_3$-	298.0405	298.0396
$C_7H_{11}O_6NO_3$-	253.0428	253.0460	$C_7H_{11}O_9NO_3$-	301.0276	301.0310
$C_8H_{11}O_6NO_3$-	265.0687	265.0719	$C_8H_{11}O_{10}NO_3$-	329.0225	329.0262
$C_7H_{11}O_7NO_3$-	269.0378	269.0412	$C_{16}H_{22}O_{14}NO_3$-	500.0882	500.0926
$C_6H_{11}O_8NO_3$-	273.0327	273.0361			

Appendix C. Proposed molecular formulae of HOM of the positive-polarity ionization experiments with 1,5-cyclooctadiene and cyclooctene

Table C.1: Proposed molecular formulae of HOM detected with 1,5-cyclooctadiene using positive-polarity ionization and reaction time of 0.63 s.

Molecular formula	Theoretical M/Z	Experimental M/Z	Molecular formula	Theoretical M/Z	Experimental M/Z
$C_8H_8OC_2H_9N_2+$	181.1335	181.1343	$C_8H_{10}O_4C_2H_9N_2+$	231.1339	231.1358
$C_8H_{10}OC_2H_9N_2+$	183.1492	183.1500	$C_8H_{12}O_4C_2H_9N_2+$	233.1496	233.1507
$C_8H_{10}O_2C_2H_9N_2+$	199.1441	199.1451	$C_8H_{12}O_7C_2H_9N_2+$	281.1343	281.1359
$C_8H_{11}OC_2H_9N_2+$	200.1519	200.1484	$C_8H_{12}O_4C_2H_9N_2+$	296.1214	296.1230
$C_8H_{12}OC_2H_9N_2+$	201.1598	201.1608	$C_{16}H_{24}O_9C_2H_9N_2+$	421.2181	421.2194
$C_7H_{10}O_3C_2H_9N_2+$	203.1390	203.1400	$C_{16}H_{22}O_{12}C_2H_9N_2+$	467.1872	467.1894
$C_9H_{12}OC_2H_9N_2+$	213.1598	213.1606	$C_{15}H_{22}O_{13}C_2H_9N_2+$	471.1821	471.1837
$C_8H_{10}O_3C_2H_9N_2+$	215.1390	215.1407	$C_{16}H_{21}O_{13}C_2H_9N_2+$	481.1664	481.1686
$C_8H_{12}O_3C_2H_9N_2+$	217.1547	217.1557	$C_{16}H_{22}O_{14}C_2H_9N_2+$	499.1770	499.1787
$C_9H_{14}O_2C_2H_9N_2+$	227.1390	227.1766			

Table C.2: Proposed molecular formulae of HOM detected with cyclooctene using positive-polarity ionization and reaction time of 0.59 s.

Molecular formula	Theoretical M/Z	Experimental M/Z	Molecular formula	Theoretical M/Z	Experimental M/Z
$C_7H_{10}OC_2H_9N_2+$	171.1503	171.1492	$C_{10}H_{16}O_3C_2H_9N_2+$	245.1878	245.1860
$C_8H_{11}OC_2H_9N_2+$	184.1570	184.1579	$C_8H_{12}O_5C_2H_9N_2+$	249.1472	249.1463
$C_8H_{12}O_2C_2H_9N_2+$	185.1648	185.1660	$C_8H_{14}O_5C_2H_9N_2+$	251.1618	251.1602
$C_7H_{12}O_2C_2H_9N_2+$	189.1598	189.1609	$C_{18}H_{22}O_1C_2H_9N_2+$	329.2465	329.2462
$C_8H_{10}O_2C_2H_9N_2+$	199.1441	199.1453	$C_{15}H_{28}O_4C_2H_9N_2+$	333.2761	333.2748
$C_8H_{12}O_2C_2H_9N_2+$	203.1598	201.1610	$C_{16}H_{26}O_4C_2H_9N_2+$	343.2618	343.2591
$C_8H_{14}O_2C_2H_9N_2+$	203.1767	203.1754	$C_{15}H_{26}O_5C_2H_9N_2+$	347.2541	347.2563
$C_9H_{12}OC_2H_9N_2+$	213.1611	213.1598	$C_{16}H_{30}O_4C_2H_9N_2+$	347.2904	347.2919
$C_9H_{14}O_2C_2H_9N_2+$	215.1768	215.1754	$C_{16}H_{24}O_5C_2H_9N_2+$	357.2384	357.2407
$C_8H_{12}O_3C_2H_9N_2+$	217.1547	217.1560	$C_{16}H_{28}O_5C_2H_9N_2+$	361.2697	361.2719
$C_8H_{14}O_3C_2H_9N_2+$	219.1717	219.1703	$C_{16}H_{26}O_6C_2H_9N_2+$	375.2490	375.2511
$C_8H_{12}O_4C_2H_9N_2+$	233.1510	233.1496	$C_{16}H_{28}O_6C_2H_9N_2+$	377.2646	377.2672
$C_9H_{16}O_3C_2H_9N_2+$	233.1875	233.1860	$C_{16}H_{24}O_7C_2H_9N_2+$	389.2282	389.2315
$C_8H_{14}O_4C_2H_9N_2+$	235.1667	235.1652	$C_{16}H_{28}O_9C_2H_9N_2+$	425.2494	425.2520

Appendix D. Extra mass spectra

D.1 Zoom into the monomer and accretion products of ∼ 10.7 s measurements of cyclooctene and 1,5-cyclooctadiene.

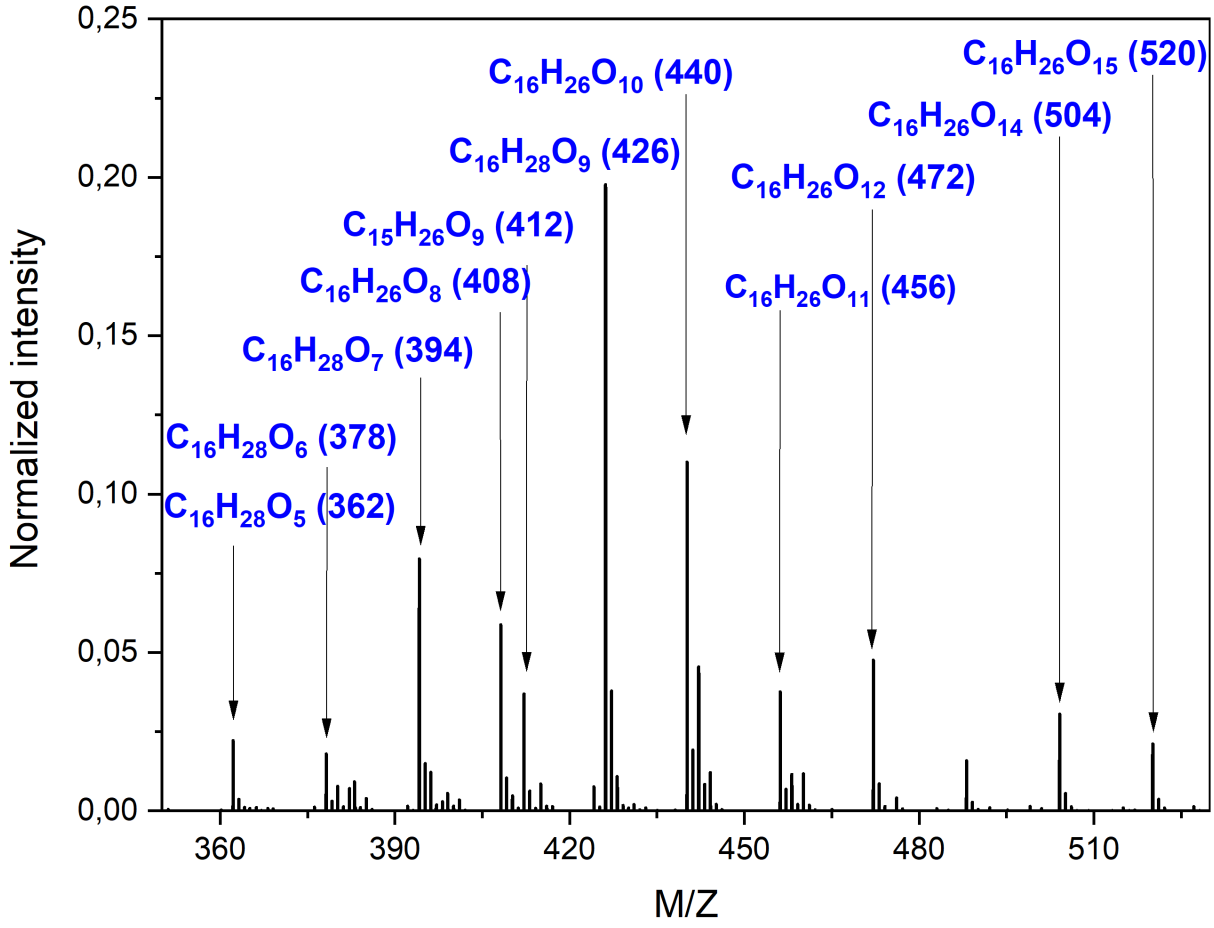

Figure D.1: A zoom of the accretion product peaks of the chemical ionization mass spectrum measured using NO_3- as the chemical ionization reagent and cyclooctene as the precursor. All products were detected as adduct of NO_3-, which is included in the M/Z ratios of products, but excluded from the molecular formulas for clarity. A concentration of 4.02 ppm of cyclooctene, and a reaction time of 10.75 s were used.

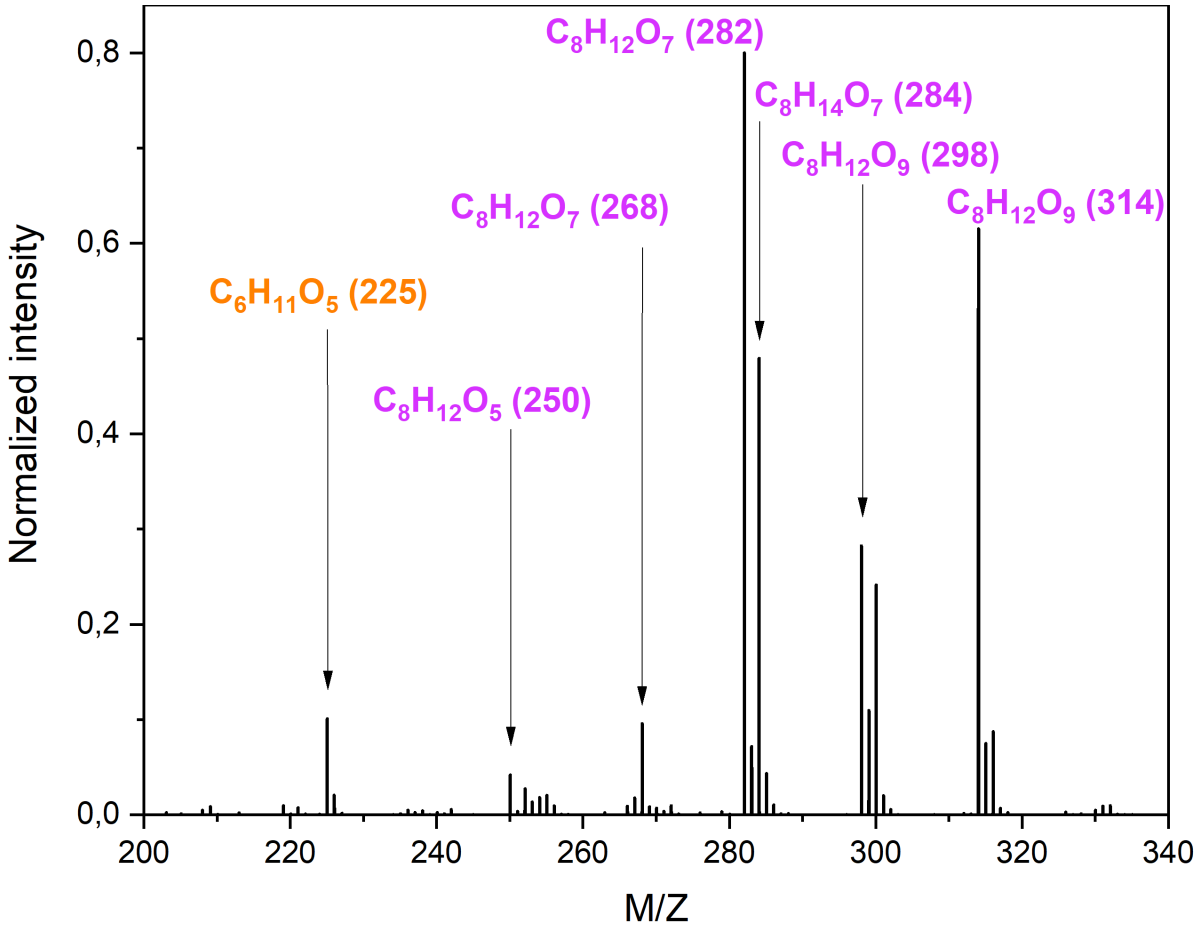

Figure D.2: A zoom of the monomer product peaks of the chemical ionization mass spectrum measured using NO_3- as the chemical ionization reagent and cyclooctene as the precursor. All products were detected as adduct of NO_3-, which is included in the M/Z ratios of products, but excluded from the molecular formulas for clarity. A concentration of 4.02 ppm of cyclooctene, and a reaction time of 10.75 s were used.

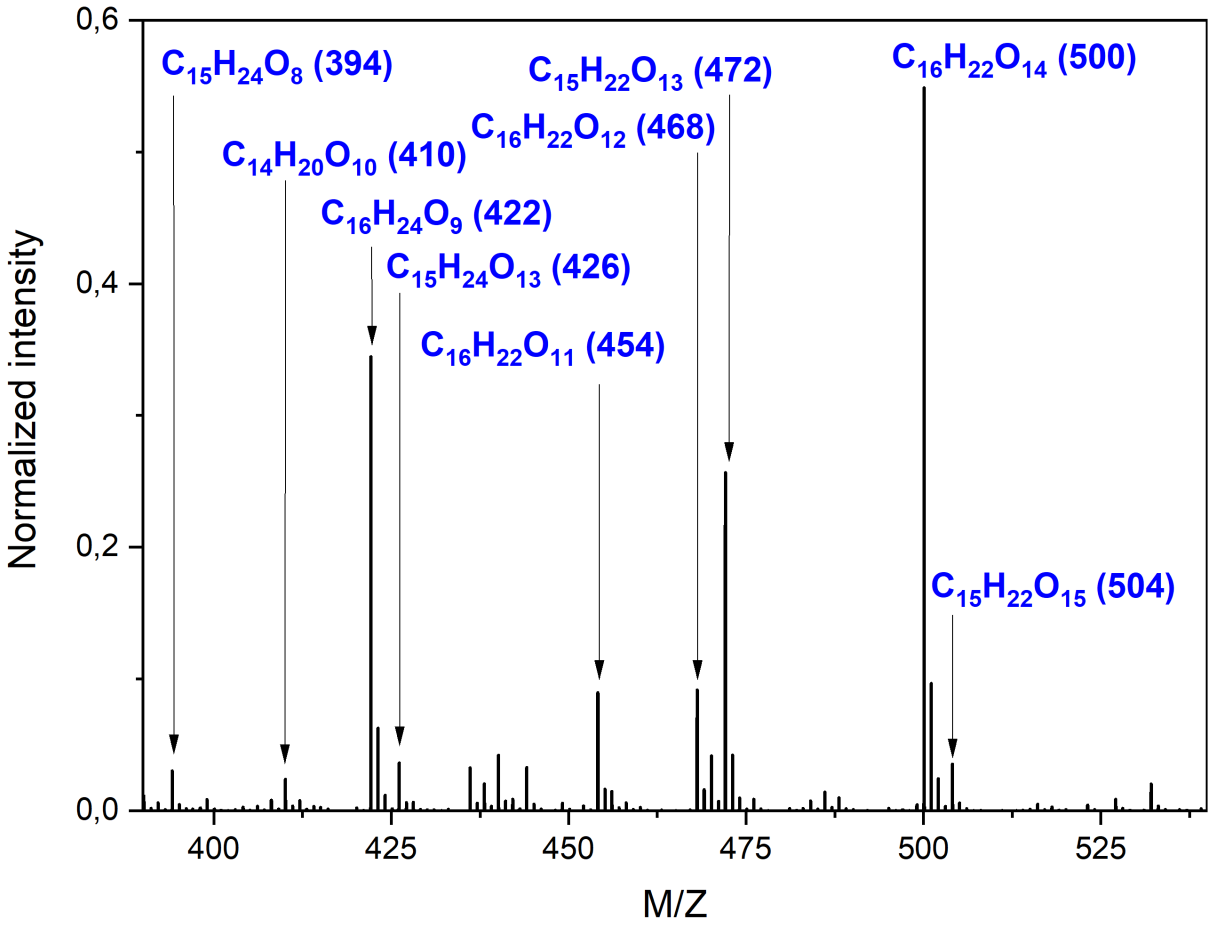

Figure D.3: A zoom of the accretion product peaks of the chemical ionization mass spectrum measured using NO_3- as the chemical ionization reagent and 1,5-cyclooctadiene as the precursor. All products were detected as adduct of NO_3-, which is included in the M/Z ratios of products, but excluded from the molecular formulas for clarity. A concentration of 6.1 ppm of 1,5-cyclooctadiene, and a reaction time of 10.70 s were used.

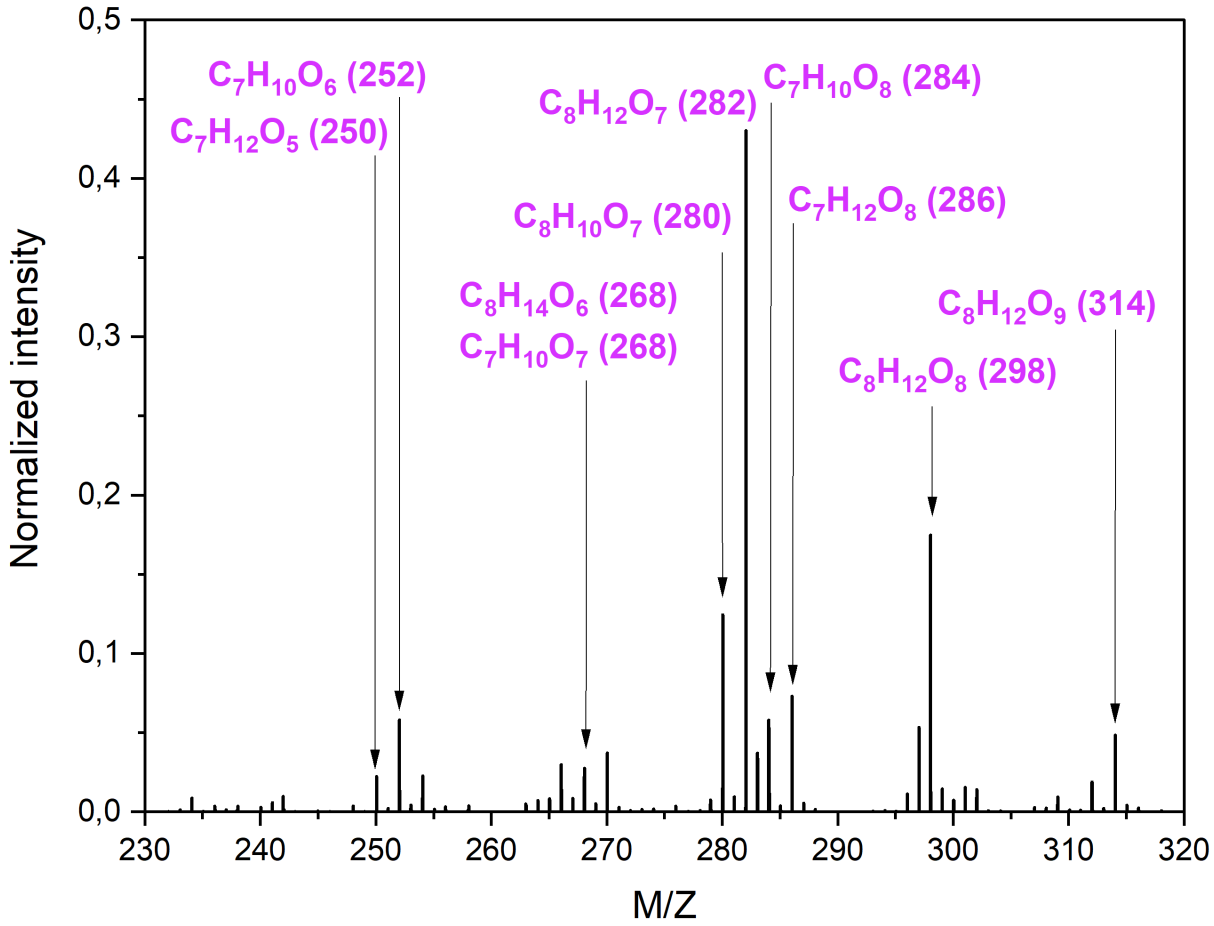

Figure D.4: A zoom of the monomer product peaks of the chemical ionization mass spectrum measured using NO_3- as the chemical ionization reagent and 1,5-cyclooctadiene as the precursor. All products were detected as adduct of NO_3-, which is included in the M/Z ratios of products, but excluded from the molecular formulas for clarity. A concentration of 6.1 ppm of 1,5-cyclooctadiene, and a reaction time of 10.70 s were used.

D.2 Positive mode spectrum of 1,5-cyclooctadiene, reaction time 0.33 s

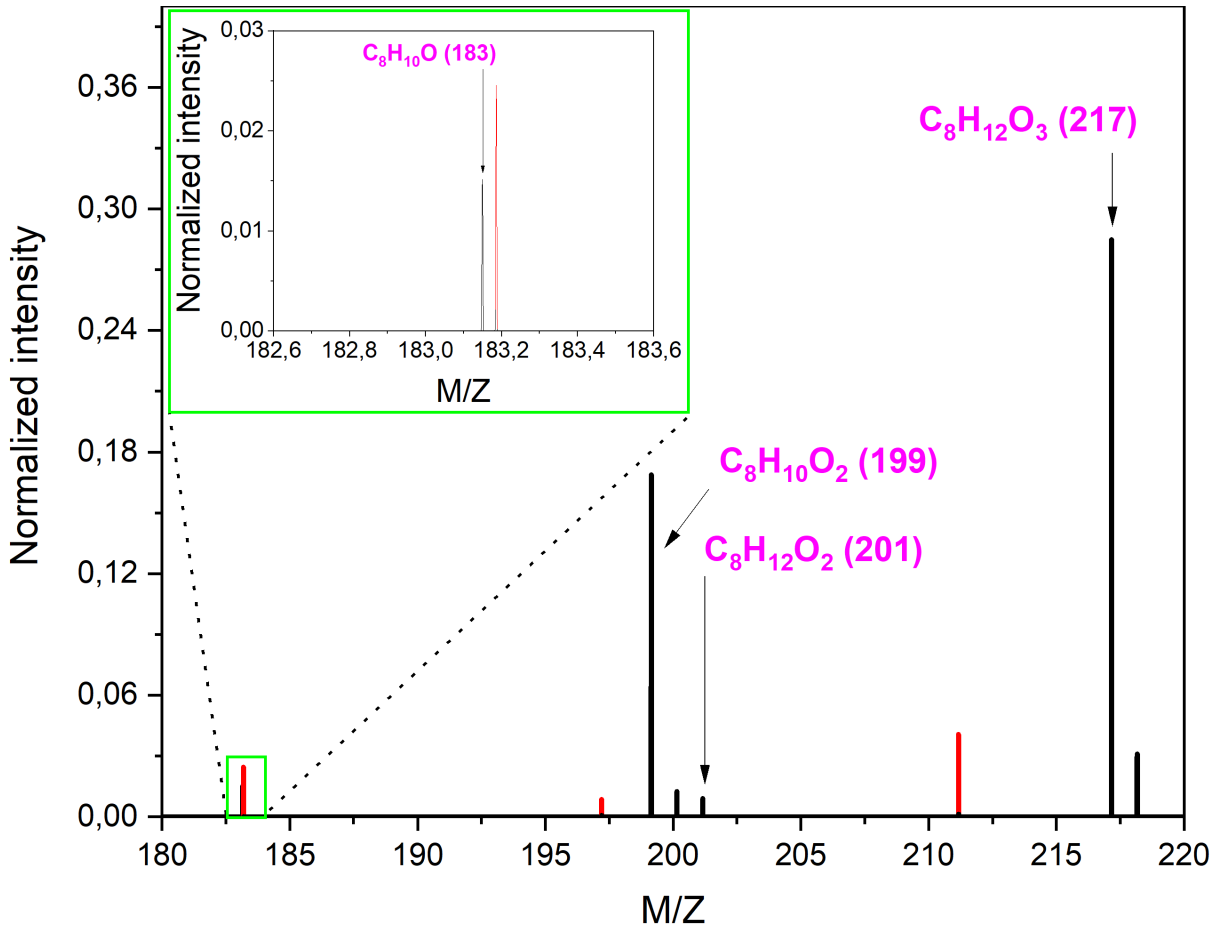

Figure D.5: Positive mode chemical ionization mass spectrum using a 3,35 ppm concentration of 1,5-cyclooctadiene as the precursor, and a reaction time of 0.33 s. All products were detected as adducts of EDA(H+) ($C_2H_9N_2+$), and the M/Z ratios include the mass of EDA(H+), but it is excluded from the molecular formulas for clarity.

Appendix E. Python programs

Two different python programs were used. The codes of these programs are presented in the following Sections.

E.1 Program for the mass spectra

```
import pandas as pd
import matplotlib.pyplot as plt
import numpy as np
# Read data and form DataFrame-object
data_files = ['C:/data/path1','C:/data/path2','C:/data/path3',
'C:/data/path4','C:/data/path5']
data_names = ['3.336 ppm', '1.668 ppm', '0.3336 ppm',
'0.1668 ppm', '0.0336 ppm']

dfs = [pd.read_csv(file) for file in data_files]

# Normalize all DataFrame-objects and name them

#normalization positive mode
#for name, df in zip(data_names, dfs):
#    max_61_row = df[df['mz'].astype(str).str.startswith('61.')]['intensity'].max()
#    max_121_row = df[df['mz'].astype(str).str.startswith('121.')]['intensity'].max()
#    max_202_row = df[df['mz'].astype(str).str.startswith('187.')]['intensity'].max()
#    reagent_max = max_61_row + max_121_row# + max_187_row
#    df['normalized_y'] = df['intensity'] / reagent_max
#    df.sort_values(by='mz', inplace=True)
#    df.name = name  # Anna DataFrame-objektille nimi


#normalization negative mode
for name, df in zip(data_names, dfs):
    max_61_row = df[df['mz'].astype(str).str.startswith('61.')]['intensity'].max()
    max_124_row = df[df['mz'].astype(str).str.startswith('124.')]['intensity'].max()
    max_187_row = df[df['mz'].astype(str).str.startswith('187.')]['intensity'].max()
```

```
    reagent_max = max_61_row + max_124_row# + max_187_row
    df['normalized_y'] = df['intensity'] / reagent_max
    df.sort_values(by='mz', inplace=True)
    df.name = name  # Name the dataframe object


# Move normalized data to an excel file
a = 0
for df in dfs:
    plt.plot(df['mz'], df['normalized_y'], label=df.name)
    with pd.ExcelWriter('30.5_cyclooctene_neg_3_MS.xlsx',
                    mode='a', if_sheet_exists='overlay') as writer:
        df.to_excel(writer, sheet_name="sheet_name", index=False, startcol=a)
        a += 3
# Plot data using python
plt.xlabel('m/z')
plt.ylabel('signal')
plt.title('Cyclooctene oxidation in a reaction time of 0.33 s')
plt.legend(title='Datasets')

# x-axis scale
plt.xlim(170, 500)

# y-axis scale
plt.ylim(0,0.01)

plt.show()
```

E.2 Program for the time series

```
import os
import pandas as pd
import matplotlib.pyplot as plt
import numpy as np

def process_files(directory):
    files = [f for f in os.listdir(directory) if f.endswith('.csv')]
```

```
    print(f"Found {len(files)} CSV files to process.")

    all_points_data = []  # Save all data from all files

    for file in files:
        filepath = os.path.join(directory, file)
        try:
            df = pd.read_csv(filepath)

# Normalization negative mode
max_61_row = df[df['mz'].astype(str).str.startswith('61.')]['intensity'].max()
max_124_row = df[df['mz'].astype(str).str.startswith('124.')]['intensity'].max()
max_187_row = df[df['mz'].astype(str).str.startswith('187.')]['intensity'].max()

# Normalization positive mode
#max_61_row = df[df['mz'].astype(str).str.startswith('61.')]['intensity'].max()
#max_121_row = df[df['mz'].astype(str).str.startswith('121.')]['intensity'].max()
#max_202_row = df[df['mz'].astype(str).str.startswith('202.')]['intensity'].max()

reagent_max = max_61_row + max_124_row + max_187_row


# Normalization
df['normalized_intensity'] = df['intensity'] / reagent_max

# Find normalized data point from all points, and add 0 values to missing points
points_data = []
for point in points:
    point_data = df[df['mz'].astype(str).str.startswith(point)]
    if not point_data.empty:
        max_y_at_point = point_data['normalized_intensity'].max()
        points_data.append({'mz_point': point, 'normalized_y': max_y_at_point})
    if point_data.empty:
        max_y_at_point = 0
        points_data.append({'mz_point': point, 'normalized_y': max_y_at_point})
all_points_data.extend(points_data)

    except pd.errors.EmptyDataError:
```

```
        print(f"Warning: {file} is empty and will be skipped.")
    except Exception as e:
        print(f"Error processing {file}: {e}")

# Create dataframe from all points
all_points_df = pd.DataFrame(all_points_data)
return all_points_df

directory = 'C:/Thesisdata/KesÃ€tyÃ¶_data/30.5/20240530_octene_short_reactor_3_neg'

# Define points from which data is fetched
points = ['408', '426', '440', '299', '315', '267']

# Process data
final_df = process_files(directory)


#Create a list for each mass to charge ratio
lista239 = []
lista241 = []
lista250 = []
lista251 = []
lista252 = []
lista254 = []
lista265 = []
lista273 = []
lista280 = []
lista267 = []
lista268 = []
lista269 = []
lista301 = []
lista297 = []
lista299 = []
lista268 = []
lista282 = []
lista285 = []
lista284 = []
lista286 = []
```

```
lista312 = []
lista298 = []
lista314 = []
lista313 = []
lista315 = []
lista329 = []
lista330 = []
lista331 = []
lista284 = []
lista376 = []
lista300 = []
lista408 = []
lista422 = []
lista440 = []
lista442 = []
lista454 = []
lista456 = []
lista426 = []
lista468 = []
lista472 = []
lista488 = []
lista500 = []
lista504 = []
lista520 = []
lista532 = []

# Sort normalized data to separate lists
for ind in final_df.index:
    mz_point = final_df['mz_point'][ind]  # Extract the value from the DataFrame
    normalized_y = final_df['normalized_y'][ind]  # Extract the normalized_y value
    tup = (mz_point, normalized_y)
    #if "250" in tup:
    #    lista250.append(tup)
    if "267" in tup:
        lista267.append(tup)
    #elif "254" in tup:
    #    lista254.append(tup)
    elif "299" in tup:
```

```
        lista299.append(tup)
    elif "408" in tup:
        lista408.append(tup)
    elif "315" in tup:
        lista315.append(tup)
    elif "426" in tup:
        lista426.append(tup)
    #elif "301" in tup:
        #lista301.append(tup)
    elif "440" in tup:
        lista440.append(tup)

# Move data to excel file
with pd.ExcelWriter('20240530_octene_short_reactor_3_neg.xlsx',
                    mode='a', if_sheet_exists='overlay') as writer:
pd.DataFrame(lista299).to_excel(writer, sheet_name="Ark1", index=False, startcol=0)
pd.DataFrame(lista267).to_excel(writer, sheet_name="Ark1", index=False, startcol=2)
pd.DataFrame(lista315).to_excel(writer, sheet_name="Ark1", index=False, startcol=4)
pd.DataFrame(lista408).to_excel(writer, sheet_name="Ark1", index=False, startcol=6)
pd.DataFrame(lista426).to_excel(writer, sheet_name="Ark1", index=False, startcol=8)
pd.DataFrame(lista440).to_excel(writer, sheet_name="Ark1", index=False, startcol=10)
```